KoG

No. 13. (2009)
ISSN 1331-1611

SCIENTIFIC-PROFESSIONAL JOURNAL OF
CROATIAN SOCIETY FOR GEOMETRY AND GRAPHICS

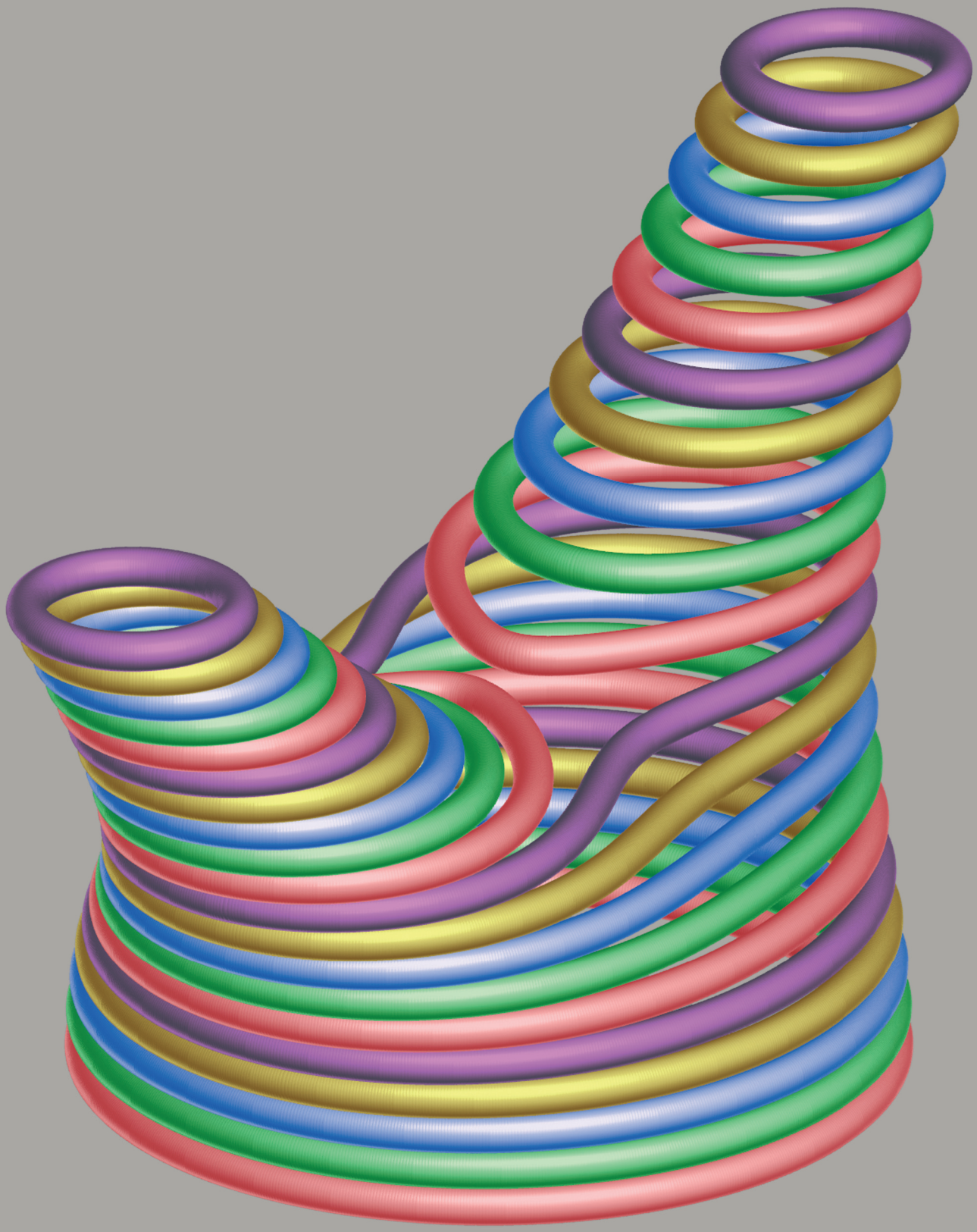

KoG

Official publication of the Croatian Society for Geometry and Graphics publishes scientific and professional papers from the fields of geometry, applied geometry and computer graphics.

Founder and Publisher

Croatian Society for Geometry and Graphics

Design

Miroslav Ambruš-Kiš

Layout

Sonja Gorjanc, Ema Jurkin

Cover Illustration

Georg Glaeser: *"Cassini–Rings", computer graphics*

Print

"O-TISAK", d.o.o., Zagreb

URL address

http://www.hdgg.hr/kog
http://hrcak.srce.hr

Edition

150

Published annually

Guide for authors

Please, see the last page.

KoG is cited in: Mathematical Reviews, MathSciNet, Zentralblatt für Mathematik

---

This issue has been financially supported by The Ministry of Science, Education and Sport of the Republic of Croatia.

ISSN 1331–1611

KoG

No. 13
Zagreb, 2009

SCIENTIFIC AND PROFESSIONAL JOURNAL OF
CROATIAN SOCIETY FOR GEOMETRY AND GRAPHICS

CONTENTS

ISSN 1331–1611

KoG

BROJ 13
Zagreb, 2009

ZNANSTVENO-STRUČNI ČASOPIS
HRVATSKOG DRUŠTVA ZA GEOMETRIJU I GRAFIKU

SADRŽAJ

VLASTA ŠČURIĆ-ČUDOVAN

Ljerka Dočkal-Krsnik

(1922. - 2009.)

Dr. sc. LJERKA DOČKAL-KRSNIK, umirovljena redovita profesorica Nacrtne geometrije na Geodetskom fakultetu Sveučilišta u Zagrebu i počasna članica našeg HDGG-a, preminula je 10. srpnja 2009. godine u Zagrebu.

Rođena je 16. travnja 1922. godine u Zlataru. Osnovnu školu i gimnaziju polazila je u Karlovcu, a na Prirodoslovno-matematičkom fakultetu u Zagrebu diplomirala je 1946. godine grupu *Nacrtna geometrija* i *Teorijska matematika*. Na istom je fakultetu 1971. godine doktorirala na temi *Plohe specijalnih krivulja u linearnim sistemima pravčastih ploha 2. reda, disertacija*.

Od 1946. do 1947. godine radila je kao profesorica Nacrtne geometrije na Industrijskoj, a od 1947. do 1949. na Tehničkoj školi u Karlovcu. Godine 1949. izabrana je za asistenticu na Katedri *Nacrtna geometrija* pod vodstvom prof. dr. Vilka Ničea na Tehničkom, kasnije Arhitektonsko-građevinsko-geodetskom fakultetu u Zagrebu. Godine 1961. birana je u zvanje predavača Nacrtne geometrije na Geodetskom odjelu AGG-a, a potom na Geodetskom fakultetu u Zagrebu. Na tom fakultetu 1968. godine postaje docenticom, izvanrednom profesoricom 1973., a redovitom profesoricom 1978. godine.

Područje znanstvenog rada Ljerke Dočkal-Krsnik bila je geometrija i to projektivna geometrija obrađena sintetičkim metodama, područje u kojem je akademik Ničе bio svjetski poznati stručnjak. Iako sam s Ljerkom radila od 1961. godine pa sve do njenog umirovljenja 1983., nisam bila upoznata (vjerojatno zbog njene skromnosti) koliko ju je akademik Ničе cijenio kao nastavnicu i znanstvenicu, već od početnih radova. Pri njezinom napredovanju u zvanjima Geodetski je fakultet svaki put izabrao akademika Ničea u komisiju za ocjenu radova pa se originali njegovih izvješća mogu naći u arhivi fakulteta. U ovoj tužnoj prilici, kad sam pripremala In Memoriam za Ljerku Dočkal-Krsnik, pročitala sam ta izvješća i zaključila kako je u prikazu njenog znanstvenog i nastavnog rada najprimjerenije citirati upravo njezinog učitelja, akademika Vilka Ničea.

"....Od 1949. g. do danas radi Ljerka Dočkal kao asistent kod već spomenute katedre. Na ovom mjestu pokazala je ona vrlo lijepe uspjehe u svom radu, unatoč poznatom velikom opterećenju asistenta kod ove katedre. Radi ovog velikog opterećenja u nastavnom radu nije se mogla sistematski baviti i naučnim radom. No unatoč tome bavila se, a i danas se uspješno bavi u granicama fizičkih mogućnosti, nekim naučnim problemima na području projektivne i nacrtne geometrije..." (Iz izvješća Vijeću Arhitektonsko-građevinsko-geodetskog fakulteta u Zagrebu, rujan 1961. godine.)

S posebnim zadovoljstvom upoznajem čitatelje KOG-a s dijelovima Ničeovih ocjena i prikaza znanstvenih radova Ljerke Dočkal-Krsnik, u nadi da će se među njima naći i čitatelj koji će posegnuti za literaturom u tom području te nastaviti njezina zanimljiva istraživanja.

Na temelju svog prvog znanstvenog rada [1] primljena je Ljerka Dočkal-Krsnik za člana Naučnog vijeća Instituta za matematiku Sveučilišta u Zagrebu. U prijedlogu da joj se taj rad prihvati kao habilitacijski akademik Ničе piše:

"... Prolazeći u takvom svom pripremnom radu geometrijska područja na kojima je zapeo njen interes, pronašla je niz problema koji do danas nisu riješeni u postojećoj literaturi, jer na njih nitko do danas nije naišao. Ti se problemi pojavljuju kao geometrijska mjesta raznovrsnih transverzala između zraka raznih pravčastih tvorevina, kao što su npr. pravčaste plohe, te kolinearno pridruženi snopovi zraka. Jedan takav dosad neriješen problem riješen je u predloženoj radnji, u kojoj se istražuje geometrijsko mjesto najkraćih transverzala od po dviju izvodnica jedne racionalne vitopere pravčaste plohe, kojima je geometrijsko mjesto nožišta poznato pod imenom "strikciona linija" takvih ploha. Geometrijsko mjesto najkraćih transverzala od bilo kojih dviju izvodnica takve vitopere pravčaste plohe dosad nije istraženo, a taj problem riješila je Ljerka Dočkal u predloženom radu.

Budući da svaka pravčasta ploha ima ∞^1 izvodnica, a svaka od njih sa svakom ima najkraću transverzalu, to takvih neprekinuto složenih najkraćih transverzala u prostoru ima ∞^2, te one čine istraženu, u naslovu radnje spomenutu, kongruenciju Ljerke Dočkal. Poznata ploha tangenata strikcione linije takve pravčaste plohe čini samo jedan singularni sastavni dio ovakve kongruencije.

U svom radu Ljerka Dočkal najprije izvodi red takve kongruencije, koji je za vitoperu pravčastu plohu n-tog stupnja jednak $(2n-1)(n-1)$. Budući da se pod redom razumijeva broj njenih zraka koje prolaze jednom točkom prostora, postavlja Ljerka Dočkal jednom točkom prostora dirni stožac na takvu plohu, te određuje nožišnu krivulju te pravčaste plohe za ovu točku kao pol. Zajedničke izvodnice unisekanata te nožišne krivulje koje prolaze tim polom daju zrake istraživane kongruencije, a njihov je broj $(2n-1)(n-1)$ njen red. Pri određivanju razreda te kongruencije, dakle broja njenih zraka u svakoj ravnini prostora, služi se Ljerka Dočkal konoidalnom pravčastom plohom onih zraka takve kongruencije, koje su usporedne s jednom ravninom prostora (direkciona ravnina tog konoida), jer stupanj tog konoida daje onda broj zraka ovakve kongruencije u po volji odabranoj ravnini prostora, a prema tome i njen razred. Poslužiši se duhovito teorijom pravčastih ploha, prenesenom na takve plohe konoidalnog sustava, dobiva ona najprije stupanj $g=(2n-1)(n-1)$ takvog konoida, a pomoću njega i razred m njene kongruencije, koji je jednak $\frac{(n-1)(3n-2)}{2}$.

Odredivši ovako red i razred opisane kongruencije kod racionalne vitopere pravčaste plohe bilo kojeg n-tog stupnja, prelazi Ljerka Dočkal na takvu kongruenciju pravčastih ploha 2. stupnja, tj. jednoplošnog hiperboloida i hiperboličkog paraboloida.

Među jednoplošnim hiperboloidima promatra Ljerka Dočkal napose jednoplošni rotacioni hiperboloid, jer opisana kongruencija baš toj plohi, koja je potpuno istražena i poznata, daje nekoliko zanimljivih novih osobina. U ovim razmatranjima služi se Ljerka Dočkal i konstruktivnim postupcima za lakše ilustrativne svrhe u ortogonalnoj i centralnoj projekciji, pomoću koje neizmjerno daleke elemente razmatra u konačnosti. Kao markantan rezultat tih razmatranja pojavljuje se ovdje činjenica, da najkraće transverzale jedne izvodnice sa svim ostalim izvodnicama istog sistema takvog hiperboloida čine poznati Plückerov konoid, koji je u matematičkoj literaturi poznat kao jedina pravčasta ploha uopće, kojoj su nožišne krivulje za bilo koji pol u prostoru krivulje 2. stupnja (elipse). Cijela istraživana kongruencija sastoji se prema tome ovdje iz sistema takvih Plückerovih konoida, koji nastaju rotacijom jednog od njih oko osi tog rotacionog hiperboloida. O kutu što ga čine izvodnice tog hiperboloida s njegovom osi ovise položaji kuspidalnih točaka i torzalnih pravaca tih konoida, koji svi zajedno čine geometrijska mjesta, koja Ljerka Dočkal u svojoj radnji istražuje. Kako Plückerov konoid osim realnih izvodnica ima i konjugirano imaginarne izvodnice, koje su od realnih odijeljene torzalnim pravcem te plohe, Ljerka Dočkal u svojoj radnji potanko istražuje i geometrijsko mjesto takvih konjugirano imaginarnih zraka njene kongruencije u okviru jednog takvog hiperboloida.

Na eliptičkom i paraboličkom hiperboloidu sva se ovakva razmatranja prilično kompliciraju, tako da će nastavak takvih razmatranja u okviru tih dviju ploha biti sadržaj kojeg daljnjeg naučnog rada. Prof. dr. Walter Wunderlich u Beču, danas jedan od prvih geometričara sintetičkog smjera u svijetu, u svom referatu o ovom radu Ljerke Dočkal u poznatom svjetskom matematičkom referatnom časopisu "Zentralblatt für mathematische Wissenschaften", dao je o njemu vrlo povoljno mišljenje, osvrnuvši se naročito na već opisane Plückerove konoide, smatrajući ih markantnim novim naučnim rezultatom na području matematičkih nauka...

...U svojim radovima ulazi Ljerka Dočkal u dosad neobrađeno geometrijsko područje, u kojemu pronalazi zanimljive probleme koje rješava na način i sredstvima koja su na punoj visini suvremenog matematičkog naučnog rada. Iz referata i diskusija Ljerke Dočkal u okviru naučnog seminara Instituta za matematiku Sveučilišta u Zagrebu vidi se, kako se u području njenog naučnog rada pojavljuju sve noviji i noviji problemi koje treba riješiti, a koje Ljerka Dočkal ima i namjeru rješavati i riješiti. Odavle se može očekivati da će se njen naučni rad nastaviti i donositi i dalje nove i lijepe rezultate...

..Na temelju svega izloženog čast nam je predložiti, da se naučni rad [1] primi kao habilitaciona radnja..." (Iz izvješća Vijeću Geodetskog fakulteta, svibanj 1967. godine)

Godine 1971., obranivši disertaciju [3] na PMF-u, promovirana je u doktora matematičkih znanosti. O toj radnji i znanstvenim radovima koji su ju slijedili Ničе piše:

"... U disertaciji se ona posvetila istraživanjima dosad neriješenih problema u području linearnih sistema ploha 2. stupnja i njihovih polarnih prostora. Problemi glavnih krivulja, simetralnih ravnina, strikcionih linija, asimptotskih stožaca itd., koji neprekinuto povezani sa svih ploha takvog sistema čine nove geometrijske tvorevine, plohe i torze, koje Lj. Dočkal u svojoj disertaciji razmatra povezano u jednoj cjelini, ne ulazeći u specijalne detalje. Podrobnijim pojedinačnim razmatranjima tih tvorevina bavi se ona kasnije u specijalnim radovima, koje ćemo odmah spomenuti. U tim svojim radovima posvetila je Lj. Dočkal naročitu pažnju onim sistemima ploha 2. stupnja, koji u dosadašnjoj matematičkoj literaturi nisu obrađivani. Sva svoja istraživanja izvodi Lj. Dočkal sintetičkom metodom projektivne geometrije, koja je u matematici najbliža Nacrtnoj geometriji.

Osim ovih problema razmatrala je i riješila Lj. Dočkal i vrlo zanimljive probleme u vezi s dva i tri kolinearno pridružena svežnja. Za ove je probleme u najmanju ruku čudno, da u dosadašnjoj matematičkoj literaturi nisu niti zapaženi, a još manje riješeni.

Prva radnja Lj. Dočkal koja je objavljena nakon njenog izbora u zvanje docenta je [4]. U ovoj se radnji Lj. Dočkal poslužila poznatom činjenicom, da svaka ravnina prostora dira tri plohe pramena ploha 2. stupnja, te da svakom točkom prostora prolazi samo jedna ploha takvog pramena. Dubljim istraživanjem ovakovih trojki točaka u prostoru, otkriva Lj. Dočkal zanimljivo prostorno preslikavanje 6. reda. Na temelju i u okviru tog preslikavanja izvodi ona u ovoj radnji prostorne krivulje 6. reda pridružene točkama jednog pravca, te opće plohe 6. reda pridružene točkama jedne ravnine.

U radnji [5] razmatrane su najkraće transverzale parova pridruženih zraka dvaju kolinearnih svežnjeva. Sve te transverzale čine kongruenciju 6. reda i 5. razreda. Nožišta tih transverzala na zrakama svakog snopa čine opću plohu 4. reda, a otkrivene su i neke druge osobine ove dosad nepoznate kongruencije.

U Glasnik matematički predana je u štampu radnja [6]. Kako svaka pravčasta ploha 2. stupnja ima svoju strikcionu liniju, istraživala je Lj. Dočkal u ovoj radnji geometrijsko mjesto strikcionih linija svih pravčastih ploha 2. stupnja jednog sistema takvih ploha. Ovo je geometrijsko mjesto opća ploha 16. reda, koja je otkrivena i istraživana u ovoj radnji. Istraženi su i specijalni slučajevi takvih ploha, naročito degeneriranih, kao i njihove važnije osobine, jer do sada takve plohe nigdje nisu razmatrane.

Daljnja radnja dr. Lj. Dočkal [7] predana je u štampu za Rad JAZU. Svaka ploha 2. stupnja ima tri simetralne ravnine, koje tu plohu sijeku u glavnim krivuljama. Sve takve glavne krivulje ploha jednog sistema ploha 2. stupnja čine opću plohu 16. reda. Istraženi su i ovdje specijalni slučajevi kao i neke osobine.

Kao posljednja, nedavno završena i za štampu u Radu JAZU predana radnja Lj. Dočkal je [8]. Postavljamo li nekom točkom prostora ravnine okomite na izvodnice neke pravčaste plohe, čine nožišta tih izvodnica na tim ravninama nožišnu prostornu krivulju tog, obzirom na tu pravčastu plohu odabranog, pola. Lj. Dočkal uzima takve polove u središtima pravčastih ploha nekog pramena ploha 2. stupnja, te istražuje sistem tako nastalih nožišnih krivulja, koje tvore jednu opću plohu 15. reda. Istraživani su i ovdje specijalni slučajevi kao i važnije osobine..."
(Iz izvješća Znanstveno-nastavnom Vijeću Geodetskog fakulteta Sveučilišta u Zagrebu, svibanj 1973. godine)

U svom posljednjem izvješću o radu Ljerke Dočkal-Krsnik, nakon kojeg je izabrana u zvanje redovitog profesora, akademik Niče daje sljedeći prikaz dvaju posljednjih Ljerkinih radova:

"... Kompleks normala ploha 2. stupnja u jednom pramenu takvih ploha poznat je i do sada temeljito istražen. Međutim, takav kompleks u nizu ploha 2. stupnja, dakle na dualnoj tvorevini pramena ploha 2. stupnja, kompleks normala je do danas nepoznat i neistražen. U radu [9] zabavila se je dr. Lj. Dočkal tim kompleksom u takovom nizu. Njen referat o tom radu na Austrijskom matematičkom kongresu u Salzburgu izazvao je veliki interes i živu diskusiju najistaknutijih matematičara.

U radu [10] otkrila je i istražila dr. Lj. Dočkal jedan do sada nezapažen problem, odnosno, geometrijsku tvorevinu, koja se, kao i kod pramena i niza, sastoji iz ∞^1 neprekinuto povezanih pravčastih ploha 2. stupnja, ali te plohe ne čine niti poznati pramen niti poznati niz. Ovaj kontinuirani linearni niz ili sistem ploha 2. stupnja tek je otkriven i obrađen u tom radu. Odaberemo li u prostoru po volji tri međusobno projektivna pramena pravaca, tada je svakoj zraci jednog pramena jedno-jednoznačno pridružena po jedna zraka drugog. Transverzale svake ovakove trojke pridruženih pravaca čine jedan sistem izvodnica neke pravčaste plohe 2. stupnja. Sama trojka tako pridruženih pravaca spada u drugi sistem takve plohe. Sa svih ∞^1 ovakovih pridruženih neprekinuto povezanih trojki zraka tih triju pramenova određeno je ∞^1 neprekinuto povezanih pravčastih ploha 2. stupnja, koji čine nov do sada nepoznat neprekinut sistem, kojim se je zabavila dr. Lj. Dočkal u toj radnji.

U ovom je radu dokazano da jedna ravnina dira tri plohe, a svakom točkom prolaze tri plohe takvog sistema. Pomoću ovog je izvedeno da i svaki pravac dira tri plohe takvog sistema. Konjugirane polare nekom pravcu obzirom na sve plohe ovakovog sistema čine pravčastu plohu 3. stupnja. Uz taj sistem ploha povezan je i kompleks njihovih normala, koji je 12. stupnja. I u ovom sistemu istražene su ploha glavnih krivulja, ploha strikcionih linija i ploha centralnih nožišnih krivulja, tako da je time zaokružen potpun prikaz ovog novootkrivenog sistema ploha 2. stupnja..."
(Iz izvješća Znanstveno-nastavnom Vijeću Geodetskog fakulteta Sveučilišta u Zagrebu, listopad 1978. godine)

Tijekom niza godina Ljerka Dočkal-Krsnik bila je voditeljica nekoliko znanstvenih projekata. O svojim je znanstvenim radovima redovito izvještavala na kongresima, savjetovanjima i drugim skupovima. Navodim ovdje neke od njih: *Austrijski kongres matematike* (Linz 1968., Beč 1973., Salzburg 1977., Insbruck 1982.), *Balkanski kongres matematičara* (Ohrid 1970., Beograd 1974.), *Jugoslavensko savjetovanje za nacrtnu geometriju nastavnika tehničkih fakulteta* (Beograd 1961., Split 1963, Sarajevo 1965., Skopje-Ohrid 1967., Ljubljana 1969., Zagreb 1971., Novi Sad 1973., Niš 1975., Herceg Novi 1977, Aranđelovac 1979., Osijek 1981., Zagreb 1990.).

Bila je članica Društva matematičara i fizičara Jugoslavije, Austrijskog matematičkog društva, Jugoslavenskog udruženja za nacrtnu geometriju i inženjersku grafiku te počasna članica Hrvatskog društva za geometriju i grafiku.

Cijeli je radni vijek Ljerke Dočkal-Krsnik bio posvećen Nacrtnoj geometriji čiji je program prilagodila potrebama Geodetskog fakulteta. Kao mlada asistentica aktivno se uključila u sastavljanje zadataka za poznati Ničeov udžbenik *Deskriptivna geometrija*, te na njihovo nadopunjavanje u svakom daljnjem izdanju. Ljerka Dočkal-Krsnik bila je vrlo cijenjena nastavnica i uzorna kolegica. U razdoblju 1968–73. obnašala je dužnost voditeljice Katedre za opće teoretske predmete, 1975–79. prodekanice za nastavu Geodetskog fakulteta, a od 1981. do 1983. bila je predstojnica Zavoda za višu geodeziju.

Bila je pravi profesor, smireno je predavala znanja na najbolji mogući način i brinula da se to znanje učvrsti. Studenti su na konstrukcijskim vježbama trebali pokazati da u potpunosti razumiju materiju, da ju mogu objasniti, nacrtati i vidjeti. Da bi to postigla bila je zajedno sa suradnikom (asistentom) na svim konstrukcijskim vježbama. Ljerka kao redoviti profesor i ja, također već kao profesor, provodile smo mnoge sate u individualnom radu sa studentima. Tako smo postizavale svoj glavni cilj – znanje studenata. Zato mi je danas, kad se susretnem s nekadašnjim studentima, drago čuti kako se vidjelo koliko nam je bilo važno da studenti shvate i nauče.

S Ljerkom raditi bilo je prelijepo, jer je ona bila čovjek u najplemenitijem smislu te riječi.

Popis radova

[1] LJ. DOČKAL, Kongruenz der Gemeinlote von Erzeugenden einer rationalen windschiefen Regelfläche *n*-ten Grades, *Glasnik Mat. fiz. i astr.* **17** (1962), No.3–4, 205–222.

[2] LJ. DOČKAL, Transversalenkomplex der zugeordneten Strahlentripe dreier kollinearzugeordneten Strahlenbündel, *Glasnik Matematički* **2** (**22**) (1967), No.2, 245–263.

[3] LJ. DOČKAL, Plohe specijalnih krivulja u linearnim sistemima pravčastih ploha 2. reda, disertacija, PMF Zagreb, 1971.

[4] LJ. DOČKAL, Über eine Abbildung sechster Ordnung, *Glasnik Matematički* **6** (**26**) (1971), No.1, 113–120.

[5] LJ. DOČKAL, Kongruenz der Gemeinlote, *Glasnik Matematički* **8** (**28**) (1973), No. 2, 273–284.

[6] LJ. DOČKAL, Die Striktionslinienfläche eines linearen Regelflächensystems 2. Ordnung, *Glasnik Matematički* **9** (**29**) (1974), No.1, 109–124.

[7] LJ. DOČKAL, Die Hauptkurvenfläche in linearen Flächensystems 2. Ordnung, *Rad JAZU* **370** (1975), 107–115.

[8] LJ. DOČKAL, Die Flächen der zentrischen Fusspunktkurven in linearen Regelflächensystems 2. Ordnung, *Rad JAZU* **370** (1975), 93–106.

[9] LJ. DOČKAL, Normalenkomplex der Flächen einer Flächenschar 2. Grades, *Rad JAZU* **386** (1980), 35–47.

[10] LJ. DOČKAL, Über einen Regelflächensystem 2. Grades das durch drei projective Strahlbüschel bestimmt ist, *Rad JAZU* **386** (1980), 49–65.

Original scientific paper
Accepted 30. 06. 2009.

GUNTER WEISS
ANA SLIEPČEVIĆ

Osculating Circles of Conics in Cayley-Klein Planes

Osculating Circles of Conics in Cayley-Klein Planes

ABSTRACT

In the Euclidean plane there are several well-known methods of constructing an osculating (Euclidean) circle to a conic. We show that at least one of these methods can be "translated" into a construction scheme of finding the osculating non-Euclidean circle to a given conic in a hyperbolic or elliptic plane. As an example we will deal with the Klein-model of these non-Euclidean planes, as the projective geometric point of view is common to the Euclidean as well as to the non-Euclidean cases.

Key words: Cayley-Klein plane, elation, pencil of conics, osculating circle, curvature centre

MSC 2010: 51N30, 51M15, 53A35

Oskulacijske kružnice konika u Cayley-Klein-ovim ravninama

SAŽETAK

U euklidskoj ravnini postoji nekoliko dobro poznatih metoda konstrukcija oskulacijske kružnice konike. Cilj je te konstrukcije "translatirati" u neke od neeuklidskih ravnina. U članku se daje opća konstrukcija oskulacijske kružnice konike zadane s pet elemenata u euklidskoj ravnini. Pokazuje se da je konstruktivna metoda primjenjiva u hiperboličkoj i eliptičkoj ravnini. Budući da je projektivno geometrijsko gledište zajedničko euklidskom i neeuklidskim slučajevima, analogne se konstrukcije koriste na Klein-ovim modelima neeuklidskih ravnina.

Ključne riječi: Cayley-Klein-ova ravnina, elacija, pramen konika, oskulacijska kružnica, središte zakrivljenosti

1 Preliminary Remark

Although the problem of constructing an osculating circle at a point of a conic seems to be anachronistic in times of numerical approximation tools, knowledge about exact constructive methods is not at all obsolete, particularly since these methods are uniformly applicable. Beyond that, with the following projective geometric constructions of osculating circles, we place particular emphasis on synthetic argumentation, which is typically for geometry. Unfortunately Projective Geometry and Non-Euclidean Geometry in the sense of F. Klein does not have much space in nowadays Mathematics education such that valuable Geometry culture is in danger of vanishing. Our article might perhaps help to counteract these facts. The paper is also to be posed into the series of articles of classical Projective and Non-Euclidean Geometry initiated by the second author, see [5] - [8].

It is hard to say, how "well-known" the presented considerations are; they could be for example exercise material to lectures on classical Projective Geometry and not considered to be valuable enough to be published. To our knowledge lectures with related content still exist in Vienna (H. Stachel, H. Havlicek) and Graz (J. Wallner, O. Röschel), where they still belong to the syllabus in teachers education in Descriptive Geometry.

2 Euclidean Osculating Circles of Conics

We start with "permissible standard givens" of a conic in the Euclidean plane, i.e. from pair of conjugate diameters $\overline{AC}$, $\overline{BD}$ of an ellipse, from a pair of line elements (A,t_A), (B,t_B) of a parabola and from a pair of asymptotes (r,s) and a point A of a hyperbola. The problem is to find the osculating circle at the given point A.

In geometry courses for engineers one usually presents the construction recipe for the hyperosculating circles at the vertex of the conic; in lectures on differential geometry for Mathematicians this recipe is also presented and the analytic equality of 4^{th}order is proved by calculation in each of the three cases. But for all three cases there is a uniform projective geometric idea for the solution of this (more general) problem. This idea uses properties of osculating resp. hyperosculating pencils of conics. This unified explanation of elementary construction of hyperosculating

circles at vertices of a conic might be not new, but it is, in our opinion, not at all so well-known as it is worthy to note.

In addition, the construction principle deduced from it can be used for all Cayley-Klein geometries, as it is shown in the following chapter only for the hyperbolic and the quasi-hyperbolic geometry (which is the dual geometry to the pseudo-Euclidean geometry) as an example.

Specifically, the construction follows two steps:

Step 1: Transform the given conic c by the standard shear transformation $\sigma_1 : c \to c'$ into another conic c', which osculates c at the point A, and has A as a vertex. The axis of the shear therefore is the tangent t_A in A. As all elations with the center N on t_A, this shear σ_1 maps the given conic c into c' which osculates the conic c at A. The osculating circle of one is also osculating circle for the other one.

Step 2: Construct the hyperosculating circle k_A of the conic c' at $A = A'$. For this one can use an additional elation σ_2 which also has t_A as its axis, but the center A and it should map c' into a hyperosculating conic c''. By demanding $c' \mapsto k_A$ the transformation σ_2 is uniquely defined; σ_2 transforms the point B' of the osculating conic c' (in the case of an ellipse this is a "neighbouring" vertex, in case of a hyperbola one of the asymptote's ideal point "at infinity", in the case of a parabola it is the additionally given point) into the point B'' of k_A. The normal from the (fixed) point $T = T' = T'' \in t_A$ ($T = t_A \cap t_B = t_{B'} \cap t_B$) to the chord $AB'' = AB'$ of circle k_A therewith passes through the center M_A of k_A.

The following figures (Figures 1-3) show the construction costs, which in each of the three cases needs only a few lines.

Elliptic case (Figure 1)
The point A is transformed into the vertex of an ellipse c' by the shear $\sigma_1 : c \to c'$ (tangent t_A at A is the axis of σ_1). Furthermore, $\sigma_2 : c' \to k_A$ with the same axis, but with center A, transforms a "neighbouring" vertex B' of c' into the point B'' of k_A. The line through the fixed point $T = T' = T''$ on t_A perpendicular to the chord $AB'' = AB'$ of the osculating circle k_A intersects the normal n of the conic c given at the point A in the center M_A of k_A.

Parabolic case (Figure 2)
The shear $\sigma_1 : c \to c'$ (axis is the tangent t_A at A) transforms the point A into the vertex of a parabola c', which osculates c. The midpoint H of the chord $\overline{AB}$, together with the point $T := t_A \cap t_B$, defines the diameter direction of the conic c, and therefore is mapped into the point H' on the line normal to t_A at T. For $\sigma_2 : c' \to k_A$ (the center is A) the line AH' is a fixed line; it contains the point $B'' = \sigma_2(B')$ of the hyperosculating conic k_A. The line through the fixed point $T = T' = T''$ perpendicular to the chord $AB'' = AH'$ of k_A passes through the sought-after curvature center M_A.

Hyperbolic case (Figure 3)
At first we construct the tangent t_A at the point A, (A is the midpoint of the tangent segment between the asymptotes). By a suitable shear σ_1 one can transform the point A into the vertex of the hyperbola c' whose asymptotes are r' and s' and the center is M'. The elation $\sigma_2 : c' \to k_A$ with center A transforms the ideal point $R' = B'$ of the asymptote r' of the conic c' into the point B'' of the hyperosculating conic k_A. Therefore, the line through the fixed point T on the tangent t_A perpendicular to $AB'' = AB'$ passes through the common curvature center M_A of the conics k_A, c' and c. As AB' is parallel to r', one only needs to draw the perpendicular line to the asymptote $r' = M'T$ at the point T.

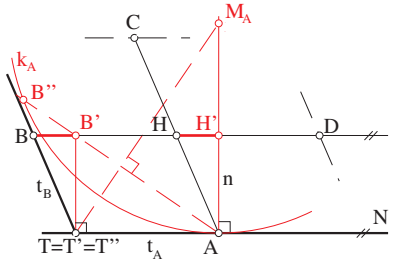

Figure1: Construction of the center M_A of the osculating circle k_A at the endpoint A of one of the given conjugate diameters of the ellipse c.

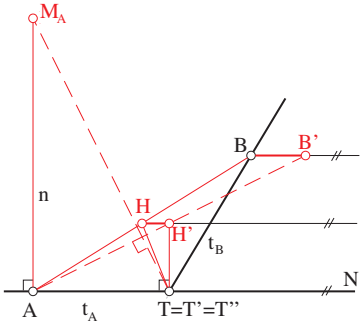

Figure 2: Construction of the center M_A of the osculating circle k_A at the point A of the parabola c given by two line elements (A,t_A), (B,t_B).

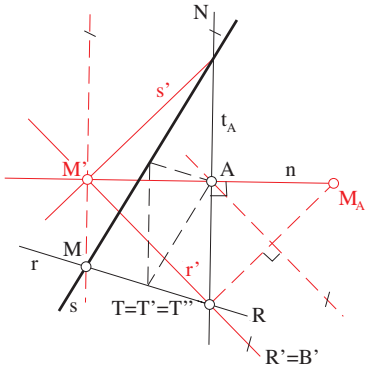

Figure 3: Construction of the curvature center M_A at the point A of the hyperbola $c$given by the pair of asymptotes (r,s) and the point A.

Remark 1 *Of course, there are other nice constructions of the Euclidean curvature circle at the point of a conic, too. We want to mention the one found in [1], which is based on the differential geometric investigations and goes as follows:*

"Choose two points P,Q on tangent t_A symmetric to A, draw the tangents from P and Q to the given conic c, receive the contact points P' and Q'. The normals p and q to the cords AP' and AQ' intersect the normal n in A in the points M_P and M_Q. Then M_A is the midpoint of the segment (M_P,M_Q). Also this construction could be transformed to CK-planes."

3 Curvature Centres of Conics which are Given by General Data in CK-planes

In the preceding chapter we started with affine-special given data of a conic. Now we choose a projective-geometric system of data defining a conic:

Let a conic c be given by two line elements (A,a), (B,b) and a point C in a (real) projective plane π equipped with an "absolute (regular or degenerated) polarity" $\pi^{\perp}$. (The plane π together with $\pi^{\perp}$ is therewith a Cayley-Klein plane, in short a CK-plane.)

These specifications of the conic c can easily be derived from all other given data, which define conic uniquely, by applying the theorems of Pappus-Pascal and Brianchon, see [2]. These givens are also appropriate for the analytic treatment of the conic, as they can be interpreted as a projective coordinate system.

Via $\pi^{\perp}$ the place of action is a projective plane with an orthogonality structure "$\perp$" and a concept of circles in the sense of Cayley-Klein; it is therefore a "projectively extended non-Euclidean plane", a CK-plane, see e.g. [3]. Among these CK-planes we want to exclude the so-called isotropic planes (see e.g. [4]) from further considerations, because their orthogonality structure $\perp$ is too degenerated. These CK-planes are treated separately in [7]. It turns out that for degenerated absolute polarity $\pi^{\perp}$ one could "swap" the two steps described in chapter 2: At first one constructs the hyperosculating parabola c' at the point A of the given conic c in the isotropic plane π with absolute point I at the ideal line u. This can be done with an elation with center A and axis a. Next, the parabola c' is transformed into the isotropic circle k with ideal point I using the shear with axis a.

In the last chapter, it will be shown that in some cases of CK-planes with degenerate absolute polarity one can easily find simplier constructions using one single elation alone.

The problem is to construct the curvature center M_A at the point A of the given conic c. (For the sake of simplicity we visualise again the Euclidean case in Figure 4, i.e. "$\perp$" and "circles" allow an elementary geometric interpretation.)

Step 1: determine the normal n of the conic c at the point A with respect to $\perp$; i.e. one needs to construct the "absolute conjugate line" n to the given tangent a of the conic c at A with respect to $\pi^{\perp}$. The absolute pole N of the normal n is a point of a and it has to be used as the center of an elation $\sigma_1 : c \to c'$ with axis a. One still needs a related pair of points to define elation σ_1 uniquely.

Step 2: the construction of a conic point D on the (fixed) collineation ray on BN using the theorem of Pappus-Pascal. (Naturally, it would be the same, if we constructed the point $E \in c$ on the collineation ray CN.) In Figure 4 the necessary lines are shown:

$$D := BN \cap AP, \quad \text{whereby,} \quad P := BC \cap \big((a \cap b) \vee (BN \cap AC)\big).$$

Step 3: determination of the 4^{th} harmonic point H to N with respect to the pair (B,D) on line BN. This point H shall be related to $H' := n \cap BN$ in σ_1 and now $\sigma_1 : c \to c'$ is uniquely determined.

Step 4: corresponds to step 2 in chapter 2 to get $\sigma_2 : c' \to k_A$. Explicitly, one only needs the center A of elation σ_2 and the fact that the point $B'' := \sigma_2(B')$ on k_A belongs to the chord $AB'' = AB'$ of k_A, which is fixed under σ_2 where $B' := \sigma_1(B)$. Therewith the wanted curvature center M_A is the intersection point of the normal n with the line s, which is the absolute-conjugate line to AB' through $a \cap b$.

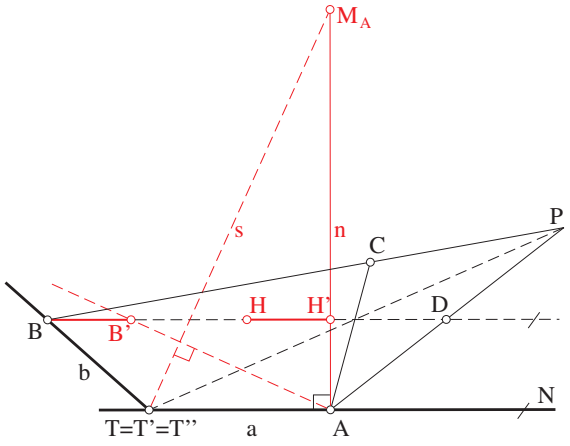

Figure 4: Construction of the curvature center M_A in a point A of a conic c, which is given by two line elements (A,a), (B,b) and an additional point C in the (projective extended) elementary geometric plane. (Explanation of the construction see above.)

4 *h*-Curvature Circles of a Conic in the Projective Model of a Hyperbolic Plane

As an example for the construction of the osculating circle in a non-Euclidean plane with regular absolute polarity $\pi^\perp$ the complete solution will be given in a hyperbolic plane, see Figure 5.

According to the projective geometric background of the idea of the construction, it is somehow natural to use the classical projective model of such a h-plane, (c.f. also [2]). This means that the place of action is essentially the inner domain of a (real) "absolute conic" u, which can be taken as an ordinary circle in elementary geometric sense. Given a conic c, the problem is to construct the h-curvature center M_A to the arbitrarily given point A (with tangent a).

It is expedient and practical to use a perspective collineation $\kappa_1 : u \to c$ to construct the conic c as collinearly related image to the absolute conic u. (In Figure 5 collineation κ_1 is defined with the center S and the axis s, and the related pair of points (A_1, A).) Note, that if s is absolute polar of S, the obtained conic c would be a circle.

Step 1: The osculating *h*-circle k of c at A has its center M on the *h*-normal n to a through A. So as a first step one needs to construct this n.

Step 2: Make A to a vertex of the conic c', which osculates c at A. For this we use a "projective shear", i.e. an elation σ_1 with axis a and centre $N \in a$, which is the absolute pole of n.

Step 3: Construct the hyperosculating circle of c' according to the description to Figure 4. In Figure 5 we used the points Q and $Q' =: \sigma_1(Q)$ to get c' from c and the special point B' and its tangent b. Finally we connect A with B' and erect the *h*-normal line to AB' through $T := a \cap b$, it intersects n in the *h*-curvature center M.

Step 4: If we do not use a graphics software like "Cinderella", where we can directly draw *h*-circles in a *h*-plane, we still have to construct the *h*-osculating circle k. This again can be done using a perspective collineation $\kappa_2 : u \to k$; it has the center M and the axis $m := \pi^\perp(M)$ and the related pair of points $(A \in c, A_2 \in u)$. Because of

$$u \overset{\kappa_1}{\longrightarrow} c \overset{\sigma_1}{\longrightarrow} c' \overset{\sigma_2}{\longrightarrow} k \overset{\kappa_2^{-1}}{\longrightarrow} u$$

The product of these perspective collineations must act as a projectivity β on u. So the mapping $\beta : c \to u \to k$ is determined by three pairs of points on u, among them A_1, A_2 and Q_1, Q_2.

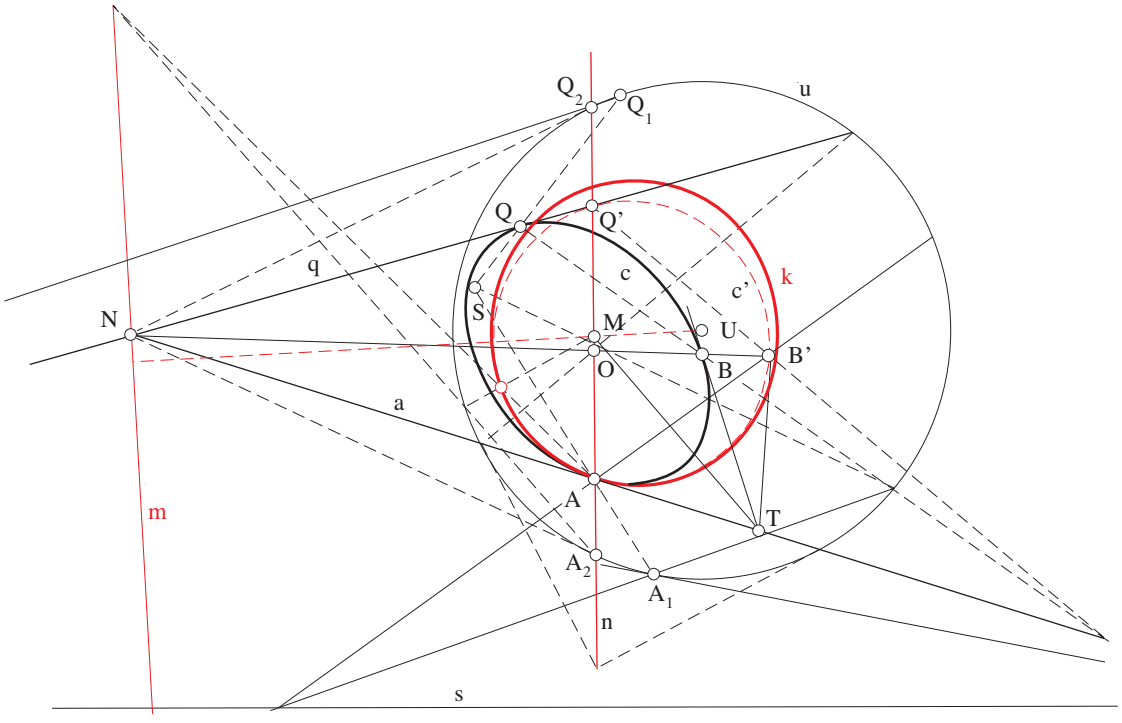

Figure 5: Osculating *h*-circle at the point A of the conic c. (Construction in the classical projective model of a *h*-plane.)

5 Curvature Circles of a Conic in the CK-Planes with Singular Absolute Polarity

To start with, we give an overview over those CK-planes, c.f. [3]:

$\pi^{\perp}$	acting in	"Absolute figure"	Name
elliptic involutoric projectivity	(ideal) line u	pair of imaginary points $I,J \in u$	Euclidean plane, $e-plane$
hyperb. involutoric projectivity	(ideal) line u	pair of real points $I,J \in u$	pseudo-Euclid. plane, $pe-plane$
elliptic involutoric projectivity	a pencil of lines u through (ideal) point U	pair of imaginary lines i,j through U	dual Euclid. plane, quasi-elliptic plane $qe-plane$
hyperb. involutoric projectivity	a pencil of lines u through (ideal) point U	pair of real lines i,j through U	dual pseudo-Euclid. plane, quasi-hyperbolic plane, $qh-plane$
degenerate inv. projectivity	(ideal) line u	point U and line u (self-dual figure)	isotropic plane, Galilean plane, $i-plane$

We treated the Euclidean case in Chapter 2 aiming at a unifying interpretation of the classical and well-known elementary constructions. We will now present constructions of osculating circles by using one single elation alone. Let us begin with

1) *Pseudo-Euclidean case*

Figure 6 shows the projective model of a pe-plane and the construction of a pe-circle osculating a conic c at the point A.

Explanation to Figure 6:
The conic c and its line element (A,a) in the pe-plane with absolute points $I,J \in u$ are given. Now we choose A as the center of an elation κ and construct its axis z: (Also this type of elations is osculation preserving!) With center A project I,J onto c getting I', J'. Intersect u with the line $u' = I'J'$, get a fixed point F and $AF =: z$. Now κ is well-defined and $\kappa(c) =: k$ is the desired osculating pe-circle.

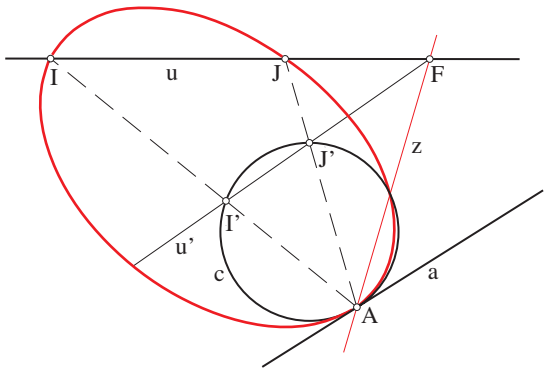

Figure 6: Osculating pe-circle at the point A of the conic c. (Construction in a projective model of a pe-plane.)

Remark 2 *The same construction principle can be performed also in the Euclidean case. The imaginary rays AI and AJ are defined by the orthogonal-involution in the pencil with vertex A and this orthogonal involution induces in c an elliptic involutoric projectivity* ρ *with involution center R. Now we had to construct the polar line r to R with respect to c; r connects the imaginary points* I' *and* J' *and therefore is parallel to the elation axis z.*

2) *Quasi-hyperbolic case*

Without loss of generality, let the absolute figure of the quasi-hyperbolic plane be a pair of parallel lines i,j. The conic c and its line element (A,a) are given. A qh-circle k is a conic k touching both absolute lines i and j. The construction is now dual to the one of Figure 6, see Figure 7.

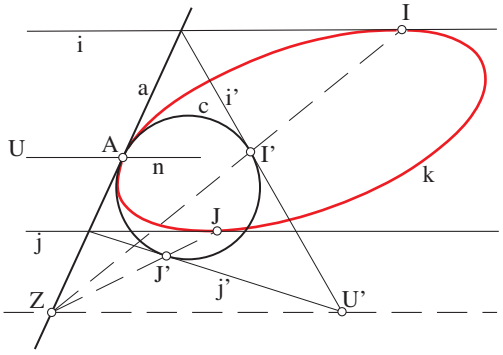

Figure 7: Osculating qh-circle at the point A of the conic c. (Construction in a qh - plane with an absolute figure $\{U;i,j\}$.)

Explanation to Figure 7:
Intersect the absolute lines i and j with the tangent a of the conic c at A. The tangents i', j' from these intersection points to c intersect at the point U' which corresponds to the absolute point U in the desired elation κ with axis a. Line UU' intersects a at the center Z of κ such that κ is well-defined by $\{Z, a, (U, U')\}$ and $k := \kappa(c)$ is the desired osculating qh-circle. Note that UA represents the qh-normal n of the c at A.

Remark 3 *The same construction principle can be performed also in the quasi-elliptic case. The construction "dualises" that of the Euclidean case. In the isotropic case, because of self-duality, one can use both, the principle of the "qh-construction" as well as that of the "pe-construction" to find the needed elation. As the construction is obvious, it can be left to the reader to practice.*

References

[1] G. BEYER, Untersuchungen zur Krümmung von Kurven zweiter Ordnung in der Ebene und Kurven vierter Ordnung erster Art im Raum. *Beiträge zur Algebra und Geometrie* **11** (1981), 65–73.

[2] H. BRAUNER, *Geometrie projektiver Räume 2*, BI. Mannheim-Wien-Zürich (1976)

[3] O. GIERING, *Vorlesungen über höhere Geometrie*, Vieweg, Braunschweig (1982)

[4] H. SACHS, *Ebene isotrope Geometrie*, Vieweg, Braunschweig-Wiesbaden, (1987)

[5] A. SLIEPČEVIĆ, Iz prizemlja više geometrije. *KoG* **5** (2001), 73.

[6] A. SLIEPČEVIĆ, Eine Anwendung der perspektive Kollineation. *KoG* **5** (2001), 51–55.

[7] A. SLIEPČEVIĆ, M. KATIĆ-ŽLEPALO, Osculating circles of conics in the isotropic plane. *Slovensky časopis pre geometriu a grafiku* **5** (2008), No.10, 21–26.

[8] A. SLIEPČEVIĆ, N. KOVAČEVIĆ, Hyperosculating circles of the conics in the Pseudo-Euclidean plane. (to be submitted).

Gunter Weiss
Technical University of Dresden
Institute for Geometry, 01062 Dresden
e-mail: Gunter.Weiss@tu-dresden.de

Ana Sliepčević
Faculty of Civil Engineering, University of Zagreb
Kačićeva 26, 10000 Zagreb
e-mail: anas@grad.hr

Original scientific paper
Accepted 19. 10. 2009.

HANS-PETER SCHRÖCKER

Orthologic Tetrahedra with Intersecting Edges

Orthologic Tetrahedra with Intersecting Edges

ABSTRACT

Two tetrahedra are called orthologic if the lines through vertices of one and perpendicular to corresponding faces of the other are intersecting. This is equivalent to the orthogonality of non-corresponding edges. We prove that the additional assumption of intersecting non-corresponding edges ("orthosecting tetrahedra") implies that the six intersection points lie on a sphere. To a given tetrahedron there exists generally a one-parametric family of orthosecting tetrahedra. The orthographic projection of the locus of one vertex onto the corresponding face plane of the given tetrahedron is a curve which remains fixed under isogonal conjugation. This allows the construction of pairs of conjugate orthosecting tetrahedra to a given tetrahedron.

Key words: orthologic tetrahedra, orthosecting tetrahedra, isogonal conjugate

MSC 2010: 51M04

Ortologni tetraedri s bridovima koji se sijeku

SAŽETAK

Dva tetraedra nazivamo ortolognim ako se pravci koji prolaze vrhovima jednog i okomiti su na odgovarajuće stranice drugog međusobno sijeku. Ovo je ekvivalentno ortogonalnosti ne-odgovarajućih bridova. Mi dokazujemo kako dodatna pretpostavka da se ne-odgovarajući bridovi sijeku ("ortopresječni tetraedar") povlači da šest sjecišta leži na jednoj kugli. Za dani tetraedar postoji općenito jednoparametarska familija ortopresječnih tetraedara. Ortogonalna projekcija geometrijskog mjesta jednog vrha na pripadajuću ravninu danog tetraedra je krivulja koja ostaje fiksnom pod djelovanjem izogonalne konjugacije. Ovo dopušta konstrukciju parova konjugiranih ortopresječnih tetraedara za dani tetraedar.

Ključne riječi: ortologni tetraedar, ortopresječni tetraedar, izogonalno konjugiranje

1 Introduction

Ever since the introduction of orthologic triangles and tetrahedra by J. Steiner in 1827 [10] these curious pairs have attracted researchers in elementary geometry. The characterizing property of orthologic tetrahedra is concurrency of the straight lines through vertices of one tetrahedron and perpendicular to corresponding faces of the second. Alternatively, one can say that non-corresponding edges are orthogonal. Proofs of fundamental properties can be found in [7] and [8]. Quite a few results are known on special families of orthologic triangles and tetrahedra. See for example [5, 6, 9, 11] for more information on orthologic tetrahedra (or triangles) which are also perspective or [3] for a generalization of a statement on families of orthologic triangles related to orthopoles.

In this article we are concerned with *orthosecting tetrahedra* — orthologic tetrahedra such that non-corresponding edges intersect orthogonally. The concept as well as a few basic results will be introduced in Section 2. In Section 3 we show that the six intersection points of non-corresponding edges necessarily lie on a sphere (or a plane). While the computation of orthosecting pairs requires, in general, the solution of a system of algebraic equations, conjugate orthosecting tetrahedra can be constructed from a given orthosecting pair. This is the topic of Section 4. Our treatment of the subject is of elementary nature. The main ingredients in the proofs come from descriptive geometry and triangle geometry.

A few words on notation: By $A_1A_2A_3$ we denote the triangle with vertices A_1, A_2, and A_3, by $A_1A_2A_3A_4$ the tetrahedron with vertices A_1, A_2, A_3, and A_4. The line spanned by two points A_1 and A_2 is $A_1 \vee A_2$, the plane spanned by three points A_1, A_2, and A_3 is $A_1 \vee A_2 \vee A_3$. Furthermore, $\mathscr{I}_n$ denotes the set of all n-tuples with pairwise different entries taken from the set $\{1,\dots,n\}$.

2 Preliminaries

Two triangles $A_1A_2A_3$ and $B_1B_2B_3$ are called *orthologic*, if the three lines

$$a_i\colon A_i \in a_i,\ a_i \perp B_j \vee B_k; \quad (i,j,k) \in \mathscr{I}_3 \tag{1}$$

intersect in a point O_A, the *orthology center* of $A_1A_2A_3$ with respect to $B_1B_2B_3$. In this case, also the lines

$$b_i\colon B_i \in b_i,\ b_i \perp A_j \vee A_k; \quad (i,j,k) \in \mathscr{I}_3 \tag{2}$$

intersect in a point O_B, the orthology center of $B_1B_2B_3$ with respect to $A_1A_2A_3$. The concept of orthologic tetrahedra is similar. Two tetrahedra $\mathbf{A} = A_1A_2A_3A_4$ and $\mathbf{B} = B_1B_2B_3B_4$ are called *orthologic*, if the four lines

$$a_i\colon A_i \in a_i,\ a_i \perp B_j \vee B_k \vee B_l; \quad (i,j,k,l) \in \mathscr{I}_4 \tag{3}$$

intersect in a point O_A, the orthology center of $\mathbf{A}$ with respect to $\mathbf{B}$. In this case, also the lines

$$b_i\colon B_i \in b_i,\ b_i \perp A_j \vee A_k \vee A_l; \quad (i,j,k,l) \in \mathscr{I}_4 \tag{4}$$

intersect in a O_B, the orthology center of $\mathbf{B}$ with respect to $\mathbf{A}$. Orthologic triangles and tetrahedra have been introduced by J. Steiner in [10]; proofs of fundamental properties can be found in [7, 8] or [1, pp. 173–174].

The symmetry of the two tetrahedra in the definition of orthology is a consequence of the following alternative characterization of orthologic tetrahedra. It is well-known but we give a proof which introduces concepts and techniques that will frequently be employed throughout this paper.

Proposition 1 *The two tetrahedra* $\mathbf{A}$ *and* $\mathbf{B}$ *are orthologic if and only if non-corresponding edges are orthogonal:*

$$A_i \vee A_j \perp B_k \vee B_l, \quad (i,j,k,l) \in \mathscr{I}_4. \tag{5}$$

Proof. We only require that the lines a_i through A_i and orthogonal to the plane $B_j \vee B_k \vee B_l$ intersect in a point O_A. The plane $A_i \vee A_j \vee O_A$ contains two lines orthogonal to the line $B_k \vee B_l$, $(i,j,k,l) \in \mathscr{I}_4$. Therefore, all lines in this plane, in particular $A_i \vee A_j$, are orthogonal to $B_k \vee B_l$.

Assume conversely that the orthogonality conditions (5) hold. Clearly, any two perpendiculars a_i intersect. We have to show that all intersection points $A_{ij} = a_i \cap a_j$ coincide. Using our freedom to translate the tetrahedron $\mathbf{A}$ without destroying orthogonality relations we can ensure, without loss of generality, the existence of the intersection points

$$\begin{aligned} V_{12} &:= (A_1 \vee A_2) \cap (B_3 \vee B_4), \\ V_{13} &:= (A_1 \vee A_3) \cap (B_2 \vee B_4), \\ V_{23} &:= (A_2 \vee A_3) \cap (B_1 \vee B_4). \end{aligned} \tag{6}$$

Consider now the orthographic projection onto the plane $A_1 \vee A_2 \vee A_3$ (Figure 1). We denote the projection of a point X by X'. By the Right-Angle Theorem of descriptive geometry,[1] the points B_1', B_2' and B_3' lie on the perpendiculars through B_4' onto the sides of the triangle $\mathbf{A} = A_1A_2A_3$. Moreover, since the plane $V_{12} \vee V_{13} \vee V_{23}$ appears in true size, the lines a_i through A_i and orthogonal to the respective face planes of $\mathbf{A}$ have projections a_1', a_2', a_3' orthogonal to the edges of the triangle $\mathbf{V} = V_{23}V_{13}V_{12}$. The triangles $\mathbf{V}$ and $\mathbf{A}$ are orthologic. Therefore the lines a_i' intersect in a point O_A' which is necessarily the projection of a common point O_A of the lines a_1, a_2, and a_3. □

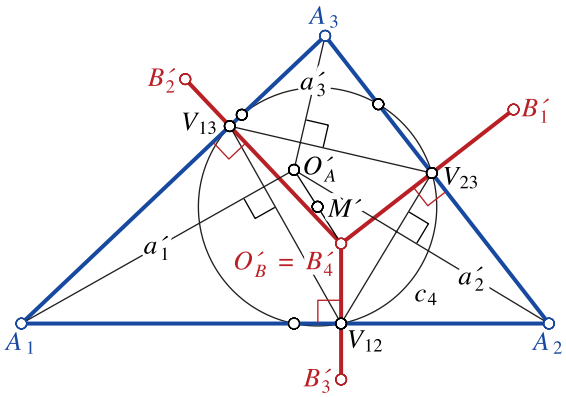

Figure 1: *Orthographic projection onto a face plane*

3 The six intersection points

The new results in this paper concern pairs of orthologic tetrahedra $\mathbf{A} = A_1A_2A_3A_4$ and $\mathbf{B} = B_1B_2B_3B_4$ such that non-corresponding edges are not only orthogonal but also intersecting. That is, in addition to (5) we also require existence of the points

$$V_{ij} := (A_i \vee A_j) \cap (B_k \vee B_l) \neq \varnothing, \quad (i,j,k,l) \in \mathscr{I}_4. \tag{7}$$

Definition 1 *We call two tetrahedra* $\mathbf{A}$ *and* $\mathbf{B}$ orthosecting *if their vertices can be labelled as* $A_1A_2A_3A_4$ *and* $B_1B_2B_3B_4$*, respectively, such that* (5) *and* (7) *hold.*

Theorem 1 *If two tetrahedra are orthosecting, the six intersection points of non-corresponding edges lie on a sphere (or a plane, if flat tetrahedra are permitted). The sphere center is the midpoint between the orthology centers.*

[1] In an orthographic projection the right angle between two lines appears as right angle if and only if one line is in true size (parallel to the image plane) and the other is not in a point-view (orthogonal to the image plane).

Proof. Denote the two tetrahedra by $\mathbf{A} = A_1A_2A_3A_4$ and $\mathbf{B} = B_1B_2B_3B_4$ such that the lines $A_i \vee A_j$ and $B_k \vee B_l$ intersect orthogonally in V_{ij} for $(i,j,k,l) \in \mathscr{I}_4$. As in the proof of Proposition 1 we consider the orthographic projection onto the plane $A_1 \vee A_2 \vee A_3$ (Figure 1). Clearly, B_4' equals the projection O_B' of the orthology center O_B of $\mathbf{B}$ with respect to $\mathbf{A}$. If it lies on the circumcircle of $A_1A_2A_3$, all perpendiculars from B_4' onto the sides of $A_1A_2A_3$ are parallel. In this case the tetrahedron $B_1B_2B_3B_4$ is flat and the theorem's statement holds. Otherwise, the points V_{12}, V_{13}, and V_{23} define a circle c_4 — the pedal circle of the point B_4' with respect to the triangle $A_1A_2A_3$. By the Right-Angle Theorem the projection O_A' of the orthology center O_A of $\mathbf{A}$ with respect to $\mathbf{B}$ is the orthology center of the triangle $A_1A_2A_3$ with respect to the triangle $V_{23}V_{13}V_{12}$. Moreover, from elementary triangle geometry it is known that the center M' of c_4 halves the segment between B_4' and O_A' [4, pp. 54–56]. Hence all circles c_i drawn in like manner on the faces of $\mathbf{A}$ have axes which intersect in the midpoint M of the two orthology centers O_A and O_B. Moreover, any two of these circles share one of the points V_{ij}. Hence, these circles are co-spherical and the proof is finished. □

The proof of Theorem 1 can also be applied to a slightly more general configuration where only five of the six edges intersect orthogonally. We formulate this statement as a corollary:

Corollary 1 *If $\mathbf{A} = A_1A_2A_3A_4$ and $\mathbf{B} = B_1B_2B_3B_4$ are two orthologic tetrahedra such that five non-corresponding edges intersect, the five intersection points lie on a sphere (or a plane).*

4 The one-parametric family of solution tetrahedra

So far we have dealt with properties of a pair of orthosecting tetrahedra but we have left aside questions of existence or computation. In this section $\mathbf{A} = A_1A_2A_3A_4$ is a given tetrahedron to which an orthosecting tetrahedron $\mathbf{B} = B_1B_2B_3B_4$ is sought.

4.1 Construction of orthologic tetrahedra

At first, we consider the simpler case of orthologic pairs. Clearly, translation of the face planes of $\mathbf{B}$ will transform an orthologic tetrahedron into a like tetrahedron (unless all planes pass through a single point). Therefore, we consider tetrahedra with parallel faces as equivalent.

The maybe simplest construction of an equivalence class of solutions consists of the choice of the orthology center O_A. This immediately yields the face normals $\mathbf{n}_i$ of $\mathbf{B}$ as connecting vectors of O_A and A_i. The variety of solution classes is of dimension three, one solution to every choice of O_A. Since five edges determine two face planes of a tetrahedron and, in case of suitable orthogonality relations, also the orthology center O_A, we obtain

Theorem 2 *If the vertices of two tetrahedra can be labelled such that five non-corresponding pairs of edges are orthogonal then so is the sixth.*

The variety of all solution classes contains a two-parametric set of trivial solutions $\mathbf{n}_1 = \mathbf{n}_2 = \mathbf{n}_3 = \mathbf{n}_4$. They correspond to orthology centers at infinity, the solution tetrahedra are flat. Note that the possibility to label the edges such that non-corresponding pairs are orthogonal is essential for the existence of non-flat solutions. If, for example, corresponding edges are required to be orthogonal only flat solutions exist.

4.2 Conjugate pairs of orthosecting tetrahedra

Establishing algebraic equations for solution tetrahedra is straightforward. Six orthogonality conditions and six intersection condition result in a system of six linear and six quadratic equations in the twelve unknown coordinates of the vertices of $\mathbf{B}$. Because of Theorem 2, only five of the six linear orthogonality conditions are independent. Therefore, we can expect a one-dimensional variety of solution tetrahedra. This expectation is generically true, as can be confirmed by computing the dimension of the ideal spanned by the orthosecting conditions by means of a computer algebra system.

The numeric solution of the system induced by the orthosecting conditions poses no problems. We used the software Bertini,[2] for that purpose. Symbolic approaches are feasible as well. One of them will be described in Subsection 4.3. It is based on a curious conjugacy which can be defined in the set of all tetrahedra that orthosect the given tetrahedron $\mathbf{A}$.

Assume that $\mathbf{B} = B_1B_2B_3B_4$ is a solution tetrahedron and denote the orthographic projection of B_i onto the face plane $A_j \vee A_k \vee A_l$ by $B_i^\star$, $(i,j,k,l) \in \mathscr{I}_4$. By the Right-Angle theorem the pedal points of all points $B_i^\star$ on the edges of $A_jA_kA_l$ are precisely the intersection points defined in (7). Three intersection points on the same face of $\mathbf{A}$ form a pedal triangle. This observation gives rise to:

[2] D. J. Bates, J. D. Hauenstein, A. J. Sommese, Ch. W. Wampler: Bertini: Software for Numerical Algebraic Geometry, `http://www.nd.edu/ sommese/bertini/`.

Definition 2 *A pedal chain on a tetrahedron is a set of four pedal triangles, each with respect to one face triangle of the tetrahedron, such that any two pedal triangles share the vertex on the common edge of their faces (Figure 2). If all vertices of pedal triangles lie on a sphere (or a plane), we speak of a spherical pedal chain.*

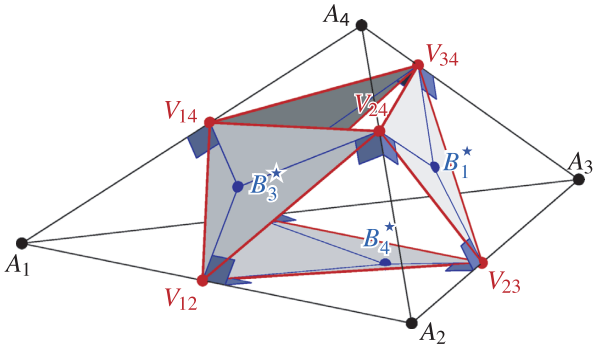

Figure 2: *A pedal chain*

If $A_1A_2A_3A_4$ and $B_1B_2B_3B_4$ are orthosecting, the proof of Theorem 1 shows that six intersection points are the vertices of a spherical pedal chain. The converse is also true:

Theorem 3 *Given the vertices V_{ij} of a spherical pedal chain on a tetrahedron $\mathbf{A} = A_1A_2A_3A_4$ there exists a unique orthosecting tetrahedron $\mathbf{B} = B_1B_2B_3B_4$ such that $A_i \vee A_j \cap B_k \vee B_l = V_{ij}$ for all $(i,j,k,l) \in \mathscr{I}_4$.*

Proof. If a solution tetrahedron **B** exists at all it must be unique since its faces lie in the planes $\beta_i := V_{ij} \vee V_{ik} \vee V_{il}$ (i, j, $k \in \{1,2,3,4\}$ pairwise different).[3]

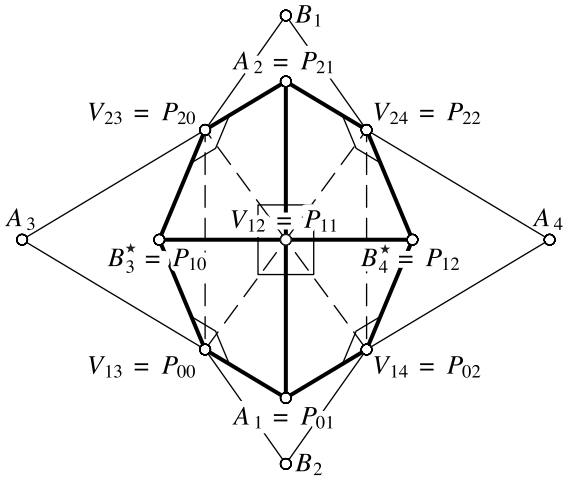

Figure 3: *Proof of Theorem 3*

In order to prove existence, we have to show that the lines $A_i \vee A_j$ and $\beta_i \cap \beta_j$ are, indeed, orthogonal for all pairwise different i, $j \in \{1,2,3,4\}$. We denote the point from which the pedal triangle on the face $A_iA_jA_k$ originates (the "anti-pedal point") by $B_l^\star$ and show orthogonality between $A_1 \vee A_2$ and $\beta_1 \cap \beta_2$ for $(i,j,k,l) \in \mathscr{I}_4$. Relabelling according to

$$\begin{aligned} P_{00} &:= V_{13}, & P_{01} &:= A_1, & P_{02} &:= V_{14}, \\ P_{10} &:= B_4^\star, & P_{11} &:= V_{12}, & P_{12} &:= B_3^\star, \\ P_{20} &:= V_{23}, & P_{21} &:= A_2, & P_{22} &:= V_{24} \end{aligned} \tag{8}$$

(Figure 3) we obtain a net of points P_{ij}. In every elementary quadrilateral the angle measure at two opposite vertices equals $\pi/2$. Thus, the net is *circular*. Such structures are extensively studied in the context of discrete differential geometry [2]. Our case is rather special since two pairs of quadrilaterals span the same plane. This does, however, not hinder application of [2, Theorem 4.21] which states that our assumptions on the co-spherical (or co-planar) position of the points P_{00}, P_{02}, P_{11}, P_{20}, and P_{22} is equivalent to the fact that the net P_{ij} is a *discrete isothermic net*. These nets have many remarkable characterizing properties. One of them, stated in [2, Theorem 2.27], says that the planes $P_{00} \vee P_{11} \vee P_{02}$, $P_{10} \vee P_{11} \vee P_{12}$, and $P_{20} \vee P_{11} \vee P_{22}$ have a line in common. In our original notation this means that the line $\beta_1 \cap \beta_2$ intersects the face normal of $A_1 \vee A_2 \vee A_3$ through $B_4^\star$ and the face normal of $A_1 \vee A_2 \vee A_4$ through $B_3^\star$. Therefore, it is orthogonal to $A_1 \vee A_2$. □

As a consequence of Theorem 3 it can be shown that tetrahedra which orthosect **A** come in conjugate pairs: Given **A** and an orthosecting tetrahedron **B** it is possible to construct a second orthosecting tetrahedron **C**. The same construction with **C** as input yields the tetrahedron **B**. This conjugacy is related to the pedal chain originating from **B**. The key ingredient is the following result from elementary triangle geometry [4, pp. 54–56]:

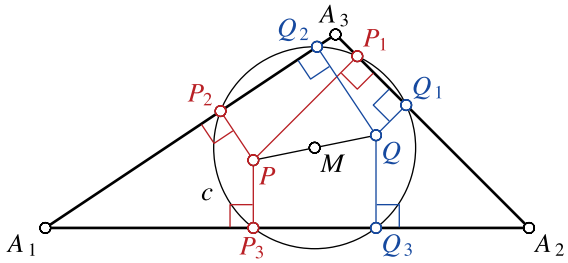

Figure 4: *Pedal circles in a triangle*

Proposition 2 *If P is a point in the plane of the triangle $A_1A_2A_3$ and c its pedal circle, the reflection Q of P in the center M of c has the same pedal circle c (Figure 4).*

[3] The case of collinear or coinciding points V_{ij} leads to degenerate solution tetrahedra whose faces contain one vertex of **A**.

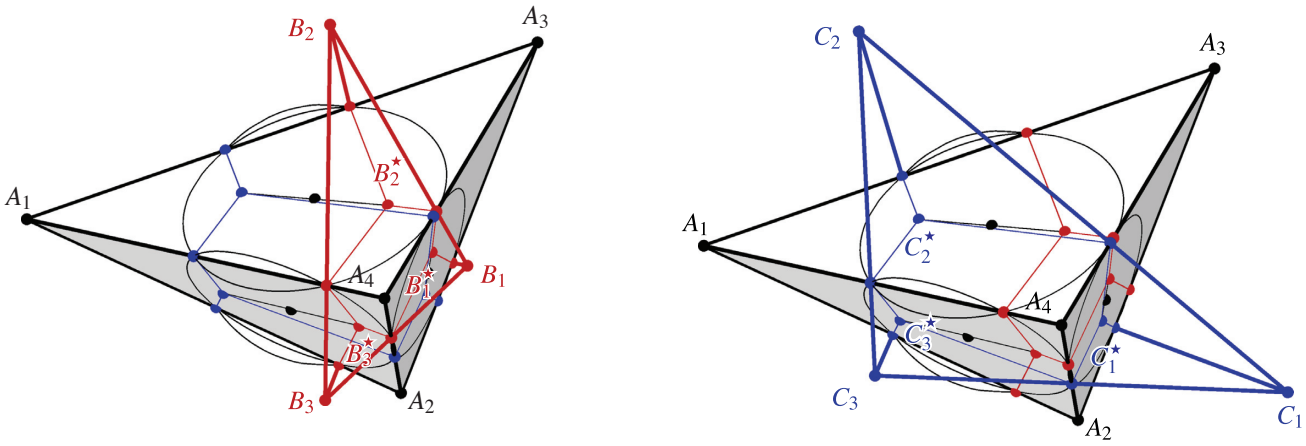

Figure 5: *A conjugate pair* **B**, **C** *of orthosecting tetrahedra.*

Suppose that **A** and **B** are orthosecting tetrahedra. The orthographic projections $B_i^\star$ of the vertices of **B** onto corresponding face planes of **A** are points whose pedal triangles form a spherical pedal chain. By reflecting $B_i^\star$ in the centers of the pedal circles on the faces of **A** we obtain points $C_i^\star$ which, according to Proposition 2, give rise to a second spherical pedal chain (with the same sphere of vertices) and, by Theorem 3, can be used to construct a second orthosecting tetrahedron **C** (Figure 5).

The points P and Q of Proposition 2 are called *isogonal conjugates* with respect to the triangle $A_1A_2A_3$. The above considerations lead immediately to

Theorem 4 *Given a tetrahedron* $\mathbf{A} = A_1A_2A_3A_4$*, the orthographic projection of all vertices* $B_i^\star$ *of orthosecting tetrahedra onto the face plane* $A_j \vee A_k \vee A_l$ *of* **A** *(with* $(i,j,k,l) \in \mathscr{I}_4$*) is a curve which is isogonally self-conjugate with respect to the triangle* $A_jA_kA_l$*.*

4.3 Computational issues

We continue with a few remarks on the actual computation of the isogonal self-conjugate curves of Theorem 4 with the help of a computer algebra system. Our first result concerns the construction of pedal chains.

Theorem 5 *Consider a tetrahedron* $\mathbf{A} = A_1A_2A_3A_4$ *and six points* $V_{ij} \in A_i \vee A_j$*,* $(i,j,k,l) \in \mathscr{I}_4$*. If three of the four triangles* $V_{ij}V_{jk}V_{ki}$*, with* $(i,j,k) \in \mathscr{I}_3$*, are pedal triangles with respect to the triangle* $A_iA_jA_k$ *then this is also true for the fourth.*

Proof. Assume that the triangles $V_{12}V_{24}V_{14}$, $V_{23}V_{24}V_{34}$, and $V_{13}V_{34}V_{14}$ are pedal triangles of their respective face triangles. We have to show that $V_{12}V_{23}V_{13}$ is a pedal triangle of $A_1A_2A_3$. As usual, the anti-pedal points are denoted by $B_1^\star$, $B_2^\star$, and $B_3^\star$. Clearly, we have $B_i^\star \vee B_j^\star \perp A_k \vee A_4$ for $(i,j,k,4) \in \mathscr{I}_4$. Denote by B_4° a point in the intersection of the three planes incident with V_{ij} and perpendicular to $A_i \vee A_j$, $(i,j,k) \in \mathscr{I}_3$. By Proposition 1 the tetrahedra **A** and $B_1^\star B_2^\star B_3^\star B_4^\circ$ are orthologic. Therefore, the face normals n_l of $A_i \vee A_j \vee A_k$ through $B_l^\star$ have a point B_4 in common ($l \neq 4$, $(i,j,k,l) \in \mathscr{I}_4$). By the Right-Angle Theorem, the intersection point $B_4^\star$ of the orthographic projections of n_1, n_2, and n_3 onto $A_1 \vee A_2 \vee A_3$ has $V_{12}V_{23}V_{13}$ as its pedal triangle. □

In order to construct a pedal chain on a tetrahedron $\mathbf{A} = A_1A_2A_3A_4$ on can proceed as follows:

1. Prescribe an arbitrary pedal triangle, say $V_{12}V_{23}V_{13}$.
2. Choose one anti-pedal point, say $B_3^\star$, on a neighbouring face. It is restricted to the perpendicular to $A_1 \vee A_2$ trough V_{12}.
3. The remaining pedal points are determined. Theorem 5 guarantees that the final completion of V_{34} is possible without contradiction.

In order to construct a spherical pedal chain, the choice of $B_4^\star$ and $B_3^\star$ needs to be appropriate. A simple computation shows that there exist two possible choices (in algebraic sense) for $B_3^\star$ such that the points V_{12}, V_{13}, V_{23}, V_{14}, and V_{24} are co-spherical (or co-planar). Demanding that the remaining vertex V_{34} lies on the same sphere yields

an algebraic condition on the coordinates of $B_4^\star$ — the algebraic equation of the isogonally self-conjugate curve i_4 from Theorem 4. We are currently not able to carry out the last elimination step in full generality. Examples suggest, however, that i_4 is of degree nine. Once a point on i_4 is determined, the computation of the corresponding orthosecting tetrahedron is trivial.

5 Conclusion and future research

We introduced the concept of orthosecting tetrahedra and presented a few results related to them. In particular we characterized the six intersection points as vertices of a spherical pedal chain on either tetrahedron. This characterization allows the construction of conjugate orthosecting tetrahedra to a given tetrahedron **A**.

In general, there exists a one-parametric family of tetrahedra which orthosect **A**. The orthographic projection of their vertices on the plane of a face triangle of **A** is an isogonally self-conjugate algebraic curve. Maybe it is worth to study other loci related to the one-parametric family of orthosecting tetrahedra. Since every sphere that carries vertices of one pedal chain also carries the vertices of a second pedal chain, the locus of their centers might have a reasonable low algebraic degree.

Moreover, other curious properties of orthosecting tetrahedra seem likely to be discovered. For example, the repeated construction of conjugate orthosecting tetrahedra yields an infinite sequence $\langle \mathbf{B}_n \rangle_{n\in\mathbb{Z}}$ of tetrahedra such that $\mathbf{B}_{n-1}$ and $\mathbf{B}_{n+1}$ form a conjugate orthosecting pair with respect to $\mathbf{B}_n$ for every $n \in \mathbb{Z}$. All intersection points of non-corresponding edges lie on the same sphere and only two points serve as orthology centers for any orthosecting pair $\mathbf{B}_n$, $\mathbf{B}_{n+1}$. General properties and special cases of this sequence might be a worthy field of further study.

Finally, we would like to mention two possible extensions of this article's topic. It seems that, with exception of Steiner's result on orthologic triangles on the sphere, little is known on orthologic triangles and tetrahedra in non-Euclidean spaces. Moreover, one might consider a relaxed "orthology property" as suggested by the anonymous reviewer: It requires that the four lines a_1, a_2, a_3, a_4 defined in (3) lie in a regulus (and not necessarily in a linear pencil). This concept is only useful if the regulus position of the lines a_i also implies regulus position of the lines b_j of (4). We have some numerical evidence that this is, indeed, the case.

References

[1] N. ALTSHILLER-COURT, *Modern Pure Solid Geometry*, Chelsea Publishing Company, New York, 2 edition, 1964.

[2] A. I. BOBENKO, Y. B. SURIS, *Discrete Differential Geometrie. Integrable Structure*, volume 98 of *Graduate texts in mathematics*. American Mathematical Society, 2008.

[3] R. GOORMAGHTIGH, A generalization of the orthopole theorem. *Amer. Math. Monthly* **36**(**8**) (1929), 422–424.

[4] R. HONSBERGER, *More Mathematical Morsels*. Math. Assoc. Amer., Washington, DC, 1991.

[5] S. R. MANDAN, Orthologic Desargues' figure. *J. Austral. Math. Soc. Ser. A* **28** (1979), 295–302.

[6] S. R. MANDAN, Special pairs of semi-bilogic and bilogic tetrahedra. *J. Austral. Math. Soc. Ser. A* **28** (1979), 303–308.

[7] J. NEUBERG, *Mémoire sur le tétraèdre*. F. Hayez, Bruxelles, 1884.

[8] J. NEUBERG, Über orthologische Tetraeder. *Monatsh. Math.* **18**(**1**) (1907), 212–218.

[9] C. SERVAIS, Un group de trois tétraèdres. *Acad. Roy. Belg. Bull. Cl. Sci. (5)* **5**(**9**) (1923), 49–54.

[10] J. STEINER, Vorgelegte Lehrsätze. *Crelle's Journal* II (1827), 287–292.

[11] V. THEBAULT, Perspective and orthologic triangles and tetrahedrons. *Amer. Math. Monthly* **59**(**1**) (1952), 24–28.

Hans-Peter Schröcker
University of Innsbruck
Technikerstraße 13, A6020 Innsbruck, Austria
e-mail: hans-peter.schroecker@uibk.ac.at

Original scientific paper
Accepted 20. 12. 2009.

GEORG GLAESER
KARLHEINZ SCHOTT

Geometric Considerations About Seemingly Wrong Tilt of Crescent Moon

Geometric Considerations About Seemingly Wrong Tilt of Crescent Moon

ABSTRACT

The following phenomenon is well-known and again and again appears as an unanswered question in literature and on internet platforms: If you see moon and sun in the sky at the same time, then the (bisector of the) crescent moon in most cases does not seem to be precisely directed at the sun. Particularly at sunset, when you would expect the bisector of the crescent moon to be horizontal, it mostly points upwards. To "prove" that, photos that seem to support this view are displayed. In this paper it is shown by means of geometry what the "wrong moon tilt" is all about and that an explanation is to be found in the nature of central or normal projections (photography is basically a central projection, at an extremely long focal length it is approximately a normal projection). The paper also deals with the reason why the seemingly wrong tilt is subjectively felt. The path of the light from the sun to the moon is in any case displayed straight (apart from minor deviations due to refraction close to the horizon), except one takes photos with a fish-eye lens.

Key words: Moon tilt, Terminator, Normal Projection

MSC 2010: 51N05, 51P05, 51M04

Geometrijska razmatranja o naizgled krivom nagibu polumjeseca

SAŽETAK

Sljedeći je fenomen dobro poznat i često se u literaturi i na internetu pojavljuje kao pitanje bez odgovora: Ako na nebu istovremeno vidite mjesec i sunce, onda simetrala polumjeseca u većini slučajeva ne izgleda usmjerena točno prema suncu. Posebno u doba sunčeva zalaska, kad očekujete da simetrala polumjeseca bude horizontalna, ona je uglavnom usmjerena prema gore. Da bismo to "dokazali" prikazujemo fotografije koje podržavaju takav pogled. U ovom se članku posredstvom geometrije objašnjava pojava "krivog nagiba mjeseca", a rješenje se nalazi u prirodi centralnog ili ortogonalnog projiciranja (naime, fotografija je temeljno centralna projekcija, ali kod izuzetno velike žarišne duljine približno je ortogonalna projekcija). U članku se također razmatra razlog zašto se naizgled krivi nagib subjektivno osjeća. Svjetlosna putanja od sunca do mjeseca u svakom se slučaju prikazuje ravno (osim kod malih odstupanja koja se javljaju zbog loma svjetlosti u blizini horizonta), i osim kod fotografija slikanih sa širokokutnim objektivom.

Ključne riječi: nagib mjeseca, ograničenje, ortogonalna projekcija

1 Introduction, Motivation

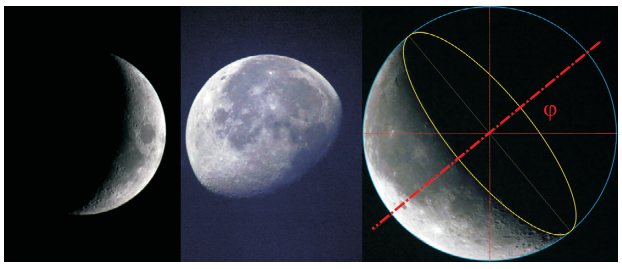

Figure 1: *Three different close-ups of the crescent moon. The outer edge appears circular, the border of the shadow (the picture of the terminator) elliptical.*

The crescent moon is composed (with an approximately equal share) of the outline of the part illuminated by the sun and the picture of the bordering line between shadow and illuminated area (in astronomy also called terminator [9]) (Fig. 1 left). In this paper we will (for the sake of simplicity) also call the more than half full moon as "crescent moon", even though the crescent is only noticeable when the moon is less than half full (in this case either the illuminated or the dark part form a crescent, see Fig. 1 middle). Roughly speaking, it is a geometrical figure, whose outline (at normal or central projection, when the center of the moon is aimed at) is approximately made out of a half circle or half ellipse (mountain ranges on the moon do not play a vital role with regard to the outline, regarding the bordering line between shadow and illuminated area they lead – due to the flatly incoming light – to noticeable deviations). This is why the following applies:

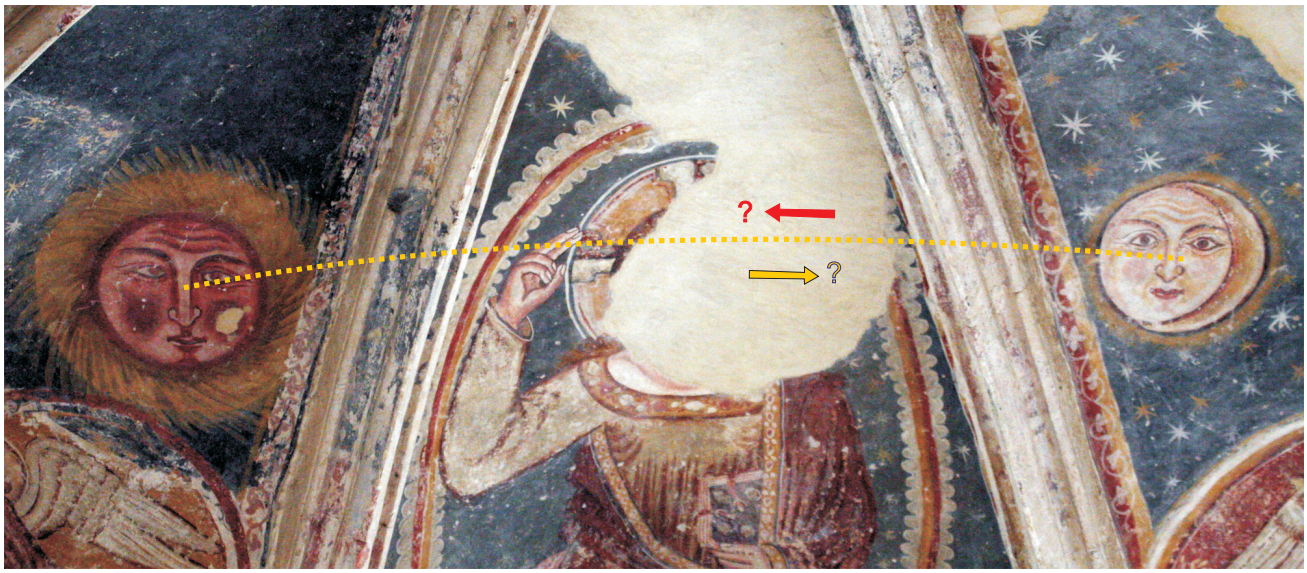

Figure 2: *Tele-photo of a fresco from the 14th century (St. Lawrence's church, Požega, Croatia). The yellow dashed line and the arrows were added.*

Lemma: *When having a normal or central projection with the center of the moon on the principal projection ray, the minor axis of the picture ellipse of the terminator of the moon is the line of symmetry of the moon crescent. As we intuitively focus on the center of the moon when looking at it with the naked eye, we always see the crescent symmetrical with regard to this axis.*

So it makes sense to take the minor axis of the ellipse in order to be able to fix with it or to measure the tilt of the crescent moon (Fig. 1 right).

Probably everyone who gazes in admiration at the waxing moon in the afternoon or at sunset or at the waning moon at sunrise, at one time asks himself whether this bisector when extended runs through the sun point.

Let us have a closer look at Fig. 2, where sun and moon are displayed next to each other. Apart from the fact that strictly speaking a waning and not a waxing moon should have been painted, this over 600-year-old painting is outstanding in various respects: First the outline of moon and sun are not exactly circular but actually elliptical (in particular the outline of the moon), secondly the moon crescent is not exactly symmetrical and thirdly the illumination caused by the sun does not seem to come from one side. The crescent is – as often described – slightly tilted. Additionally one could add that the painting is produced on an approximately spherical ceiling so that the distortion in the original is even stronger than it seems on the photo. In the course of this paper we will show that all these phenomena are surprisingly linked to the "wrong tilt" of the moon crescent[1].

2 Photographs on which sun and moon are shown at the same time

Sun and moon have both a diameter of half a degree on the firmament.This is an optical angle that can be completely captured by our eyes – the "external branch" of our brain – without moving the eye apple. In order to be able to photograph sun and moon in a way that they both fill the picture, one needs a focal length of about 2000 mm. The angular distance sun - moon is now always at least several degrees (otherwise there is new moon or the crescent of the moon is so thin that it cannot be seen with the naked eye). At half moon the deviation is 90°, which already requires a distinct wide-angle lens (20 mm focal length). Until the full moon is reached the angle increases up to 180°, so that both sun and moon can only be photographed at the same time with special fish eye lenses that are definitely not linear.

The in geometry common perspective projection is a central projection of the space onto a plane. The same process is relevant for photography, where the projection center is the center of the lens system and the projection plane is the light sensitive sensor plane. The central projection is linear, which means straight lines – for example light rays – are portrayed straight. This also applies to wide-angle photography in good approximation (The quality of wide-angle lenses is often determined by this criterion).

[1]Let us mention in passing: The face of the moon seems to be rather female, the face of the sun rather male. That is for someone who is a native speaker of English or Romance language obvious. In Germanic languages, however, the moon is male and the sun female.

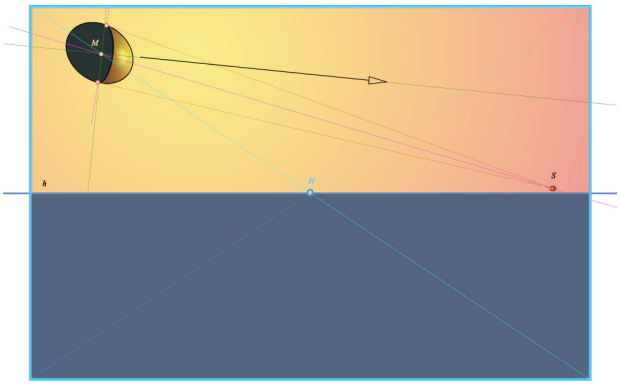

Figure 3: *"Photograph" showing sun and moon, simulated by means of the computer, so that the moon diameter could be enlarged. Two ellipses form the boundary of the moon crescent. The minor axis of the picture ellipse of the terminator (black with arrow) is directed above the sun point. The blue frame symbolizes the sensor plane.*

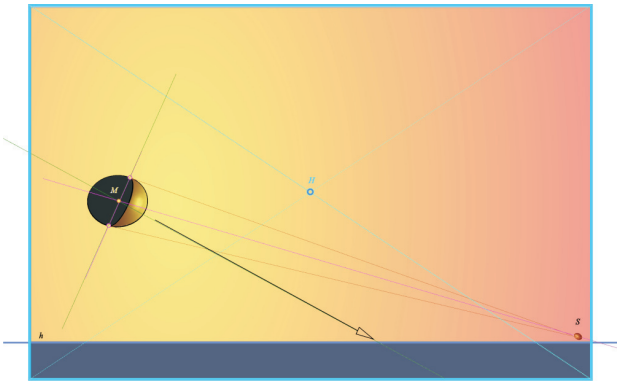

Figure 4: *Another "photo" of the same situation, this time with a different camera tilt. The minor axis of the picture of the terminator is now directed below the sun point.*

The outline of a sphere that fully lies in front of the observer is – under the condition of such a projection – generally an ellipse whose main axis runs through the main point H (the intersection of the optical axis with the sensor plane, hence planimetrically speaking the intersection of the diagonals of the chips) (Fig. 3 and 4, [8],[1]).

A general circle in front of the observer (in our case the terminator) is displayed as an ellipse whose axes in general do not go through the main point. There is just the following exception: If the axis of the circle (the perpendicular of the circular plane in the circle's center point) hits the principal ray (the optical axis), the minor axis of the picture ellipse runs through H ([3]) for reasons of symmetry. As the axis of the terminator is the direction of the light rays, the following applies

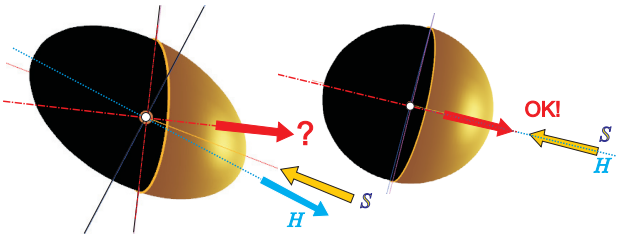

Figure 5: *If you want to enlarge details taken from a wide-angle photo even more, it becomes even more obvious: The two ellipses (the outline of the sphere and the picture of the terminator) generally have no common axis of symmetry. If the picture of the connecting straight line to the sun runs through the main point H of the picture, the crescent is however symmetrical and is directed at the sun indeed.*

Theorem 1: *In a photograph where not the center of the moon is focused at, the moon crescent has an elliptical boundary on both sides and is in general not symmetrical. Only if the light ray goes through the center point of the moon in the picture through the main point H (the center point of the sensor), both ellipses have a common line of symmetry (the minor axis of the terminator and the main axis of the outline ellipse). The direction of the minor axis of the picture of the terminator therefore is not directed at the sun point in general. If H lies below the connecting line of moon point and sun point, the minor axis is directed above the sun point; is H above, the minor axis is directed below the sun point.*

As clear as this theorem seems to be in geometry: On the wide-angle photo of the moon it can hardly be noticed that we are dealing with a double elliptical crescent, because the crescent appears naturally so small that this circumstance does not become obvious in the photo.

If one photographs sun and moon simultaneously with a wide angle lens, one should consider that the connecting straight line between sun point and moon point runs through the center of the picture, for example by positioning the moon point in one corner and the sun point in the opposite corner (Fig. 6).

If one photographs under the condition of a bigger distance between sun and moon point with a fish eye lens (Fig. 7), we get a distortion of straight lines: fish eye lenses are not linear and in general increase the above mentioned deviations upwards or downwards. Yet, due to rotation symmetry of the lenses around the optical axis, straight lines, which meet the optical axis, are portrayed as straight radial rays. Circles are portrayed oval but not elliptical. Therefore the following applies:

Figure 6: *Photo with 20 mm focal length (optical angle about 90°). Despite extremely high resolution (22 megapixel) the moon (top, right) also appears blurred in the magnification (framed white) due to the small size in the picture, but obviously elliptically distorted.*

Theorem 2: *If taking photos with a fish eye lens and if it is not explicitly the moon center focused at, the moon crescent appears as being framed by not elliptical ovals on both sides. The crescent is only then symmetrical and aims at the sun point if the connecting line between sun point and moon point is a radial ray through the middle of the picture.*

In Fig. 7 sun and moon were photographed in a way that sun point and moon point are approximately on a picture diagonal. The (natural not visible) sun ray through the moon center is colored red and is also displayed straight in the fish eye picture. The crescent that is limited by two ovals has the red line as a line of symmetry. (Note: In the picture also the vapor trail of a plane is visible. This vapor plane is displayed – in contrast to the horizon – almost straight, because it is approximately radial.)

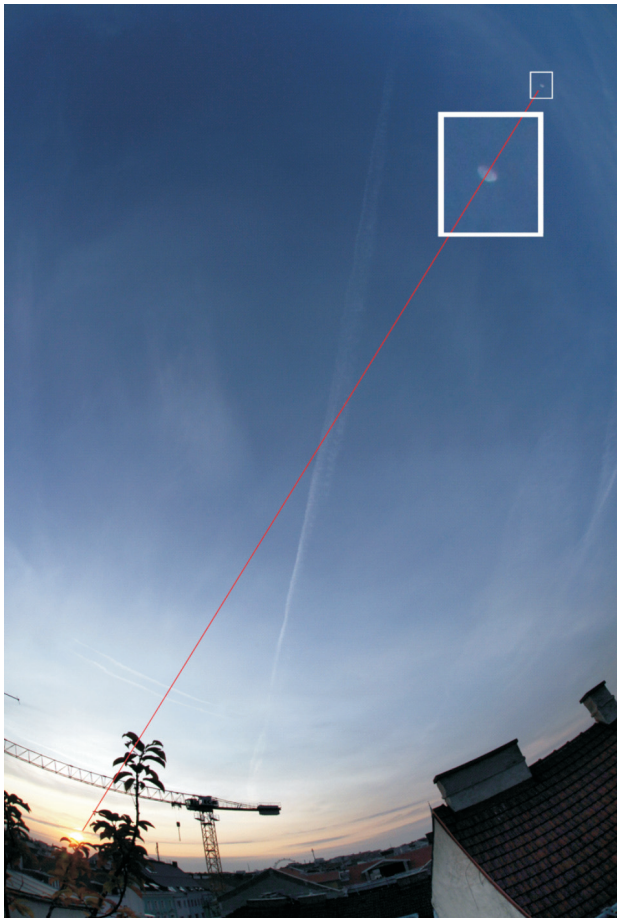

Figure 7: *Similar situation, but a few days later when the angle distance between sun and moon point has extremely increased. That is why a fish eye lens (15mm) had to be used.*

3 Close-up of the moon and the seemingly wrong tilt of the crescent

We now deal with close-ups of the moon, which can only be produced by means of an efficient telephoto lens. Here the moon center is automatically moved into the center of the picture. The respective representation is an extreme magnification of the center of an ordinary perspective and in good approximation a normal projection. The outline of the moon sphere is circular, the terminator elliptical. The center of this ellipse is the projection of the moon center. The vertices of the image ellipse lie diametral on the sphere's outline: The connecting line of these points in space has "principal position", hence is parallel to the sensor plane. The minor axis is orthogonal to the connection of the two vertices (Fig.1 right) and according to the theorem of the right angle normal projection of the circle axis ([7], [2], [17]). Hence, the following applies:

Theorem 3: *When dealing with close-ups of the moon, we almost have a normal projection. The minor axis of the picture ellipse of the terminator is the normal projection of the light ray through the moon center. The points of intersection of the circum-circle and the terminator (the end points of the crescent) are the vertices in the picture.*

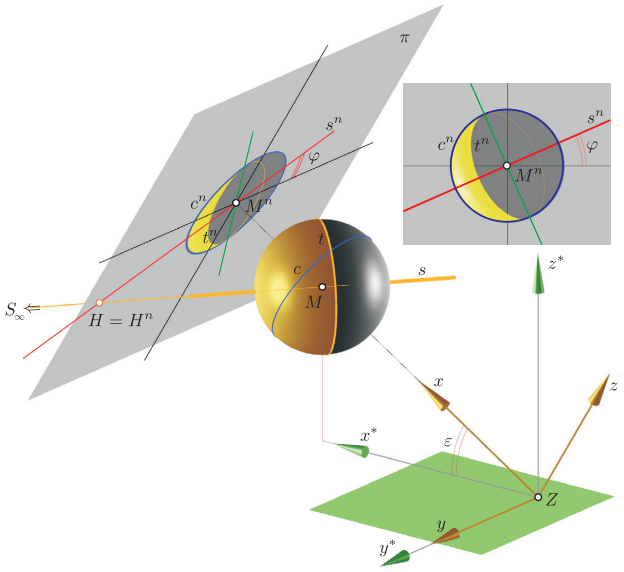

Figure 8: *Normal projection of the moon onto the sensor plane π. The sun rays direction s turns into direction s^n, the outline c of the moon turns into the circle c^n, the terminator t into the crescent edge t^n. s^n is the minor axis of the ellipse t^n.*

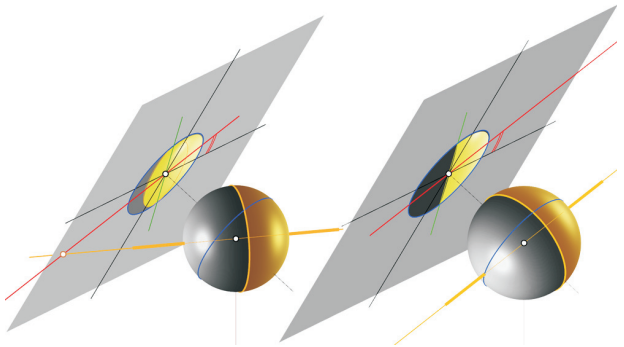

Figure 9: *The same crescent tilt φ as in Fig. 8, yet at 3/4-moon or half moon (sun rays parallel to the picture plane π).*

If you photograph the moon in a way that the lower part or frame of the camera (and hence the border of the rectangular sensor) is horizontal, then one can measure the rotation angle of the picture ellipse well. According to Theorem 3 this angle can practically have any size between -90° and +90° and can only be determined when the length of the minor axis (half minor axis b), hence indirectly the "thickness" of the crescent, is taken into consideration as well:

Theorem 4: *Only the simultaneous interpretation of direction and length of the minor axis of the picture ellipse of the terminator makes it possible to reconstruct the light rays in space.*

For better understanding, some special cases are to be mentioned (here b again defines the length of the half minor axis and r defines the moon radius):

- Having a half moon ($b = 0$) the sun rays are necessarily parallel to the sensor plane (Fig. 9 right). At sunrise or sunset the line of symmetry of the crescent is therefore horizontal, no matter how high the moon is in the sky.
- At new or full moon ($b = r$) the sun rays have the direction of the optical axis (= direction of the projection). The tilt of the circle that has mutated into an ellipse is undefined.
- If one defines the quarter and three quarter moon a week after full moon or new moon, then $b = r/\sqrt{2} \approx 0,7r$. One comes from the picture to the direction to the sun by imagining the minor axis as normal projection of an axis tilted by 45° (Fig. 8 or Fig. 9 left).

Now we want to derive a formula for the tilt of the minor axis or "bulbousness" of the ellipse (a comparable formula can also be found in [5]). Imagine the lens center is the origin of a Cartesian coordinate system. For matters of simplicity we define the optical axis as x-axis, the horizontal direction of the sensor plane as y-direction and the line of steepest slope of the sensor plane as z-direction. The direction to the moon is also given through $\vec{m} = (1,0,0)$, the one to the sun is defined by the direction vector $\vec{s} = (s_x, s_y, s_z)$. Its normal projection onto the sensor plane has the components $\vec{s}_n = (0, s_y, s_z)$. We measure the angle φ to the y-axis by scaling / normalizing $\vec{s}_n$ and multiplying by $\vec{y} = (0,1,0)$:

$$\cos\varphi = \vec{s}_n \cdot \vec{y} = s_y / \sqrt{s_y^2 + s_z^2} \qquad (1)$$

Moon and sun coordinates (in horizontal polar coordinates given through their azimuth angles α, α^* or their difference $\delta = \alpha^* - \alpha$ and elevation angle ε and ε^*) may be at disposal (for example by means of relevant software). Let us look at the Cartesian coordinates in a coordinate system which has the same y-axis, whose z-axis is however vertical: There the direction vector to the sun has the components

$$\vec{s}^* = (s_x^*, s_y^*, s_z^*) = (\cos\varepsilon^* \cdot \cos\delta, \cos\varepsilon^* \cdot \sin\delta, \sin\varepsilon^*) \qquad (2)$$

Relative to the coordinate system that is twisted around the elevation angle ε the following applies:

$$\vec{s} = (s_x^* \cos\varepsilon + s_z^* \sin\varepsilon, s_y^*, -s_x^* \sin\varepsilon + s_z^* \cos\varepsilon) \qquad (3)$$

If we again insert (2) in (3), φ can be calculated directly by inserting

$$s_y = \cos\varepsilon^* \sin\delta,\ s_z = -\cos\varepsilon^* \cos\delta \sin\varepsilon + \sin\varepsilon^* \cos\varepsilon \quad (4)$$

in (1). The tilt ψ of the sun rays to the picture plane is equivalent to the complementary angle to the negativ x-axis $-\vec{m}$, determined through

$$\cos\psi = -\vec{s}\cdot\vec{m} = -s_x/\sqrt{s_y^2 + s_z^2} \quad (5)$$

with $s_x = \cos\varepsilon^* \cos\delta \cos\varepsilon + \sin\varepsilon^* \sin\varepsilon$.

This cosine value is also a measure for the thickness of the picture of the terminator.

4 Human perception of the direction of light rays from sun to moon

In order to be able to perceive sun and moon at the same time, human beings have to move their head (or at least roll the eyes balls when keeping the head stiff). After it was proved through various experiments that human beings can only perceive quite small optical angles in one complete picture (and then almost perceives a normal projection), the brain has to do the job of gathering all the individual impressions gained by moving the eye balls. Here only a limited "impression similar to a photo" can be created: One cannot fix together individual photos showing single parts of an object without manipulation[2]. Most likely a spherical picture develops which must be interpreted by the brain by comparing optical angles. Looking at straight lines (without any other straight line as a reference) is in particular at optical angles of over 90° a rather deceitful venture. One cannot even compare the simultaneous observation of sun and moon with observing a vapor trail of an airplane about which one knows that it runs parallel to the base plane (which is rarely the case considering the sun-moon condition, most likely at moonrise and simultaneous sunset but then one cannot notice any tilt of the moon crescent).

If one wants to assess the tilt of the crescent, one automatically and necessarily refers to the picture of the moon, which one gets through direct sighting, and this is – according to the considerations made in Section 3 – tilted like the normal projection of the sun rays.

In the following we want to deal with frequent claims and questions arising in connection with the moon tilt:

1. A simple but didactically helpful animation about the "development" of the moon crescent can be found on [13]. Pictures and animations that are much more demanding and only comprehensible with some previous knowledge can be found on [14].

2. The so-called AUBERT's phenomenon claims that one must turn and instinctively swing the head when trying to perceive larger angle areas. This is sometimes used as the only explanation for the phenomenon of the "wrong tilt" of the moon crescent ([11]). According to what we have heard so far, this is however not true.

3. In [4] it is assumed that the direction of the normal projection of the sun rays is equivalent to the tangent on the great circle in the sky that connects moon M and sun S and that has the observer Z as the center. This is – planimetrically speaking – correct, because the mentioned great circle obviously lies in the optical plane MSZ and appears projective, hence in the picture it cannot be differentiated from the sun ray SM at that moment. Having a normal projection on the picture plane, the optical plane is projective and the great circle always appears as a straight line. One could therefore apply the following trick in order to estimate the tilt of the projection of the terminator: One points with the stretched arm at the moon crescent and turns the arm to the sun in the optical plane. The direction in which the index finger starts indicates the tilt. This trick makes us suppose that the light ray in the sky is crooked, which is, however, not true. As mentioned it can only be compared to the situation *in the beginning*.

   Unfortunately many participants in internet discussions are often "tempted to rely on the crooked line". Didactically speaking, it therefore does not seem useful to introduce the great circle at the beginning of the explanation of this phenomenon: The tilt is only to be determined by the effect of the central and normal projections and by considering various preconditions. Consequently the explanation of the moon tilt given in [16] is not correct as far as it relies on the crooked line, whereas the explanation in [6] is wrong due to the fact that the effect of the perspective is not taken into consideration.

[2] For example for a "panorama photo" stripes that actually come from the picture centers of various photos are usually fixed together. The margins of these stripes must be contracted in order to compensate for the perspectively caused enlargement. After having fixed the stripes together, the picture that is framed by various crooked lines is cut into a rectangle ([2]).

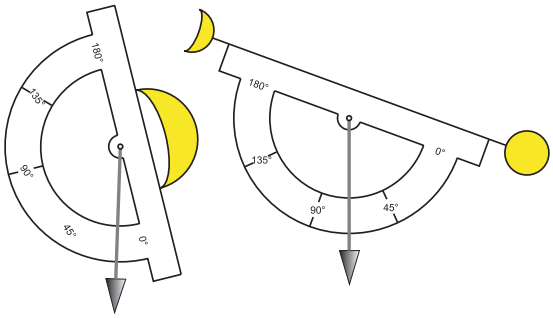

Figure 10: *"True" and "expected" tilt of the moon crescent.*

4. On internet pages people differentiate between "true" and "expected" moon tilt, which is explained by a figure comparable to Fig. 3. There the expected tilt is seen as a projection of the connection moon - sun on a vertical plane which owns – as a normal – the angle bisector of the outlines of moon and sun ([5], [16]). If one agrees on certain requirements (e.g. that the connecting line of sun and moon runs through the center of the picture and both points have the same distance from the margin of the picture; additionally that the picture plane is tilted if the moon is not quite low), this "expected" tilt can be defined mathematically and can be compared with the tilt at normal projection (there called "true tilt") (Fig. 10). The difference of the angles can then be named "supposed mistake".

5. It would be tempting to assume that the line of symmetry of the moon crescent indicates the motion direction of the crescent. This is however at least not the case if the path of the moon is steeper or less steep than the one of the sun.

   Is, for example, as in Fig. 11 (moonset in Vienna on the 25th of October 2009, at about 10pm) the moon path flatter by about 10° than the sun path, then due to the different heights of the paths e.g. at half moon a clear deviation downwards is noticable[3].

   In order to test our Formula (4) and the respective formula in [5] (there "Formel 2") [4], we insert the values $\delta = 83,1°$, $\varepsilon = 2,6°$ and $\varepsilon^* = -47,5°$ and get according to both formulas $\varphi \approx -48°$. This value is determined graphically correct to one degree for the middle position of the moon in Fig. 11.

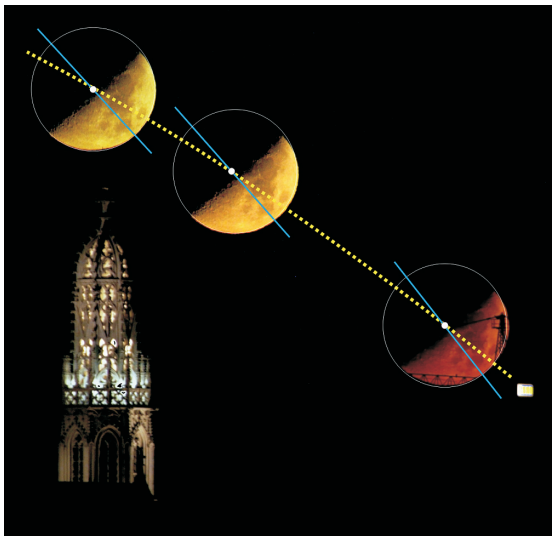

Figure 11: *Set of the waxing half moon. On that day the path of the moon was flatter than the path of the sun. That is why the crescent is directed more downward.*

The fact that the moon does not always culminate at the same elevation angle as the sun can be easily realized with the educational (and simplified) simulation [10]. Here we do not deal with small deviations (as the one of the path planes of the earth or the moon, which is at the most $\pm 5°$), but with enormous differences: The full moon moves in the winter so high as the sun in the summer and the other way round (difference in the elevation angle approximately 47°). At equinox we have a deviation of about $\pm 23,5°$ at half moon, whereas new and full moon culminate approximately as high as the sun.

5 Summary

When having a close-up or when a human being is the observer, the moon crescent appears as a symmetrical object which is restricted by a half circle and a half ellipse with the moon center point as center. The minor axis of the half ellipse shows into the direction of the normal projection of the sun rays on the projection plane – and therefore generally not "to the sun". Only when also considering the length of the minor axis, the position of the sun can be determined. If you photograph sun and moon at the same time with a wide-angle lens, then the moon crescent is in general restricted by two ellipses that have no shared line

[3] In Fig. 11 two peculiarities are worth mentioning: First, the moon – such as the sun – is colored red briefly before reaching the horizon and secondly, the usually circle shaped outline appears flatter. Both are consequences of the refraction of the flatly incoming light into the gradually becoming more dense atmosphere of the earth.

[4] To determine the equatorial coordinates [15] was used, which – by means of [12] – were changed into horizontal coordinates.

of symmetry. That is why we cannot speak of a direction of the moon crescent in case of a wide-angle photograph.

If sun point and moon point are on one straight line through the center of the photo, the moon crescent is symmetrical and the line of symmetry is directed at the sun point. Something similar applies to photographs with fisheye lenses. Theories which want to explain the phenomenon of the "wrong moon tilt" with crooked light rays are incorrect. Exclusively geometrical characteristics of different kinds of projections are involved.

References

[1] HEINRICH BRAUNER, *Lehrbuch der Konstruktiven Geometrie*, Springer Verlag Vienna, 1986

[2] GEORG GLAESER, *Geometrie und ihre Anwendungen in Kunst, Natur und Technik, 2. Auflage*, Spektrum akademischer Verlag Heidelberg, 2007

[3] FRITZ HOHENBERG, *Konstruktive Geometrie in der Technik, 2. Aufl.*, Springer Verlag Vienna, 1961

[4] BERNHARD SCHÖLKOPF, *The moon tilt illusion*, Perception 27(10), 1229-1232 (08 1998)

[5] KARLHEINZ SCHOTT, *Das Phänomen der "falsch" geneigten Mondsichel*, http://falsche-mondneigung.jimdo.com

[6] BURKARD STEINRÜCKEN, *Über gerade und gekrümmte Linien am Himmel - oder: Warum zeigt die Mondsichel nicht genau zur Sonne?*, http://www.sternwarte-recklinghausen.de/files/mondsichel.pdf

[7] WALTER WUNDERLICH, *Darstellende Geometrie I*, B.I. Mannheim, 96,96a, S.49ff. 1967

[8] WALTER WUNDERLICH, *Darstellende Geometrie II*, B.I. Mannheim, 133/133a, S.142ff, 1967

[9] JOHN WOODRUFF UND GOTTFRIED RIEKERT, *Lexikon der Astronomie*, Delius Klasing, 2007. Definition see also http://en.wikipedia.org/wiki/Lunar_terminator

[10] HELMER ASLAKSEN, *A simplified model of the tilt of the waxing or waning Moon in different parts of the world*, http://www.math.nus.edu.sg/aslaksen/applets/eclipticmoon/eclipticmoon.html

[11] *Astronomie: Sonne auf Abwegen*, GEO magazin Nr. 11/06, http://www.geo.de/GEO/natur/kosmos/51729.html

[12] *Caligo – Den Sternen etwas näher*, Umrechnungsprogramm von äquatorialen in horizontale Himmelskoordinaten, http://www.freewebs.com/projektarbeit/

[13] *Educational Software EduMedia*, http://www.edumedia-sciences.com/en/a426-the-crescent-moon

[14] *Educational Software MMSD*, http://planetariumweb.madison.k12.wi.us/mooncal/crescent-tilt/Crescent

[15] *Starry Night*, Astronomisches Simulationsprogramm, http://www.starrynight.com/

[16] STEPHAN MAYER, *Warum zeigt die Neigung der Mondsichel nicht genau zur Sonne?*, http://www.psy-mayer.de/links/Mondneigung.pdf

[17] HELGRID MÜLLER, *Kreisdarstellung in normaler Axonometrie*, http://lehrer.schule.at/helgrid_mueller/darste/normaxo/kreiseaxo.pdf

Georg Glaeser

University of Applied Arts Vienna
Department of Geometry
Oskar Kokoschka-Platz 2, 1010 Vienna, Austria

email: georg.glaeser@uni-ak.ac.at

Karlheinz Schott

D-96129 Strullendorf / Geisfeld

email: kh.schott@yahoo.de

Original scientific paper
Accepted 23. 12. 2009.

SONJA GORJANC

Pedal Surfaces of First Order Congruences

Pedal Surfaces of First Order Congruences

ABSTRACT

This paper is an overview of the pedal surfaces P_n^{n+2} for first order line congruences. We describe their construction, prove their algebraic properties, derive parametric and implicit equations and visualize these new resulting surfaces with the program *Mathematica* in seven examples.

Key words: congruence of lines, pedal surface of congruence, pinch-point, singular point

MSC 2010: 51N20, 51N15, 51M15, 65D18

Nožišne plohe kongruencija prvog reda

SAŽETAK

U radu je dan pregled nožišnih ploha P_n^{n+2} za kongruencije prvog reda. Opisana je njihova konstrukcija, dokazana su njihova algebarska svojstva, izvedene su parametarske i implicitne jednadžbe za opći slučaj, a za sedam primjera, pomoću programa *Mathematica*, vizualizirani su njihovi oblici.

Ključne riječi: kongruencija, nožišna ploha kongruencije, kuspidalna točka, singularna točka

1 Introduction

Congruence C is a set of lines in a three-dimensional space (projective, affine or Euclidean) depending on two parameters [3]. The line $l \in C$ is said to be a *ray* of the congruence. The *order* of an algebraic congruence is the number of its rays passing through an arbitrary point; the *class* of a congruence is the number of its rays lying in an arbitrary plane. C_n^m denotes an mth *order* nth *class* congruence. A point is a *singular point* of a congruence if ∞^1 rays pass through it. A plane is a *singular plane* of a congruence if it contains ∞^1 rays.

In Euclidean space $\mathbb{E}^3$, the *pedal surface* of a congruence C_n^m with respect to a pole P is the locus of the foot points of perpendiculars from the point P to the rays of the congruence C_n^m. The order of the pedal surface of C_n^m for the pole P is $2m+n$ [11].

2 First order line congruences

According to [16, p. 64], [22, pp. 1184-1185], [19, p. 32], there are only two types of first order line congruences directed by loci of points. Their rays intersect two curves or the same curve twice.

The *first type* is the type of nth class congruences C_n^1, their rays are transversals of one straight line d and one nth order curve c^n which cuts this straight line at $n-1$ points. These curves are called the *directing lines* of C_n^1. The intersection points of d and c^n can be multiple points of c^n with the highest multiplicity $n-2$ for a space curve and $n-1$ for a plane curve. Some of these points can coincide, and there are cases when d is the tangent line of c^n, the tangent at inflection, etc. If c^n is a plane curve, it must contain an $(n-1)$-ple point which is the intersection point of d and the plane of c^n. All singular points of C_n^1 lie on its directing lines c^n and d, and all singular planes of C_n^1 are the planes of the pencil $[d]$ (see Fig. 1).

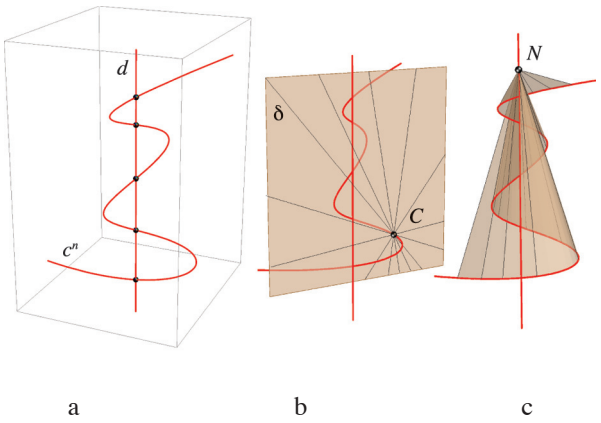

Figure 1: *The directing lines of C_n^1 are shown in figure a. For a point $C \in c^n$, the rays of C_n^1 form a pencil of lines in the plane through d (figure b) and for $N \in d$ they form an nth degree cone with the vertex N (figure c).*

The *second type* of first order line congruences consists only of 3rd class congruences and their rays are bisectors of a twisted cubic k^3. Unlike the first type congruence C_3^1, this type will be denoted by K_3^1.

The properties of the first order congruences (the construction of their rays, singular points and planes, focal properties, etc.) can be found in [2].

3 Pedal surfaces of C_n^1

In [1] the authors define one transformation of three-dimensional projective space where corresponding points lie on the rays of the 1st order, nth class congruence C_n^1 and are conjugate with respect to a proper quadric Ψ. This transformation, called $(n+2)$-degree inversion, maps a straight line to an $(n+2)$-order space curve, and a plane to an $(n+2)$-order surface which contains an n-ple straight line.

Proposition 1 *The pedal surface of the first type congruence C_n^1 with respect to a pole P is an $(n+2)$-order surface with n-ple straight line d containing the curve c^n and the absolute conic of $\mathbb{E}^3$.*

PROOF: Orthogonality in Euclidean space $\mathbb{E}^3$ means conjugacy with respect to the absolute conic. The plane through a point A is orthogonal to a line l iff it is the polar plane of the point at infinity on the line l with respect to any sphere with the center A. Thus, the pedal surface of a congruence C_n^1 with respect to a pole P is the image of the plane at infinity given by the $(n+2)$-degree inversion with respect to C_n^1 and any sphere with the center P. According to [1], it is an $(n+2)$-order surface with an n-ple straight line d containing the curve c^n and the absolute conic of $\mathbb{E}^3$. □

In the following, P_n^{n+2} denotes the pedal surface of C_n^1.

Proposition 2 *If the directing line d lies in the plane at infinity, the pedal surface P_n^{n+2} splits into an $(n+1)$-order surface with the $(n-1)$-ple line d and the plane at infinity.*

PROOF: This proposition follows from the property of the $(n+2)$-degree inversion which is given in theorem 4 [1] (see examples 4.5.). □

Proposition 3 *If the directing curve c^n lies in the plane at infinity, the pedal surface P_n^{n+2} splits into an $(n+1)$-degree ruled surface with the n-ple line d and the plane at infinity.*

PROOF: This proposition follows from the property of the $(n+2)$-degree inversion which is given in theorem 3 [1] (see examples 4.6.). □

3.1 Construction of the pedal surface P_n^{n+2}

It is clear that any plane through the n-ple line of an $(n+2)$-order surface intersects this surface at its n-ple line and one conic. If the surface contains the absolute conic, this intersection conic is a circle.

In any plane δ through the directing straight line d, the rays of C_n^1 form the pencil of lines (C), where the point $C \notin d$ is the intersection of the plane δ and the directing curve c^n. If a pole P is in the general position with respect to the directing lines of the congruence C_n^1, the feet of perpendiculars from P to the rays of the pencil (C) form a circle c with the diameter $\overline{CP'}$, where P' is the orthogonal projection of P onto δ. For a given pole P, the path of the point P' is the circle k lying in the plane through P perpendicular to d. The diameter of k is $\overline{PP_d}$, where P_d is the orthogonal projection of P onto d.

Thus, we can regard the pedal surface P_n^{n+2} as the system of circles in the planes through the n-ple line d with the end points of diameters on the curve c^n and the circle k (see Fig. 2). The diameters of the circles c lie on the rulings of one $(n+2)$-degree ruled surface with the directing lines c^n, d and k [14, p. 186], [16, p. 90].

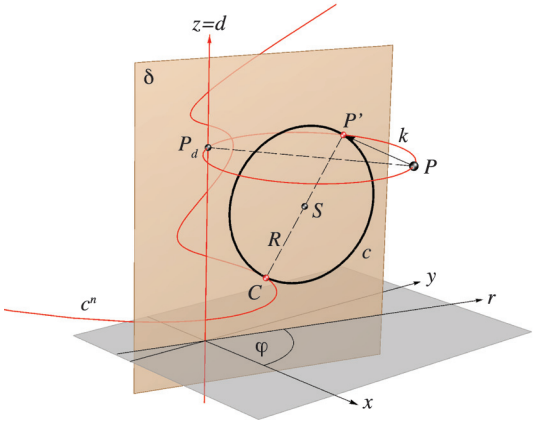

Figure 2: *One system of the curves on P_n^{n+2} can be constructed as circles in the planes through d with the end points of the diameters on c^n and k.*

3.2 Singularities of P_n^{n+2}

The highest singularity which a proper P_n^{n+2} can possess is an $(n+1)$-ple point. If such a point exists, it must lie on its n-ple line. Namely, if P_n^{n+2} had an $(n+1)$-ple point A out of d, every line through A which cuts d would cut P_n^{n+2} at $2n+1$ points. This is possible only in the case if this line lies entirely on P_n^{n+2}, but then the surface must break up into the plane through A and d and one ruled surface of the degree $n+1$.

Proposition 4 *An $(n+1)$-ple point exists on P_n^{n+2} iff a pole P lies on d. The highest number of such points on P_n^{n+2} is two only if c^n lies in the plane perpendicular to d.*

PROOF: If a pole P lies on d, then every circle c passing through P, and it is the $(n+1)$-ple point of P_n^{n+2} because every straight line through P (except d) intersects P_n^{n+2} at P and only one additional point on c. Inversely, if $N^{n+1} \in d$ is an $(n+1)$-ple point, every circle c must pass through it. Namely, if some circle c did not pass through N^{n+1}, every line in the plane of c passing through N^{n+1} would cut P_n^{n+2} at $n+3$ points, which is impossible. It is possible only if $N^{n+1} = P$, because the circle k must break up into a pair of isotropic lines with the double point P. If there exists one more $(n+1)$-ple point O on d, it must lie on c^n because all circles c pass through P and O. It is possible only if c^n is a planar curve with an $(n-1)$-ple point O. It is elementary that in such a case c^n lies in the plane perpendicular to d (Thales' theorem). □

Any other point $N \in d$ is an *n-planar* point – the tangent cone at N splits into n planes through d. Namely, n circles c pass through $N \in d$ and the planes of these circles form the splitting tangent cone ST_N^n of P_n^{n+2} at N. If some of these tangent planes coincide, the touching point is the *pinch-point* of P_n^{n+2}. The tangent planes at an n-planar point can be real or imaginary. Depending on the number of real and imaginary tangent planes, as well as the number of coinciding planes, we distinguish different types of n-planar points. To calculate the number of these types we use the *partition function*[1] $p : \mathbb{N} \cup \{0\} \to \mathbb{N}$ [21].

Proposition 5 *The number of types of the splitting tangent cones ST^n at n-planar points is*

$$\sum_{s=0}^{s=\lfloor \frac{n}{2} \rfloor} p(s) \cdot p(n-2s).$$

PROOF: Any cone ST^n consists of s $(0 \le s \le \lfloor \frac{n}{2} \rfloor)$ pairs of imaginary planes and $n-2s$ real planes. The number of different multiplicities of these planes equals the sum of the corresponding partitions. □

Proposition 6 *The number of types of pinch-points on P_n^{n+2} is*

$$-1 - \lfloor \frac{n}{2} \rfloor + \sum_{s=0}^{s=\lfloor \frac{n}{2} \rfloor} p(s) \cdot p(n-2s).$$

PROOF: The number of possibilities that no planes of ST^n coincide is $1 + \lfloor \frac{n}{2} \rfloor$. In all other cases, at least two tangent planes coincide and the touching point is the pinch-point of P_n^{n+2}. □

Proposition 7 *On the pedal surface P_n^{n+2} exist $4(n-1)$ pinch-points.*

PROOF: Every plane δ of the pencil $[d]$ cuts P_n^{n+2} at the n-ple line d and one circle c. The intersection points N_1, N_2 of d and c are the touching points of δ and P_n^{n+2}. But, through each of the points N_1 and N_2 other $n-1$ tangent planes pass. The correspondence between the planes of the pencil $[d]$, where corresponding planes have the same touching point, is an involution of the order $2(n-1)$. This involution has $4(n-1)$ double elements [13, p. 48] which are the coinciding tangent planes through the points on the n-ple line, and their touching points are the pinch-points of P_n^{n+2} [18, p. 317]. These points can be real or imaginary. □

Except for the points on the n-ple line d, the highest singularity which P_n^{n+2} can possess is a double point.

Proposition 8 *The maximal number of real double points on P_n^{n+2} is:*

n, if c^n is a space curve,

$n+1$, if c^n is a planar curve.

PROOF: If D is the double point of P_n^{n+2}, it is a double point for every section of P_n^{n+2} through D. Thus, the circle c in the plane through D and the line d splits into a pair of isotropic lines through D. This is the case when the end points of the diameter $\overline{CP'}$ coincide, i.e. circle k intersects the curve c^n at the point D. Therefore, if c^n is a space curve, P_n^{n+2} can possess at most n double points in the plane of the circle k. But if c^n is a plane curve in the plane of k, then c^n and k can possess $n+1$ intersection points which do not lie on d. □

3.3 Parametric equations of P_n^{n+2}

Let the directing lines of C_n^1 be the axis z and the curve c^n given by the following parametrization:

$$\mathbf{r}_{c^n}(\varphi) = (x_{c^n}(\varphi), y_{c^n}(\varphi), z_{c^n}(\varphi)),\ x_{c^n}, y_{c^n}, z_{c^n} : [0, \pi) \to \mathbb{R}. \tag{1}$$

Let (p_x, p_y, p_z) be the coordinates of the pole P.

[1] A partition of a positive integer n is a way of writing n as a sum of positive integers. The number of partitions of n is given by the partition function $p(n)$ where $p(0) = 1$ by convention. The partition function is implemented in *Mathematica* as `PartitionP[n]` or `NumberOfPartitions[n]` in the *Mathematica* package `Combinatorica'`.

Let (r,z), where $|r| = \sqrt{x^2+y^2}$, be the coordinates in the plane $\delta(\varphi)$ given by the equation $y = x\tan\varphi$ if $\varphi \in [0,\pi)$, $\varphi \neq \pi/2$, and $x = 0$ if $\varphi = \pi/2$ (see Fig. 2).

The coordinates of the points $C, P' \in \delta(\varphi)$ are

$$r_C(\varphi) = \sqrt{x_{c^n}(\varphi)^2 + y_{c^n}(\varphi)^2}, \qquad z_C(\varphi) = z_{c^n}(\varphi)$$
$$r_{P'}(\varphi) = p_x\cos\varphi + p_y\sin\varphi, \qquad z_{P'}(\varphi) = p_z. \quad (2)$$

$R(\varphi)$ is the radius and $S(r_S(\varphi), z_S(\varphi))$ is the center of the circle c in the plane $\delta(\varphi)$:

$$R(\varphi) = \frac{\sqrt{(r_C(\varphi) - r_{P'}(\varphi))^2 + (z_C(\varphi) - p_z)^2}}{2}$$
$$r_S(\varphi) = \frac{r_C(\varphi) + r_{P'}(\varphi)}{2}$$
$$z_S(\varphi) = \frac{z_C(\varphi) + p_z}{2} \quad (3)$$

Since the parametric equations of the circle c in the plane $\delta(\varphi)$ are

$$r(\theta) = R(\varphi)\sin\theta + r_S(\varphi)$$
$$z(\theta) = R(\varphi)\cos\theta + z_S(\varphi), \quad \theta \in [0,2\pi), \quad (4)$$

the parametric equations of the surface P_n^{n+2} are the following:

$$x(\theta,\varphi) = \cos\varphi\,(R(\varphi)\sin\theta + r_S(\varphi))$$
$$y(\theta,\varphi) = \sin\varphi\,(R(\varphi)\sin\theta + r_S(\varphi))$$
$$z(\theta,\varphi) = R(\varphi)\cos\theta + z_S(\varphi), \quad (5)$$
$$\varphi \in [0,\pi),\ \theta \in [0,2\pi).$$

3.4 Implicit equation of P_n^{n+2}

According to [1], the plane at infinity cuts P_n^{n+2} at the absolute conic and n rays of C_n^1. These rays pass through the point at infinity of the directing line d and can be real or imaginary. Therefore, the polynomial of the highest degree in the implicit equation of P_n^{n+2} can be written in the form $(x^2+y^2+z^2)H^n(x,y)$, where $H^n(x,y)$ is the homogeneous polynomial of degree n.

Theorem 1 *If an nth order surface in $\mathbb{E}^3$ which passes through the origin is given by the equation*

$$F(x,z,y) = f_m(x,y,z) + f_{m+1}(x,y,z) + \cdots + f_n(x,y,z) = 0,$$

where $f_k(x,y,z)$ $(1 \le k \le n)$ are homogeneous polynomials of degree k, then the tangent cone at the origin is given by the equation $f_m(x,y,z) = 0$.

The proof of this theorem is given in [9, p. 251].

Thus, since the axis z is the n-ple line of P_n^{n+2}, the implicit equation of P_n^{n+2} takes the following form:

$$(x^2+y^2+z^2)H_1^n(x,y) + H^{n+1}(x,y,z) + H_2^n(x,y) = 0, \quad (6)$$

where H_j^i are homogeneous polynomials of degree i.

From eq. (4), by using the standard coordinate transformation formulas for Cartesian and cylindrical coordinates, it is possible to determine the polynomials H_j^i for every P_n^{n+2}.

4 Examples of P_n^{n+2}

4.1 P_1^3 – pedal surfaces of linear congruences

The pedal surfaces of linear congruences C_1^1 are cubics which contain the absolute conic. It was shown in [11] that in the general case if C_1^1 is a hyperbolic linear congruence, seven real straight lines exist on the pedal surface P_1^3; if C_1^1 is elliptic, three real straight lines exist on P_1^3; if C_1^1 is parabolic, then P_1^3 contains one double point and five real straight lines and two of them are counted twice. Figure 3 shows three types of parabolic cyclides obtained as the pedal surfaces of the hyperbolic linear congruence.

4.2 P_2^4 – pedal surfaces of 1st order 2nd class congruences

A complete classification of the pedal surfaces of C_2^1 is given in [6]. If there are no directing lines of C_2^1 in the plane at infinity, the pedal surface P_2^4 is a quartic with a double straight line. These surfaces are classified in five types depending on the number of real straight lines on them. According to propositions 4 and 8, there are at most two triple points (see Fig. 4) and at most three real double points (see Fig. 5c) on the pedal surfaces P_2^4.

The points on the double line d are bi-planar points – tangent cones split into two planes through d. These points can be isolated (two tangent planes are imaginary), binodal (the tangent planes are real and different) or pinch-points (coinciding tangent planes). The pinch-points of P_2^4 separate the intervals with isolated and binodal points on d and there are at most four real pinch-pints on d (see Fig. 5a).

If one directing line d or c^2 lies in the plane at infinity, the pedal surface P_2^4 splits into the plane at infinity and into a cubic surface.

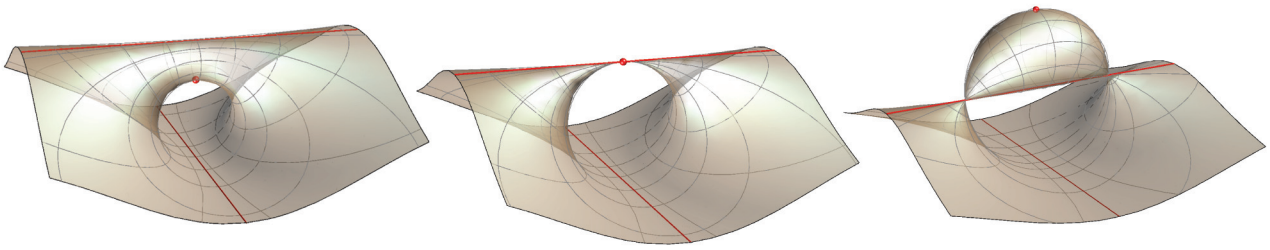

a b c

Figure 3: *The directing orthogonal lines of C_1^1 are the axis z, placed in the horizontal plane, and the line parallel to the axis y in the plane $x = 1$. For three different positions of the pole P on the axis x ($x_P = \frac{1}{2}, 1, 2$), the pedal surface is the ring, spindle and horn parabolic cyclide [4, pp. 371-373] in the case a, b and c, respectively.*

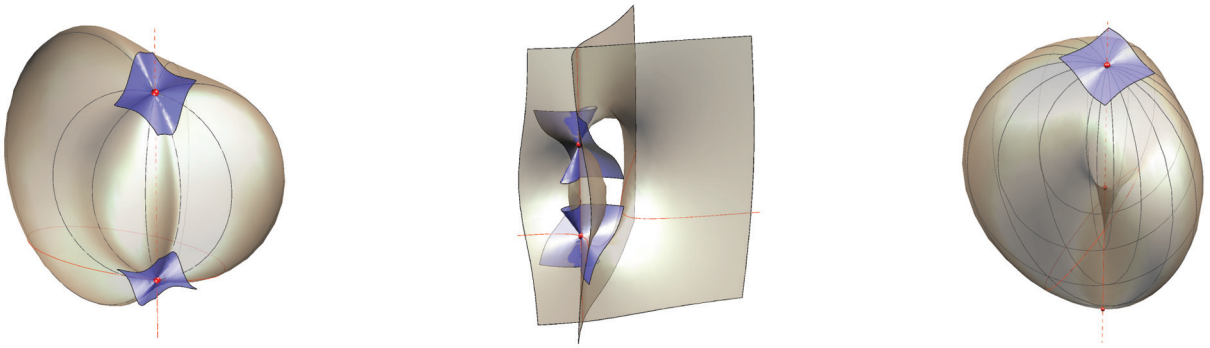

a b c

Figure 4: P_2^4 *with triple points and 3rd order tangent cones. The directing elements are: figure a* – $c^2(x^2+4y^2-2x+4y=0, z=0)$, $P(0,0,2)$; *figure b* – $c^2(x^2-y^2-2x=0, z=0)$, $P(0,0,2)$; *figure c* – $c^2(x^2+y^2+2x+4y=0, x-y+z=0)$, $P(0,0,8)$. *Except the triple points, all points on the double line are isolated in the case a, and binodal in the case b. In the case c, two pinch-points separate the segments with isolated and binodal points on the double line.*

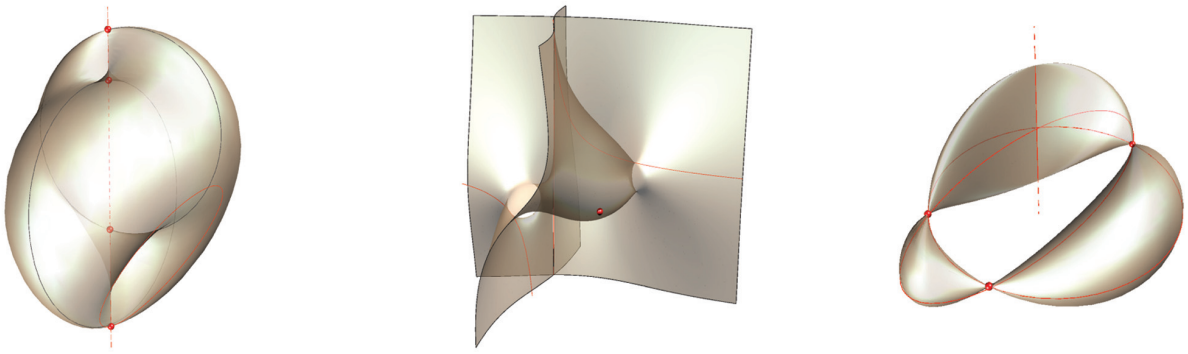

a b c

Figure 5: P_2^4 *with four real pinch-points is shown in figure a. The directing elements are* c^2 $(x^2+0.5y^2+x+y=0, x+y+z=0)$ *and* $P(1,1,5)$. *The pedal surface in figure b has no real pinch-points and its directing elements are* c^2 $(yz=1, x=1)$ *and* $P(2.5, 2.-0.3)$. *The directing elements for* P_2^4 *in figure c are* c^2 $(x^2+6y^2-x-4y=0, z=0)$ *and* $P(1,1,0)$. *Three conical points of this surface are the intersection points (different from the origin) of* c^2 *and the circle k.*

4.3 Special P_4^6 directed by Viviani's curve

Special sextics with a quadruple line P_4^6 are elaborated in detail in [5]. They are obtained as the pedal surfaces of one special first order fourth class congruence C_4^1 directed by the axis z and Viviani's curve – the intersection of the sphere $(x+\sqrt{2})^2+y^2+(z+\sqrt{2})^2=4$ and the cylinder $(x+z+\sqrt{2})^2+2y^2=2$ (see Fig. 6). Viviani's curve is given by the following parametrization:

$$\mathbf{r}(\varphi)=4\sqrt{2}\,\frac{1+3\cos 2\varphi}{(3+\cos 2\varphi)^2}\left(-2(\cos\varphi)^2,-\sin 2\varphi,(\sin\varphi)^2\right),\quad \varphi\in[0,\pi). \tag{7}$$

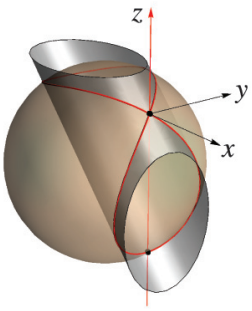

Figure 6: *The origin is the double point of Viviani's curve c^4 (the intersection of a sphere and cylinder) and the axis z cuts c^4 at one more regular point $z_0=-2\sqrt{2}$.*

The highest singularity which P_4^6 can possess is a quintuple point. According to the type of its 5th degree tangent cone, we distinguish six types of quintuple points on P_4^6 [5]. Three of them are shown in Figure 7. The points on the axis z are quadri-planar points of P_4^6, their tangent cones split into four planes through z. These tangent planes can be real and different, real and coinciding or imaginary. According to proposition 5, we distinguish nine types of quadri-planar points: *type* 1 – four real and different tangent planes; *type* 2 – two real and different planes and a pair of imaginary planes; *type* 3 – two different pairs of imaginary planes; *type* 4 – one double plane and two different single real planes; *type* 5 – one double plane and a pair of imaginary planes; *type* 6 – a pair of double real planes; *type* 7 – a double pair of imaginary planes; *type* 8 – one triple plane and one single plane; *type* 9 – one quadruple plane. On the axis z the intervals with quadri-planar points of types 1–3 are bounded by the points of the types 4–9 which are the pinch-points of P_4^6. Since four rays of C_4^1 in the plane at infinity are given by the equation $(2x^2+y^2)^2=0$, the point at infinity on the axis z is the pinch-point of type 7. The type of a quadri-planar point depends on the factorization of the homogeneous 4th degree polynomial in x and y which represents its cone. Based on the conditions given in [20], we made a program in *Mathematica 6* (available online: www.grad.hr/sgorjanc/pinch_points.nb) which calculates the coordinates z_0 of the pinch-points of P_4^6 for every choice of pole P. According to proposition 7, the highest number of real pinch-points of P_4^6 is twelve. Three examples are shown in Fig. 8.

The following is shown in [5]: iff a pole P lies on the part of one parabola, P_4^6 has two real conical points; iff P lies on one 5th degree ruled surface, P_4^6 has at least one real conical point.

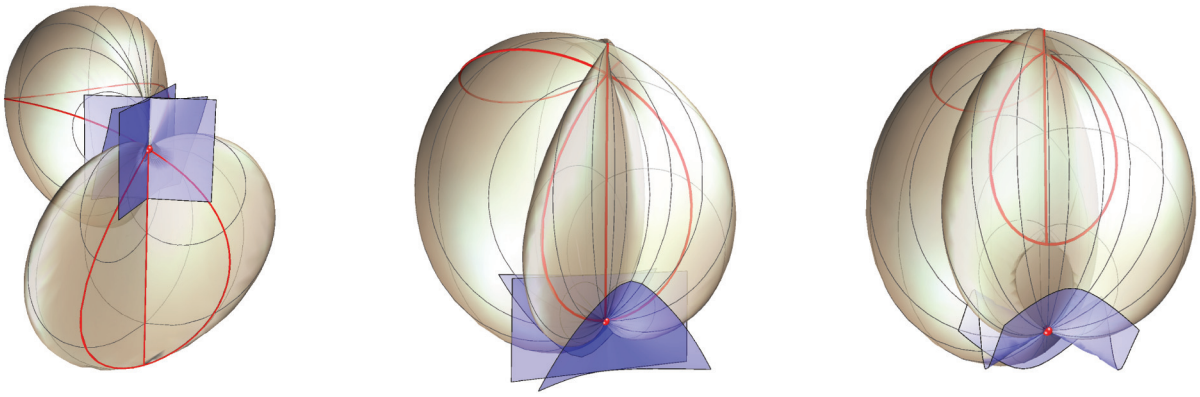

a b c

Figure 7: *If $P=O$, the tangent cone at P splits into two planes and one 3rd degree cone (a). If $P=(0,0,-2\sqrt{2})$, the tangent cone at P splits into a 4th degree cone and one plane (b). For all other positions of a pole $P\in z$, the tangent cones at P are proper 5th degree cones with a quadruple line z. Such a cone with an isolated quadruple line is shown in figure c.*

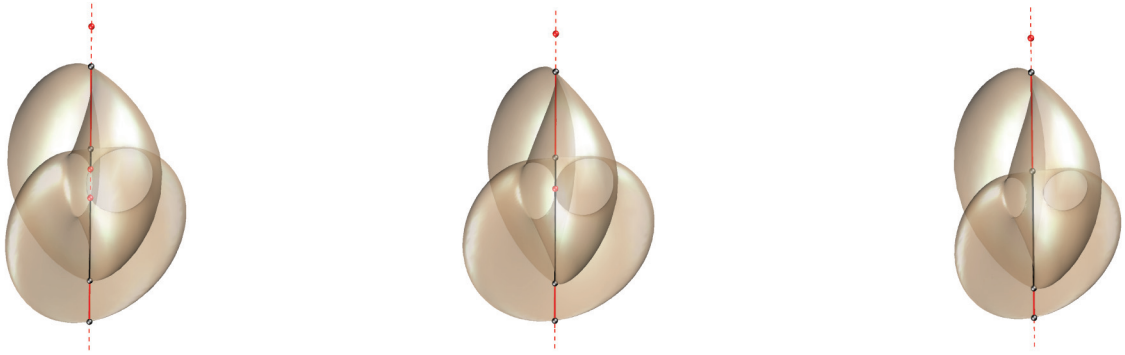

a b c

Figure 8: *The surfaces P_4^6 with 12, 10 and 8 real pinch-points are shown in figures a, b and c, respectively. The pinch-points counted twice (types 6 and 7) are indicated by red color. Other pinch-points (types 4 and 5) are black. Besides the highlighted pinch-points, every surface P_4^6 has a pinch-point of type 7 at infinity. The segments on the axis z contain quadruple points of type 1 (black), type 2 (red) and type 3 (dashed red).*

4.4 Special P_{2k}^{2k+2} directed by roses

Roses or *rhodonea* are curves which can be expressed by the following polar equations:

$$r(\varphi)=\cos n\varphi \quad \text{or} \quad r(\varphi)=\sin n\varphi, \quad n\in\mathbb{R}. \tag{8}$$

If $n=2k-1$, $k\in\mathbb{N}$, the curves close at a polar angle π and have n petals. They are algebraic curves of the order $n+1$, with only one singular point – an n-ple point in the origin [12, pp. 358-369]. According to the multiple-angle formula $\cos n\varphi=\sum_{i=0}^{\lfloor\frac{n}{2}\rfloor}(-1)^i\binom{n}{2i}(\cos\varphi)^{n-2i}(\sin\varphi)^{2i}$ and the standard coordinate transformation formulas, their implicit equation is

$$(x^2+y^2)^k-\tau^{2k-1}=0, \quad \text{where} \tag{9}$$

$$\tau^{2k-1}=\sum_{i=0}^{k}(-1)^i\binom{2k-1}{2i}x^{2k-1-2i}y^{2i}. \tag{10}$$

It is clear ([9, p. 251], [17, p. 27]) that $2k-1$ tangent lines at the origin are given by

$$\tau^{2k-1}=0. \tag{11}$$

Some examples are shown in Fig. 9.

Let the axis z and the curve c^{2k} given by equations

$$(x^2+y^2)^k-\tau^{2k-1}=0, \quad ax+by+z=0, \tag{12}$$

be the directing lines of a congruence C_{2k}^1. The curve c^{2k} is the intersection of one $2k$-order cylinder and a plane through the origin (see Fig. 10a). The singular points of C_{2k}^1 lie on its directing lines c^{2k} and z (see Fig. 10b and Fig. 10c). The rays of C_{2k}^1 through the origin O form the pencil of lines (O) in the plane $ax+by+z=0$, and the other lines through O are not regarded as the rays of C_{2k}^1. The pedal surface P_{2k}^{2k+2} of C_{2k}^1 with respect to a pole P is a $(2k+2)$-order surface with $2k$-ple line z (see Fig. 10d).

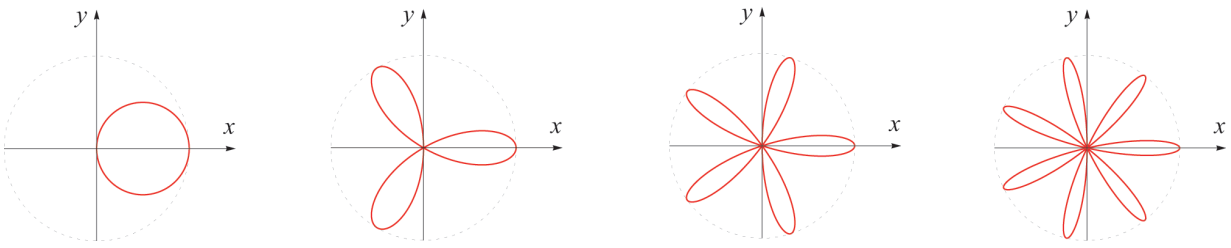

a b c d

Figure 9: *The curves $r(\varphi)=\cos n\varphi$ for n equal to 1, 3, 5 and 7 are shown in figures a, b, c and d, respectively.*

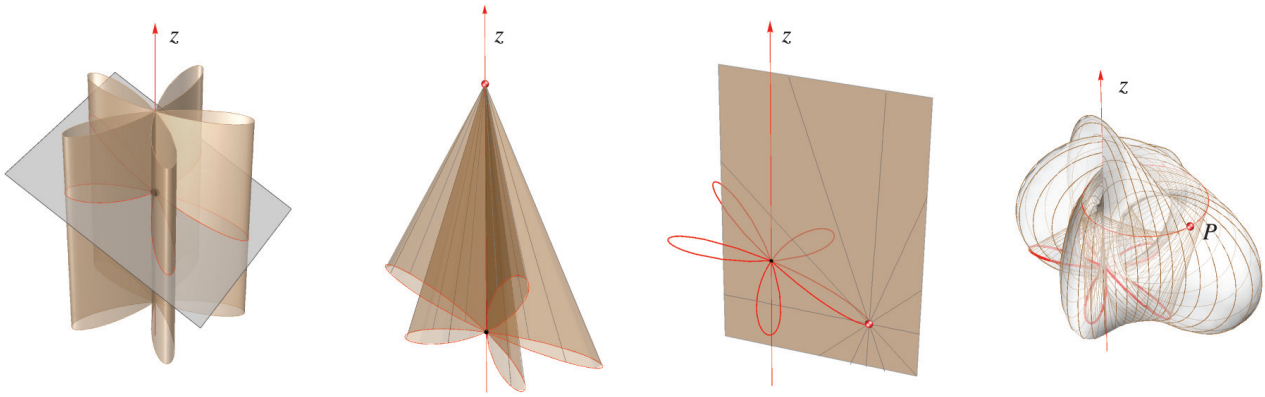

a b c d

Figure 10: *c^{2k} is the intersection of one $2k$-degree cylinder with a $(2k-1)$-ple line z and a plane through the origin (a). The rays of C^1_{2k} through a point on z form a $2k$-degree cone with a $(2k-1)$-ple line z (b). The rays of C^1_{2k} through a point $C \in c^{2k}$ form the pencil of lines (C) in the plane though z and C (c). The pedal surface P^{2k+2}_{2k} is a system of circles in the planes through z, with the end points of its diameters on c^{2k} and k. These diameters lie on the rulings of one $(2k+2)$-degree ruled surface (d).*

In every plane through z, the coordinates of $C \in c^{2k}$ are given by

$$(r_C(\varphi), z_C(\varphi)) = \cos n\varphi(1, -a\cos\varphi - b\sin\varphi). \tag{13}$$

From (13) and eqs. (2) – (5), we obtain the parametric equations of P^{2k+2}_{2k} which enable them to be visualized using the program *Mathematica*. Some examples are shown in Fig. 11.

Since every plane through the axis z cuts P^{2k+2}_{2k} at the circle c and the $2k$-ple line z, the equation of P^{2k+2}_{2k} in the cylindrical coordinates (r,φ,z) is

$$r^{2k} \cdot ((r - r_S(\varphi))^2 + (z - z_S(\varphi))^2 - R^2(\varphi)) = 0. \tag{14}$$

From (14), by using eqs. (13), (2), (3) and the standard coordinate transformation formulas, we obtain the following implicit equation of P^{2k+2}_{2k}:

$$(x^2+y^2+z^2)(x^2+y^2)^k + H^{2k+1}(x,y,z) + H^{2k}(x,y) = 0, \tag{15}$$

where

$$\begin{aligned} H^{2k+1}(x,y,z) &= -(p_x x + p_y y + p_z z)(x^2+y^2)^k \\ &\quad - (x^2+y^2 - axz - byz)\tau^{2k-1} \\ H^{2k}(x,y) &= (p_x x + p_y y - ap_z x - bp_z y)\tau^{2k-1}. \end{aligned} \tag{16}$$

The plane at infinity cuts P^{2k+2}_{2k} at the absolute conic and the pair of isotropic lines counted k times. These isotropic lines are the rays of C^1_{2k} and also the rulings of the rose-cylinder given by the first equation in (12). Thus, the point at infinity on the axis z is the pinch-point of P^{2k+2}_{2k}.

If we translate the origin into $Z_0(0,0,z_0)$, then (from eq. (15) and according to theorem 1) we obtain the following equation of the splitting tangent cone at Z_0:

$$\begin{aligned} &(z_0^2 - p_z z_0)(x^2+y^2)^k + (x(p_x + az_0 - ap_z) \\ &+ y(p_y + bz_0 - bp_z))\tau^{2k-1} = 0. \end{aligned} \tag{17}$$

The surface P^{2k+2}_{2k} has a $(2k+1)$-ple point iff P lies on the axis z. In this case, all coefficients in eq. (17) are equal to zero, and the tangent cone at P, in the coordinate system with the origin P, is given by the following equation:

$$p_z z(x^2+y^2)^k - (x^2+y^2 - axz - byz)\tau^{2k-1} = 0. \tag{18}$$

If $P = O$, the tangent cone at P splits into one 2nd degree cone and $(2k-1)$ planes through the axis z

$$(x^2+y^2 - axz - byz)\tau^{2k-1} = 0. \tag{19}$$

Three examples are shown in Fig 12.

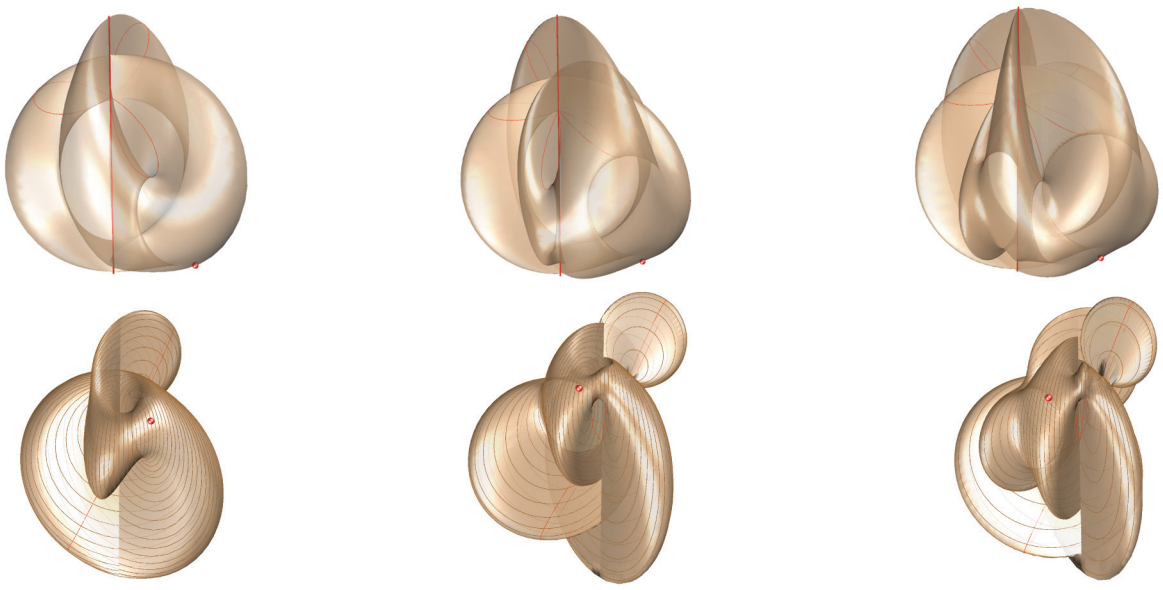

a b c

Figure 11: *The pedal surfaces* P_{2k}^{2k+2} *for the poles* $P(-1,1,-2)$, $P(-1,1,1)$ *and* $k=2,3,4$ *are shown in figures a, b and c, respectively.*

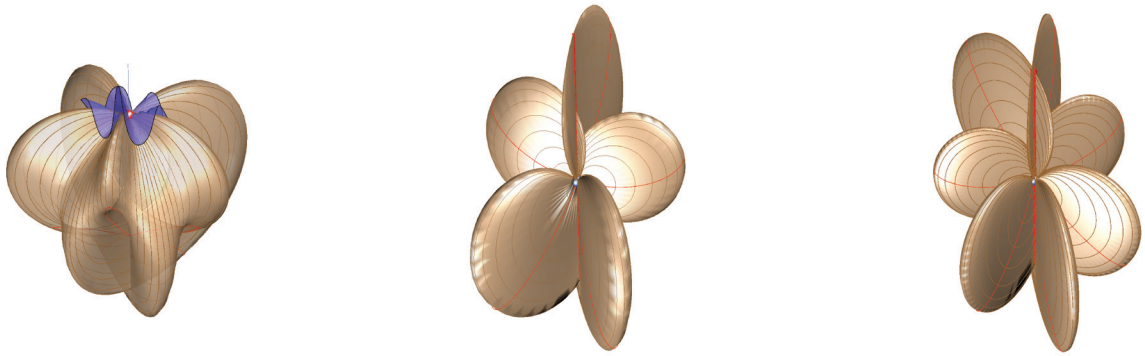

a b c

Figure 12: *The surface* P_6^8, *directed by the 5-petalled curve in the plane* $x+y+z=0$ *and the pole* $P(0,0,2)$, *and its 7th degree tangent cone at P, are shown in figure a. The pedal surfaces, directed by the 5-petalled and 7-petalled curves in the plane* $x+y+z=0$ *and* $P=O$, *are shown in figures b and c, respectively.*

According to proposition 8, P_{2k}^{2k+2} possesses the highest number of real double points if the directing curve c^{2k} and the circle k lie in the same plane. It is the case that $a=b=p_z=0$ when c^{2k} and k have $4k$ intersection points. But $2k-1$ points coincide with O, two points are the absolute points of the plane $z=0$, thus only $2k-1$ intersection points can lie besides the axis z and be real. Since $2k-1$ is an odd number, at least one real double point exists on P_{2k}^{2k+2} if $a=b=p_z$=0.

The pedal surfaces directed by the roses in the plane $z=0$ are elaborated in detail in [7]. Some examples are shown in Fig. 13.

In this case ($a=b=0$), if a pole P lies on the axis z, the

equation (15) takes the form

$$(x^2+y^2)P^{2k}(x,y,z)=0, \tag{20}$$

where

$$P^{2k}(x,y,z)=(x^2+y^2)^{k-1}(x^2+y^2+z^2-p_z z)-\tau^{2k-1}. \tag{21}$$

Thus, the pedal surface splits into a pair of isotropic planes through the axis z and one $2k$-order surface given by $P^{2k}(x,y,z)=0$. The line z is a $(2k-2)$-ple line of these surfaces with two $(2k-1)$-ple points, the origin O and the pole P (see Fig. 14).

Especially, if $P=O$, the tangent cone at P splits into $2k-1$ planes given by equation $\tau^{2k-1}=0$ (see Fig. 15).

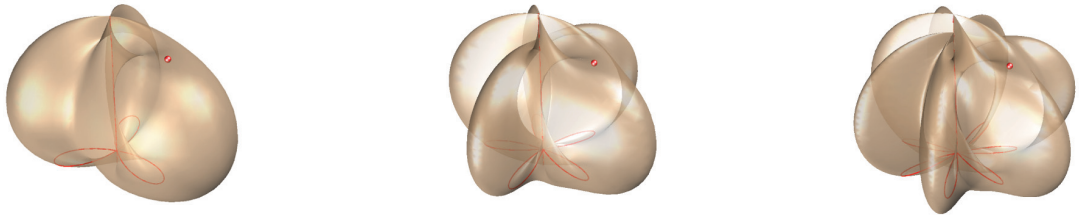

a b c

Figure 13: *The pedal surfaces for the pole $P(1,0,2)$ and 3, 5 and 7-petalled roses in the plane $z=0$ are shown in figures a, b and c, respectively.*

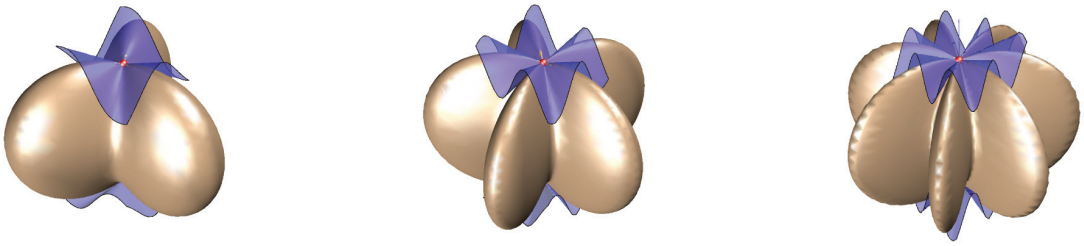

a b c

Figure 14: *The pedal surfaces for the pole $P(0,0,2)$ and 3, 5 and 7-petalled roses in the plane $z=0$ with 3, 5 and 7-degree tangent cones at P and O are shown in figures a, b and c, respectively.*

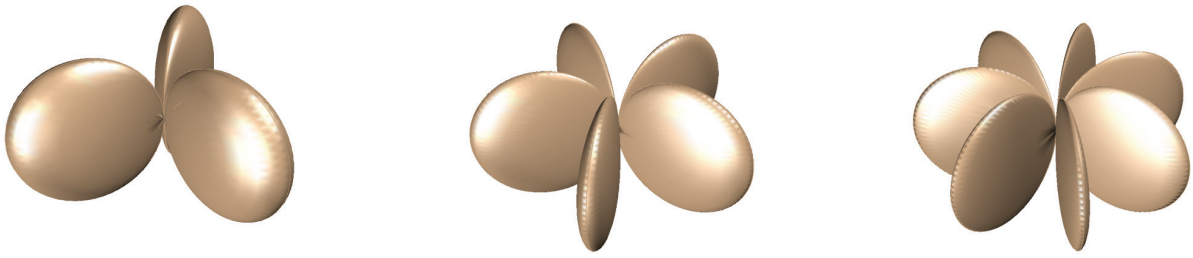

a b c

Figure 15: *The pedal surfaces for the pole $P=O$ and 3, 5 and 7-petalled roses in the plane $z=0$ are shown in figures a, b and c, respectively.*

4.5 P_n^{n+2} of $C_n^1(c^n,d)$ with d at infinity

If the directing line d lies in the plane at infinity (α^∞), then α^∞ is the singular plane of $C_n^1(c^n,d^\infty)$. Thus, its image given by the $(n+2)$-degree inversion with respect to $C_n^1(c^n,d^\infty)$ and any sphere with the center P splits into α^∞ and the image D_{n-1}^{n+1} of the singular line d^∞ which is an $(n+1)$-order surface with the $(n-1)$-ple line d^∞ (see theorem 4 [1]). In this case the circle k splits into a line through P perpendicular to the pencil of planes $[d^\infty]$ and one line at infinity. The planes through d^∞ cut D_{n-1}^{n+1} into the circles with the end points of diameters on k and c^n. Three examples are shown in Fig. 16.

4.6 P_n^{n+2} of $C_n^1(c^n,d)$ with c^n at infinity

If the directing curve c^n lies in the plane α^∞, the intersection point $D^\infty=\alpha^\infty\cap d$ must be the $(n-1)$-ple point of $c^{n\infty}$. In this case α^∞ is the singular plane of $C_n^1(c^{n\infty},d)$ and its image given by the $(n+2)$-degree inversion with respect to $C_n^1(c^{n\infty},d)$ and any sphere with the center P splits into α^∞ and the image R_n^{n+1} of $c^{n\infty}$ which is one $(n+1)$-degree ruled surface with the n-ple line d (see theorem 3 [1]). In the plane $\delta\in[d]$ the ruling of R_n^{n+1} is perpendicular to the rays of C_n^1 and passes through P', i. e. the circle c splits into this ruling and the line at infinity. Three examples are shown in Fig. 17.

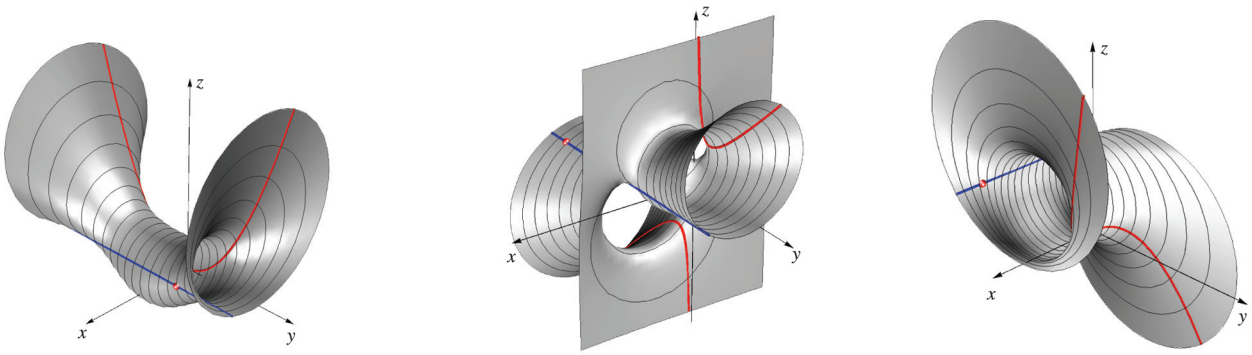

a b c

Figure 16: *a* $-D_1^3$ *defined by* d^∞ *in the plane* $y=0$, c^2 *given by equations* $x=0$ *and* $z=\frac{y^2}{2}$ *and* $P(2,1.5,1)$.
b $-D_1^3$ *defined by* d^∞ *in the plane* $y=0$, c^2 *given by equations* $x=0$ *and* $y^2-yz+1=0$ *and* $P(3,-4,1)$.
c $-D_2^4$ *defined by* d^∞ *in the plane* $x=0$, c^3 *given by equations* $y=\frac{x^2}{5}$ *and* $z=\frac{x^3}{10}$ *and* $P(3,-4,2)$.

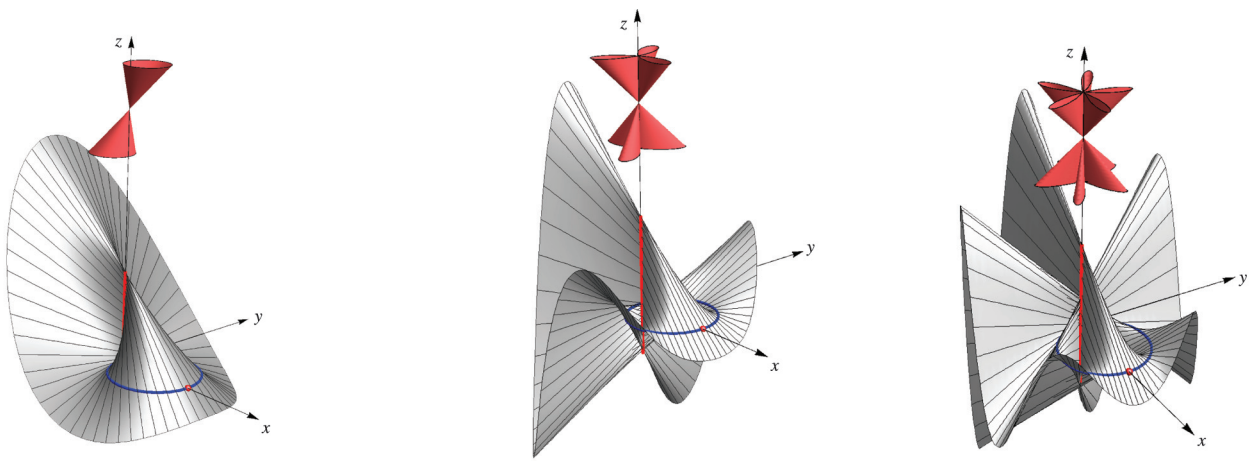

a b c

Figure 17: *The pedal ruled surfaces for the pole* $P(2,0,0)$, *axis z and 1, 3 and 5-petalled roses in the plane at infinity are shown in figures a, b and c, respectively. These directing roses are the curves at infinity of the highlighted red cones.*

5 Pedal surfaces of K_3^1

5.1 Congruence K_3^1

Twisted cubics k^3 may be divided into four types according to the different sections of the curve by the plane at infinity. These are the *cubical parabola*, *cubical hyperbolic parabola*, *cubical ellipse* and *cubical hyperbola* if the plane at infinity meets the curve at three coincident points, at two coincident points and one real point, at one real and two imaginary points and at three real and different points, respectively [15, p. 353].

Below we will use the following canonical form of a twisted cubic $k^3 = (k_1(t), k_2(t), k_3(t))$

$$\mathbf{k}(t) = \left(\frac{a_1 t}{k}, \frac{a_2 t + b_2 t^2}{k}, \frac{a_3 t + b_3 t^2 + c_3 t^3}{k}\right),\ t \in \mathbb{R}, \qquad (22)$$

where k equals 1, $1-t$, $1+t^2$ or $1-t^2$ which specify a cubical parabola, cubical parabolic hyperbola, cubical ellipse or cubical hyperbola, respectively [4, pp. 69-76], [8, p. 928]. Specially, for $k = 1+t^2$, $a_1 = b_2$, $a_2 = b_3 = 0$, $a_3 = c_3$, eq. (22) represents a cubical circle.

These curves for $a_1 = b_2 = c_3 = 1$ and $a_2 = a_3 = b_3 = 0$, lying on the corresponding 2nd degree cones, are shown in Fig. 18.

The union of the tangent and secant lines of a twisted cubic k^3 fill up the projective space $\mathbb{P}^3$ and the lines are pairwise disjoint, except at the points of the curve itself [10, p. 90]. Thus, the system of lines meeting a twisted cubic twice is the 1st order 3rd class congruence K_3^1 with the singular points on the directing curve k^3. The rays of K_3^1 can be expressed by the following equations:

$$\frac{x-k_1(u)}{k_1(v)-k_1(u)} = \frac{y-k_2(u)}{k_2(v)-k_2(u)} = \frac{z-k_3(u)}{k_3(v)-k_3(u)}, \qquad (23)$$
$$(u,v) \in \mathbb{R}^2.$$

5.2 Pedal surface PK_2^5

Let P be any finite point in $\mathbb{E}^3$ and k^3 the directing curve of K_3^1. The pedal surface of K_3^1 with respect to the pole P is denoted PK_2^5. The rays of K_3^1 through any point $K \in k^3$ form a 2nd degree cone ζ_K with the vertex K (see Fig. 19a). The feet of the perpendiculars from P on the rulings of ζ_K lie on the sphere σ_K with the diameter $\overline{PK}$. Thus, we can regard the pedal surfaces PK_2^5 as the system of the 1st kind of quartic curves – the intersection curves of ζ_K and σ_K (see Fig. 19b).

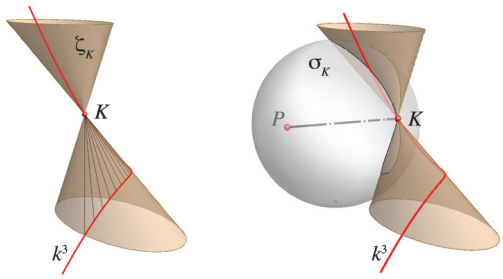

a b

Figure 19: *The rays of K_3^1 through $K \in k^3$ form a 2nd degree cone ζ_K with the vertex K (a). σ_K is a sphere with the diameter $\overline{PK}$. The intersection curve of ζ_K and σ_K lies on the pedal surface PK_3^5 (b).*

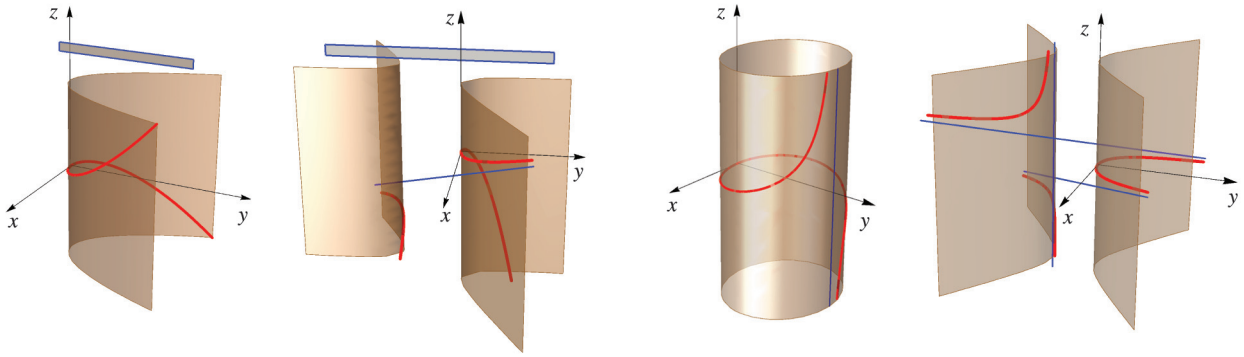

a b c d

Figure 18: *The cubical parabola, parabolic hyperbola, ellipse and hyperbola are shown in figures a, b, c and d, respectively. Their points at infinity are:* $(0:0:1:0)$ *counted three times in case a,* $(1:1:1:0)$ *and* $(0:0:1:0)$ *counted twice in case b,* $(0:0:1:0)$ *and the pair of imaginary points* $(\pm i:-1:\mp i:0)$ *in case c and* $(\pm 1:1:\pm 1:0)$, $(0:0:1:0)$ *in case d, where the points are expressed in standard homogeneous Cartesian coordinates.*

Proposition 9 *The pedal surface PK_2^5 is a 5th order surface passing through the pole P and the absolute conic.*

PROOF: The proof of this proposition is given in [11]. □

Proposition 10 *The twisted cubic k^3 is the double curve of PK_2^5 and ten pinch-points exist on it.*

PROOF: For every point $K \in k^3$, the intersection curve of ζ_K and σ_K is a 4th order space curve with the double point K. The tangent lines of this curve at K are the intersection rulings of the cone ζ_K and the plane through K perpendicular to PK. Thus, there are two tangent planes of PK_2^5 at $K \in k^3$, determined by the tangent line of k^3 at K and two tangent lines of the curve $\zeta_K \cap \sigma_K$ at K. If the two tangent lines of $\zeta_K \cap \sigma_K$ at K are real and different, coinciding or imaginary, K is the binodal point, pinch-point or isolated point of PK_2^5, respectively (see Fig. 20). The proof that on a 5th order surface with a double twisted cubic ten pinch-points can exist is given in [18, p. 312]. These points can be real or imaginary. □

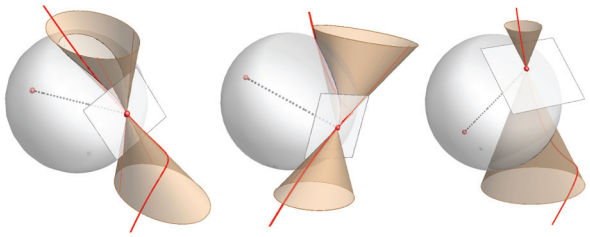

a b c

Figure 20: *On the twisted cubic the intersection curve of σ and ζ has a node, cusp or isolated double point shown in figure a, b and c, respectively.*

Proposition 11 *If the pole P lies on the directing curve k^3, P is the triple point of PK_2^5.*

PROOF: It is clear that if $P \in k^3$, then every curve $\zeta_K \cap \sigma_K$, $K \in k^3$ passes through P. The tangent lines of $\zeta_K \cap \sigma_K$ at P are the result of an $(1,1)$ correspondence between one second degree envelope cone with the vertex P and one pencil of planes through the line passing through P. Thus, according to the Chasles formula [13, p. 40], these tangent lines form a third degree cone with a vertex P. Namely, every tangent line of $\zeta_K \cap \sigma_K$ at P is the intersection of the plane through P perpendicular to PK (the tangent plane of σ_K at P), and the tangent plane of ζ_K at P. The planes through P perpendicular to PK, $K \in k^3$ form a second degree envelope cone with a vertex P. Since the tangent planes of ζ_K at P are determined by the lines PK and t_P, where t_P is the tangent line of k^3 at P, they form the pencil of planes $[t_P]$. □

Proposition 12 *The ray at infinity of K_3^1 lies on the pedal surface PK_3^5.*

PROOF: Orthogonality in Euclidean space means polarity with respect to the absolute conic – a line l with the point at infinity L^∞ is perpendicular to a plane π with the line at infinity p^∞ iff L^∞ is the pole of p^∞ with respect to the absolute conic. Every ray of K_3^1 cuts PK_3^5 at two double points on k^3 and the intersection point with the corresponding plane through P perpendicular to this ray. Since the ray at infinity corresponds with the pencil of planes, every point on it lies on PK_3^5. □

According to the straight lines at infinity, we divide the pedal surfaces PK_3^5 into the following four types:

Type I PK_3^5 has one real straight line counted three times at infinity. The directing curve k^3 is a cubical parabola.

Type II PK_3^5 has two real straight lines at infinity, and one of them is counted twice. The directing curve k^3 is a cubical hyperbolic parabola.

Type III PK_3^5 has one real and a pair of imaginary straight lines at infinity. The directing curve k^3 is a cubical ellipse.

Type IV PK_3^5 has three real and different straight lines at infinity. The directing curve k^3 is a cubical hyperbola.

5.3 Parametric and implicit equations of PK_2^5

Let the pole P be given by the vector $\mathbf{p} = (p_x, p_y, p_z)$, and let the directing line k^3 of K_3^1 be the twisted cubic given by the vector function (22). The ray of K_3^1 passing through the points $K(u), K(v) \in k^3$ can be expressed by the following equation:

$$\mathbf{r}_1(u,v) = \mathbf{k}(u) + s\,\mathbf{d}(u,v), \quad s \in \mathbb{R}, \tag{24}$$

where $\mathbf{d}(u,v)$ is the direction vector of the line $K(u)K(v)$, i.e. $\mathbf{d}(u,v) = \mathbf{k}(v) - \mathbf{k}(u)$.

The plane through the pole P, perpendicular to the ray $K(u)K(v)$, is given by the following vector equation:

$$(\mathbf{r}_2(u,v) - \mathbf{p}) \cdot \mathbf{d}(u,v) = 0. \tag{25}$$

Since the point on the pedal surface PK_2^5 is the intersection of the ray (24) and the plane (25), for this point the parameter s satisfies the following equation:

$$s(u,v) = \frac{(\mathbf{p} - \mathbf{k}(u)) \cdot \mathbf{d}(u,v)}{\|\mathbf{d}(u,v)\|^2}. \tag{26}$$

Thus, the parametric equations of PK_2^5 are:

$$\begin{aligned} x(u,v) &= k_1(u) + d_1(u,v) \cdot s(u,v) \\ y(u,v) &= k_2(u) + d_2(u,v) \cdot s(u,v) \\ z(u,v) &= k_3(u) + d_3(u,v) \cdot s(u,v), \quad (u,v) \in \mathbb{R}^2. \end{aligned} \tag{27}$$

This parametrization does not yield satisfactory *Mathematica* visualizations of PK_2^5. Therefore, to draw figures 21 and 22 we used the implicit equations of PK_2^5 which can be derived from the equations of corresponding spheres σ and cones ζ.

For any point $K(t) \in k^3$, $t \in \mathbb{R}$, the implicit equation of the sphere $\sigma_{K(t)}$ is the following:

$$\left(x-\frac{p_x+k_1(t)}{2}\right)^2+\left(y-\frac{p_y+k_2(t)}{2}\right)^2+\left(z-\frac{p_z+k_3(t)}{2}\right)^2=$$
$$\frac{1}{4}\left((p_x-k_1(t))^2+(p_y-k_2(t))^2+(p_z-k_3(t))^2\right). \qquad (28)$$

The implicit equation of the cone $\zeta_{K(t)}$ can be derived by eliminating parameters u and v from the following parametric equations:

$$x = k_1(t)+u\cdot d_1(t,v)$$
$$y = k_2(t)+u\cdot d_2(t,v)$$
$$z = k_3(t)+u\cdot d_3(t,v) \quad (u,v)\in\mathbb{R}^2. \qquad (29)$$

Now, if we eliminate the parameter t from the corresponding implicit equations of $\zeta_{K(t)}$ and $\sigma_{K(t)}$, we obtain the implicit equation of PK_3^5. According to propositions 9, 12 and theorem 1 this equation takes the following form:

$$(x^2+y^2+z^2)H_1^3(x,y,z)+H^4(x,y,z)$$
$$+H_2^3(x,y,z)+H^2(x,y,z)=0, \qquad (30)$$

where $H^i(x,y,z)$ are homogeneous polynomials of degree i. The equation $H_1^3(x,y,z)=0$ represents three rays of K_3^1 at infinity and $H^2(x,y,z)=0$ represents the tangent cone of PK_3^5 at the origin.

Equation (30) depends on nine parameters $(a_1,a_2,a_3, b_2,b_3,c_3,p_x,p_y,p_z)$ and it is incongruously to write them here even for the special cases. As an appendix to this paper, the reader can download one *Mathematica* notebook available on-line: `http://www.grad.hr/sgorjanc/pedalsKP53.nb`.

5.4 Examples of PK_2^5

We consider PK_2^5 where the directing twisted cubic is given by eq. (22) for

$$a_1=b_2=c_3=1, \quad a_2=a_3=b_3=0. \qquad (31)$$

Type I – the directing curve k^3 is a cubical parabola given by eqs. (22) and (31) for $k=1$. The pedal surface has a real line at infinity counted three times. In the standard Cartesian coordinates $(x:y:z:w)$, this line is given by the equations $x^3=0$, $w=0$. See Fig. 21a and Fig. 22a.

Type II – the directing curve k^3 is a cubical hyperbolic parabola given by eqs. (22) and (31) for $k=1-t$. The pedal surface has two real lines, one of them counted twice, at infinity. They are given by the equations $x(x-y)^2=0$, $w=0$. See Fig. 21b and Fig. 22b.

Type III – the directing curve k^3 is a cubical ellipse given by eqs. (22) and (31) for $k=1+t^2$. The pedal surface has one real and a pair of imaginary lines at infinity. They are given by the equations $(x^2+y^2)(x+z)=0$, $w=0$. See Fig. 21c and Fig. 22c.

Type IV – the directing curve k^3 is a cubical hyperbola given by eqs. (22) and (31) for $k=1-t^2$. The pedal surface has three real lines at infinity. They are given by the equations $(x-y)(x+y)(x-z)=0$, $w=0$. See Fig. 21d and Fig. 22d.

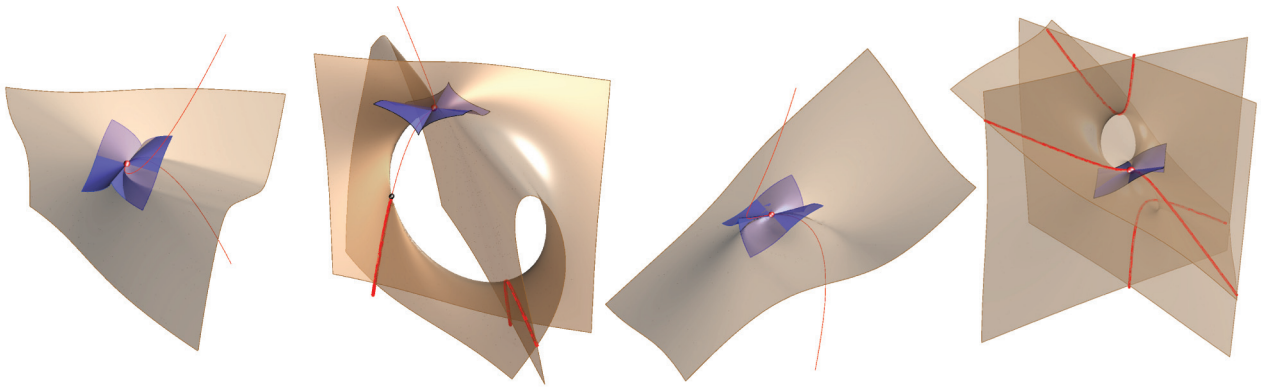

a b c d

Figure 19: *PK_3^5 of types I, II, III and IV, for $P(0,0,0)$, are shown in figures a, b, c and d, respectively. The 3rd degree tangent cone at P has a cuspidal edge.*

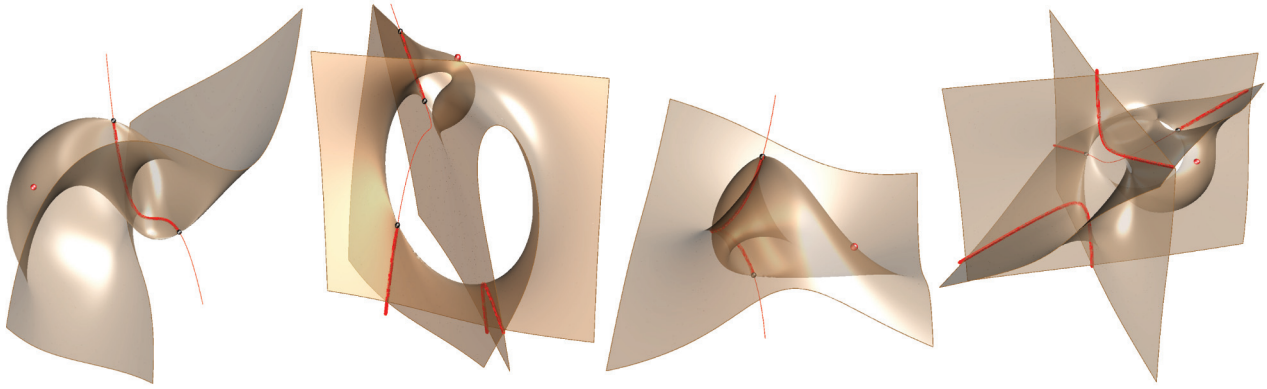

a b c d

Figure 22: *Figure a – PK_3^5 type I for $P(4,4,0)$; figure b – PK_3^5 type II for $P(2,-1,3)$; figure c – PK_3^5 type III for $P(1,2,0)$; figure d – PK_3^5 type IV for $P(5,-1,3)$.*

References

[1] V. BENIĆ, S. GORJANC, Inversion of degree $n+2$. Acta Mathematica Hungarica, **122** , 3, 237-253, (2009)

[2] V. Benić, S. Gorjanc, (1,n) Congruences. KoG, 10 , 5-12, (2006)

[3] Encyclopaedia of Mathematics - SpringerLink. Edited by M. Hazewinkel, available on-line: http://eom.springer.de/C/c024910.htm

[4] K. FLADT, A. BAUR, Analytische Geometrie spezieller Flächen und Raumkurven. Friedr. Vieweg & Sohn, Braunschweig, (1975)

[5] S. GORJANC, V. BENIĆ, Special Sextics with Quadruple Line, Math. Commun. Vol. **14**, No. 1, 85-103, (2009)

[6] S. GORJANC, Classification of the Pedal Surfaces of (1,2) Congruences. PhD thesis, Mathematical department, Faculty of Science, University of Zagreb, (2001) (in Croatian).

[7] S. GORJANC, Special nth Order Surfaces with (n-2)-ple Line. Proc. of 13th International Conference on Geometry and Graphics, Dresden, (2008)

[8] A. GRAY, Modern Differential Geometry of Curves and Surfaces with Mathematica. CRC Press, Boca Raton, (1998)

[9] J. HARRIS, Algebraic Geometry. Springer, New York, (1995)

[10] J. HARRIS, Algebraic Geometry: A First Course. Springer, New York, (1992)

[11] E. KRANJČEVIĆ, Die Fusspunktflächen der linearen Kongruenzen, Glasnik matematički, 3 (23), 269-274, (1968)

[12] G. LORIA, Spezielle algebraische und transzendente ebene Kurven. B. G. Teubner, Leipzig-Berlin, (1910)

[13] E. MÜLLER, J. L. KRAMES, Konstruktive Behandlung der Regelflächen, Franc Deuticke, Leipzig und Wien, (1931)

[14] V. NIČE, Synthetic Geometry, Školska knjiga, Zagreb, (1956) (in Croatian).

[15] G. SALMON, A Treatise on the Analytic Geometry of Three Dimensions, Vol.I., Chelsea Publishing Company, New York, (1958)

[16] G. SALMON, A Treatise on the Analytic Geometry of Three Dimensions, Vol.II. Chelsea Publishing Company, New York, (1965)

[17] G. SALMON, Higher Plane Curves. Chelsea Publishing Company, New York, (1960)

[18] R. STURM, Die Lehre von den geometrischen Verwandtschaften, Band IV. B. G. Taubner, Leipzig-Berlin, (1909)

[19] R. STURM, Liniengeometrie, II. Teil. B. G. Taubner, Leipzig, (1893)

[20] R. VIHER, On the Multiple Roots of the 4th Degree Polynomial, KoG, 11, 25-31,(2007)

[21] Wikipedia – The Free Encyclopedia. Available on-line: http://en.wikipedia.org/wiki/Integer_partition

[22] K. ZINDLER, Algebraische Liniengeometrie, Encyklopädie der Mathematischen Wissenschaften, Band III, 2. Teil, 2. Hälfte. A., pp. 1184-1185, B. G. Teubner, Liepzig, (1921-1928)

Sonja Gorjanc

Faculty of Civil Engineering, University of Zagreb
Kačićeva 26, 10000 Zagreb, Croatia

e-mail: sgorjanc@grad.hr

The author would like to thank her colleague Vladimir Benić and Prof. Otto Röschel for their valuable suggestions which have improved the quality of this paper.

Original scientific paper
Accepted 28. 12. 2009.

NORMAN JOHN WILDBERGER

Chromogeometry and Relativistic Conics

Chromogeometry and Relativistic Conics

ABSTRACT

This paper shows how a recent reformulation of the basics of classical geometry and trigonometry reveals a three-fold symmetry between Euclidean and non-Euclidean (relativistic) planar geometries. We apply this *chromogeometry* to look at conics in a new light.

Key words: chromogeometry, conics, relativistic geometry

MSC 2010: 51N25, 83A05

Kromogeometrija i relativističke konike

SAŽETAK

U radu se pokazuje kako novija formulacija osnova klasične geometrije i trigonometrije otkriva trostruku simetriju između euklidske i neeuklidskih (relativističkih) ravninskih geometrija. Primjenjujemo kromogeometriju kako bismo konike vidjeli u novom svjetlu.

Ključne riječi: kromogeometrija, konike, relativistička geometrija

Pythagoras, area and quadrance

To measure a line segment in the plane, the ancient Greeks measured the *area of a square constructed on it*. Algebraically, the parallelogram formed by a vector $v = \overrightarrow{A_1A_2} = (a,b)$ and its perpendicular $B(v) = (-b,a)$ has area

$$Q = \det \begin{pmatrix} a & b \\ -b & a \end{pmatrix} = a^2 + b^2. \qquad (1)$$

The Greeks referred to building squares as 'quadrature', and so we say that Q is the **quadrance** of the vector v, or the quadrance $Q(A_1,A_2)$ between A_1 and A_2. This notion makes sense over any field.

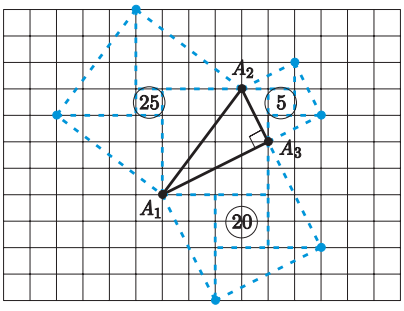

Figure 1: *Pythagoras' theorem:* $5 + 20 = 25$

If $Q_1 = Q(A_2,A_3)$, $Q_2 = Q(A_1,A_3)$ and $Q_3 = Q(A_1,A_2)$ are the quadrances of a triangle $\overline{A_1A_2A_3}$, then Pythagoras' theorem and its converse can together be stated as: A_1A_3 *is perpendicular to* A_2A_3 *precisely when*

$$Q_1 + Q_2 = Q_3.$$

Figure 1 shows an example where $Q_1 = 5$, $Q_2 = 20$ and $Q_3 = 25$. As indicated for the large square, these areas may also be calculated by subdivision and (translational) rearrangement, followed by counting cells.

There is a sister theorem—the *Triple quad formula*—that Euclid did not know, but which is fundamental for *rational trigonometry*, introduced in [2]: A_1A_3 *is parallel to* A_2A_3 *precisely when*

$$(Q_1 + Q_2 + Q_3)^2 = 2\left(Q_1^2 + Q_2^2 + Q_3^2\right).$$

Figure 2 shows an example where $Q_1 = 5$, $Q_2 = 20$ and $Q_3 = 45$.

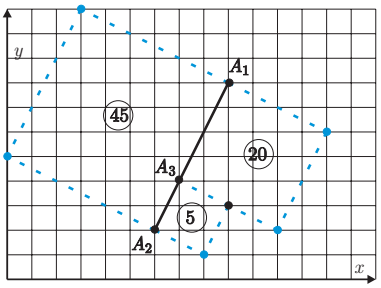

Figure 2: *Triple quad formula:* $(5 + 20 + 45)^2 = 2\left(5^2 + 20^2 + 45^2\right)$

In terms of side lengths $d_1 = \sqrt{Q_1}, d_2 = \sqrt{Q_2}$ and $d_3 = \sqrt{Q_3}$, and the semi-perimeter $s = (d_1 + d_2 + d_3)/2$, observe that

$$\begin{aligned}
&(Q_1+Q_2+Q_3)^2 - 2\left(Q_1^2+Q_2^2+Q_3^2\right)\\
&= 4Q_1Q_2 - (Q_1+Q_2-Q_3)^2 = 4d_1^2d_2^2 - \left(d_1^2+d_2^2-d_3^2\right)^2\\
&= \left(2d_1d_2 - \left(d_1^2+d_2^2-d_3^2\right)\right)\left(2d_1d_2 + \left(d_1^2+d_2^2-d_3^2\right)\right)\\
&= \left(d_3^2 - (d_1-d_2)^2\right)\left((d_1+d_2)^2 - d_3^2\right)\\
&= (d_3-d_1+d_2)(d_3+d_1-d_2)(d_1+d_2-d_3)(d_1+d_2+d_3)\\
&= 16(s-d_1)(s-d_2)(s-d_3)s.
\end{aligned}$$

Thus Heron's formula in the usual form

$$\text{area} = \sqrt{s(s-d_1)(s-d_2)(s-d_3)}$$

may be restated in terms of quadrances as

$$\begin{aligned}
16\,\text{area}^2 &= (Q_1+Q_2+Q_3)^2 - 2\left(Q_1^2+Q_2^2+Q_3^2\right)\\
&\equiv A(Q_1,Q_2,Q_3).
\end{aligned}$$

This more fundamental formulation deserves to be called **Archimedes' theorem**, since Arab sources indicate that Archimedes knew Heron's formula. The Triple quad formula is the special case of Archimedes' theorem when the area is zero. The function $A(Q_1,Q_2,Q_3)$ will be called **Archimedes' function**.

In Figure 3 the quadrances are $Q_1 = 13$, $Q_2 = 25$ and $Q_3 = 26$, so $16\,\text{area}^2 = 1156$, giving $\text{area}^2 = 289/4$ and $\text{area} = 17/2$.

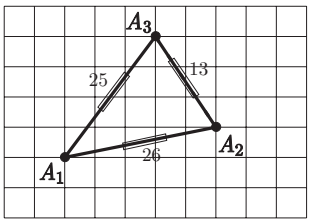

Figure 3: $16\,\text{area}^2 = (13+25+26)^2 - 2\left(13^2+25^2+26^2\right)$
$= 1156$

Irrational side lengths are not needed to determine the area of a rational triangle, and in any case when we move to more general geometries, we have no choice but to give up on distance and angle.

Blue, red and green geometries

Euclidean geometry will here be called **blue geometry**. We now introduce two relativistic geometries, called *red* and *green*, which arise from Einstein's theory of relativity. These rest on alternate notions of perpendicularity, but they share the same underlying affine concept of area as blue geometry, and indeed the same laws of rational trigonometry, as will be explained shortly.

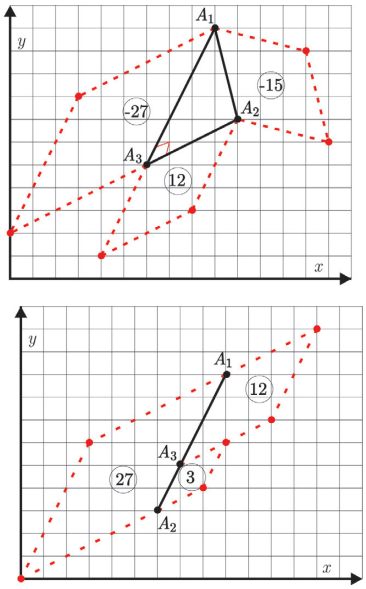

Figure 4: *Red Pythagoras' theorem and Triple quad formula*

Define the vector $v = \overrightarrow{A_1A_2} = (a,b)$ to be **red perpendicular** to $R(v) = (b,a)$. This mapping is easily visualized: it corresponds to Euclidean reflection in a line of slope 1 or -1. A **red square** is then a parallelogram with sides v and $R(v)$, and hence (signed) area

$$Q^{(r)} = \det\begin{pmatrix} a & b \\ b & a \end{pmatrix} = a^2 - b^2 \tag{2}$$

which we call the **red quadrance** between A_1 and A_2. Figure 4 illustrates that both Pythagoras' theorem and the Triple quad formula hold also using red quadrances and red perpendicularity, where the areas of the red squares can be computed as before by subdivisions, (translational) rearrangement and counting cells—or by applying the algebraic formula for the red quadrance.

In a similar fashion the vector $v = \overrightarrow{A_1A_2} = (a,b)$ is **green perpendicular** to $G(v) = (-a,b)$. This corresponds to Euclidean reflection in a vertical or horizontal line. A **green square** is a parallelogram with sides v and $R(v)$, and hence (signed) area

$$Q^{(g)} = \det\begin{pmatrix} a & b \\ -a & b \end{pmatrix} = 2ab \tag{3}$$

which we call the **green quadrance** between A_1 and A_2.

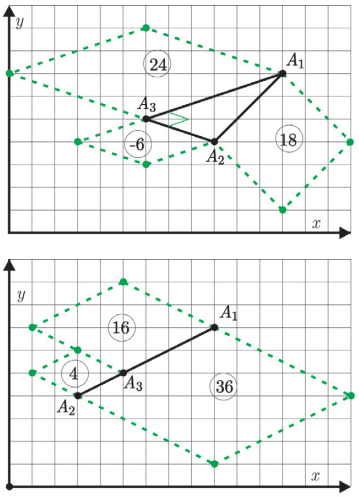

Figure 5: *Green Pythagoras' theorem and Triple quad formula*

Figure 5 shows Pythagoras' theorem and the Triple quad formula in the green context. This version of relativistic geometry corresponds to a basis of null vectors in red geometry.

All three geometries can be defined over a general field, not of characteristic two.

Spreads and rational trigonometry

The three quadratic forms

$$Q^{(b)}(a,b) = a^2 + b^2$$
$$Q^{(r)}(a,b) = a^2 - b^2$$
$$Q^{(g)}(a,b) = 2ab$$

have corresponding dot products

$$(a_1,b_1) \cdot_b (a_2,b_2) \equiv a_1a_2 + b_1b_2$$
$$(a_1,b_1) \cdot_r (a_2,b_2) \equiv a_1a_2 - b_1b_2$$
$$(a_1,b_1) \cdot_g (a_2,b_2) \equiv a_1b_2 + a_2b_1.$$

Together with $a_1b_2 - a_2b_1 = 0$ describing parallel vectors, these are the four simplest bilinear expressions in the four variables.

In rational trigonometry, one wants to work over general fields, so the notion of angle is not available, but it is important to realize that the dot product is not necessarily the best replacement. Instead we introduce the related notion of *spread* between two lines (not between rays), which in the blue framework is the square of the sine of the angle between the lines (there are actually many such angles, but the square of the sine is the same for all).

The **blue, red** and **green spreads** between lines l_1 and l_2 with equations

$$a_1x + b_1y + c_1 = 0 \qquad \text{and} \qquad a_2x + b_2y + c_2 = 0$$

are respectively the numbers

$$s^{(b)}(l_1,l_2) = \frac{(a_1b_2 - a_2b_1)^2}{(a_1^2 + b_1^2)(a_2^2 + b_2^2)}$$
$$s^{(r)}(l_1,l_2) = -\frac{(a_1b_2 - a_2b_1)^2}{(a_1^2 - b_1^2)(a_2^2 - b_2^2)}$$
$$s^{(g)}(l_1,l_2) = -\frac{(a_1b_2 - a_2b_1)^2}{4a_1b_1a_2b_2}.$$

These quantities are undefined when the denominators are zero. The negative signs in front of $s^{(r)}$ and $s^{(g)}$ insure that, for each of the colours, the *spread at any of the three vertices of a right triangle (one with two sides perpendicular) is the quotient of the opposite quadrance by the hypotenuse quadrance*. See [3] for a proof of this, and other facts about rational trigonometry, in a wider context.

In Figure 1 the spreads at A_1 and A_2 are $1/5$ and $4/5$ respectively, in the upper diagram of Figure 4 the spreads at A_1 and A_2 are $-4/5$ and $9/5$ respectively, and in the upper diagram of Figure 5 the spreads at A_1 and A_2 are $-1/3$ and $4/3$ respectively. In each case the spread at the right vertex is 1, and the other two spreads sum to 1.

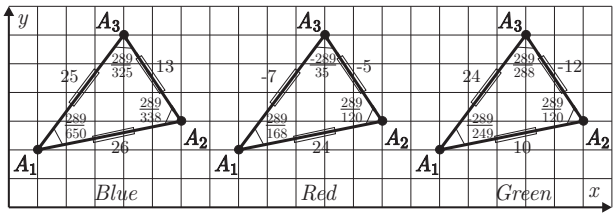

Figure 6: *Blue, red and green quadrances and spreads*

Figure 6 allows you to compare the various quadrances and spreads of a fixed triangle in each of the three geometries. Note the common numerators of the spreads, arising because $A(Q_1,Q_2,Q_3) = \pm 4 \times 289$ is up to sign the same in each geometry, with a plus sign in the blue situation and a negative sign in the red and green ones.

Aside from Pythagoras' theorem and the Triple quad formula, the main laws of rational trigonometry are: for a triangle with quadrances Q_1, Q_2 and Q_3, and spreads s_1, s_2 and s_3 :

$$\frac{s_1}{Q_1} = \frac{s_2}{Q_2} = \frac{s_3}{Q_3} \quad \text{(Spread law)}$$

$$(Q_1 + Q_2 - Q_3)^2 = 4Q_1Q_2(1 - s_3) \quad \text{(Cross law)}$$

$$(s_1 + s_2 + s_3)^2 = 2(s_1^2 + s_2^2 + s_3^2) + 4s_1s_2s_3 \quad \text{(Triple spread formula).}$$

As shown in [2], these laws are derived using only Pythagoras' theorem and the Triple quad formula. Since these latter two results hold in all three geometries, the Spread law, Cross law and Triple spread formula also hold in all three geometries.

For any points A_1 and A_2 the square of $Q^{(b)}(A_1,A_2)$ is the sum of the squares of $Q^{(r)}(A_1,A_2)$ and $Q^{(g)}(A_1,A_2)$, and for any lines l_1 and l_2

$$\frac{1}{s^{(b)}(l_1,l_2)}+\frac{1}{s^{(r)}(l_1,l_2)}+\frac{1}{s^{(g)}(l_1,l_2)}=2.$$

The first statement follows from the Pythagorean triple identity

$$\left(x^2+y^2\right)^2=\left(x^2-y^2\right)^2+(2xy)^2$$

while the latter follows from the identity

$$\left(a_1^2+b_1^2\right)\left(a_2^2+b_2^2\right)-\left(a_1^2-b_1^2\right)\left(a_2^2-b_2^2\right)-4a_1b_1a_2b_2$$
$$=(a_1b_2-a_2b_1)^2.$$

So in Figure 6 there are three linked (signed) Pythagorean triples, namely $(13,-5,-12)$, $(25,-7,24)$ and $(26,24,10)$, and three triples of harmonically related spreads.

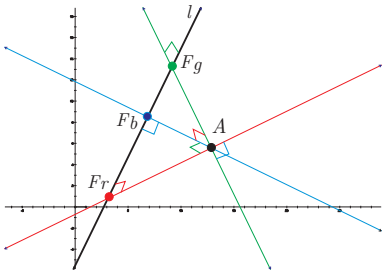

Figure 7: *Three altitudes from a point to a line*

Figure 7 shows the three coloured altitudes from a point A to a line l, and the feet of those altitudes. Note that the blue and red altitudes are green perpendicular and similarly for the other colours. The three triangles formed by the four points are each **triple right triangles**, containing each a blue, red and green right vertex.

Most theorems of planar Euclidean geometry have universal versions, valid in each of the three geometries. *This is a large claim that deserves further investigation*. In the red and green geometries, circles and rotations become rectangular hyperbolas and Lorentz boosts. There are no equilateral triangles in the red and green geometries, so results like Napoleon's theorem or Morley's theorem will not have (obvious) analogs.

To see some chromogeometry in action, let's have a look at conics in this more general framework.

The ellipse as a grammola

In the real number plane, one usually defines an *ellipse* as the locus of a point X whose ratio of distance from a fixed point (focus) to distance from a fixed line (directrix) is constant and less than one, and hyperbolas and parabolas similarly with eccentricities greater than one and equal to one. By squaring this condition, we can discuss the locus of a point whose ratio of *quadrance* from a fixed point to a fixed line is constant. By quadrance from a point X to a line l we mean the obvious: construct the altitude line n from X to l, find its foot F and measure $Q(X,F)$. Let's call such a locus a **conic section**. Over a general field we cannot distinguish 'ellipses' from 'hyperbolas', although parabolas are always well defined.

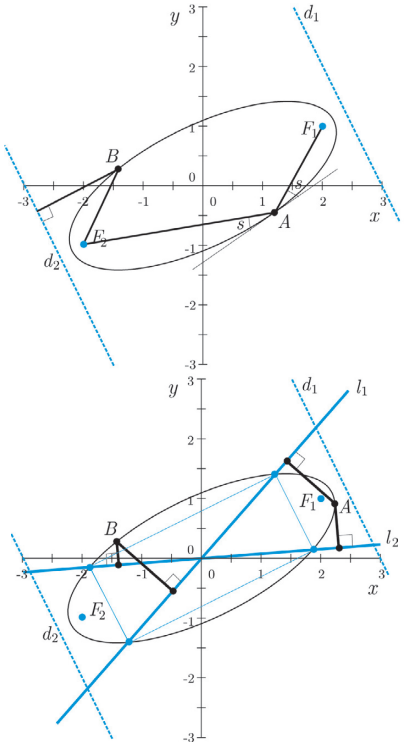

Figure 8: *Two views of the ellipse* $2x^2-4xy+5y^2=6$

The upper diagram in Figure 8 shows the central ellipse

$$2x^2-4xy+5y^2=6$$

with foci at $F_1=[2,1]$ and $F_2=[-2,-1]$, corresponding directrices d_1 and d_2 with respective equations $2x-y+6=0$ and $2x-y-6=0$, and eccentricity $e=\sqrt{5/6}$. The familiar reflection property may be recast as: *spreads* between a tangent and lines to the foci from a point on the ellipse are equal.

The lower diagram in Figure 8 illustrates a (perhaps?) novel definition of an ellipse. It is motivated by the fact that a circle is the locus of a point X whose quadrances to two fixed perpendicular lines add to a constant. Define a **grammola** to be the locus of a point X such that the sum of the quadrances from X to two fixed non-perpendicular intersecting lines l_1 and l_2 is constant. This definition works for each of the three colours. It turns out that the lines l_1 and l_2 are unique; we call them the **diagonals** of the grammola (see [2, Chapter 15]). The **corners** of the grammola are the points where the diagonal lines intersect it, and determine the **corner rectangle**. In the blue setting over the real numbers a grammola is always an *ellipse*, while in the red and green settings a grammola might be an ellipse, or it might be a hyperbola.

The ellipse of Figure 8 is a blue grammola with blue diagonals

$$\left(14+5\sqrt{6}\right)x-23y=0 \quad \text{and} \quad \left(14-5\sqrt{6}\right)x-23y=0.$$

The blue quadrances of the sides of the corner rectangle are 12 and 2, whose product 24 is the squared area. The lower diagram in Figure 8 shows the usual foci and directrices of the grammola and its diagonals and corners. The quadrances from any point on the conic to the two diagonals sum to 6. The blue spread between the two diagonals is an invariant of the ellipse—in this case $s_b = 24/49$.

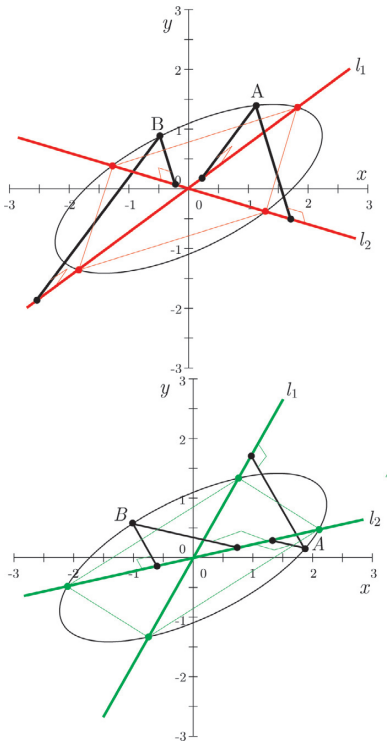

Figure 9: *Ellipse as red and green grammola*

The ellipse can also be described as a red grammola, as in the upper diagram of Figure 9. The red diagonals are

$$\left(\sqrt{22}+2\right)x-9y=0 \quad \text{and} \quad \left(\sqrt{22}-2\right)x+9y=0$$

and the **red corner rectangle** has sides parallel to the red axes of the ellipse, and red quadrances $3+\sqrt{33}$ and $3-\sqrt{33}$, whose product is -24. The four red corners have rather complicated expressions in this case. The red spread between the red diagonals is $s_r = -8/3$.

The same ellipse may also be viewed as a green grammola, as in the lower diagram of Figure 9. The green diagonals are

$$\left(-5+\sqrt{15}\right)x+5y=0 \quad \text{and} \quad \left(-5-\sqrt{15}\right)x+5y=0$$

and the **green corner rectangle** has sides parallel to the green axes of the ellipse, and green quadrances $4+2\sqrt{10}$ and $4-2\sqrt{10}$, whose product is again -24. Except for a sign, the three squared areas of the blue, red and green corner rectangles are the same. The green spread between the green diagonals is $s_g = -3/2$.

The relationship between the blue, red and green spreads of an ellipse is

$$\frac{1}{s_b}+\frac{1}{s_r}+\frac{1}{s_g}=1.$$

The ellipse as a quadrola

Another well known definition of an ellipse is as the locus of a point X whose sum of distances from two fixed points F_1 and F_2 is a constant k. To determine a universal analog of this, we consider the locus of a point X such that the quadrances $Q_1 = Q(F_1,X)$ and $Q_2 = Q(F_2,X)$, together with a number K, satisfy Archimedes formula $A(Q_1,Q_2,K)=0$. This is the quadratic analog to the equation $d_1+d_2=k$, just as the Triple quad formula is the analog to a linear relation between three distances.

Such a locus we call a **quadrola**. This algebraic formulation applies to the relativistic geometries, and also extends to general fields. The notion captures both that of ellipse and hyperbola in the Euclidean setting, and while it is in general a different concept than a grammola, it is possible for a conic to be both, as is the case of an ellipse in Euclidean (blue) geometry.

The upper diagram in Figure 10 shows that in the red geometry, a new phenomenon occurs: our same ellipse as a quadrola has *two pairs* of foci $\{F_1,F_2\}$ and $\{G_1,G_2\}$. Each of these points is also a focus in the context of a conic section, and there are two pairs of corresponding directrices $\{d_1,d_2\}$ and $\{h_1,h_2\}$. Directrices are parallel or red perpendicular, and intersect at points on the ellipse, and

tangents to these **directrix points** pass through two foci, forming a parallelogram which is both a *blue* and a *green rectangle*. It turns out that the red spreads between a tangent and lines to a pair of red foci are equal, as shown at points A and B.

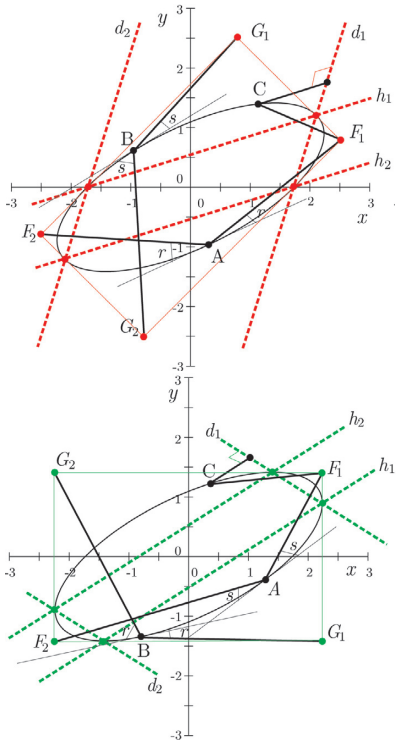

Figure 10: *Red and green foci and directrices*

The lower diagram in Figure 10 shows the same ellipse as a green quadrola, with again two pairs of green foci, two pairs of corresponding green directrices (which are parallel or green perpendicular), and the tangents at directrix points forming a blue and red rectangle.

The red and green directrix points are easy to find: they are the limits of the ellipse in the null and the coordinate directions. So the red and green directrices and foci are also then simple to locate geometrically. This is not the case for the usual (blue) foci and directrices, and suggests that considering ellipses from the relativistic perspectives can be practically useful. In algebraic geometry the 'other' pair of blue foci are not unknown; they require complexification and a projective view (see for example [1, Chapter 12]).

When we put all three coloured pictures together, as shown in Figure 11, another curious phenomenon appears—there are three pairs of coloured foci that appear to be close to the intersections of directrices of the opposite colour. The reason for this will become clearer later when we consider parabolas.

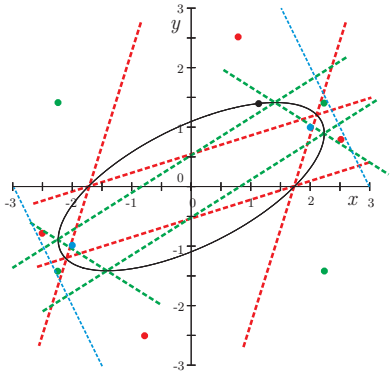

Figure 11: *Three sets of foci and directrices*

Hyperbolas

Over the real numbers some of what we saw with ellipses extends also to hyperbolas, although there are differences. The central hyperbola shown in Figure 12 with equation

$$7x^2 + 6xy - 17y^2 = 128$$

is a red quadrola with red foci $F_1 = [3,1]$ and $F_2 = [-3,-1]$, meaning that it is the locus of a point $X = [x,y]$ such that

$$A\left((x-3)^2 - (y-1)^2, (x+3)^2 - (y+1)^2, 64\right) = 0.$$

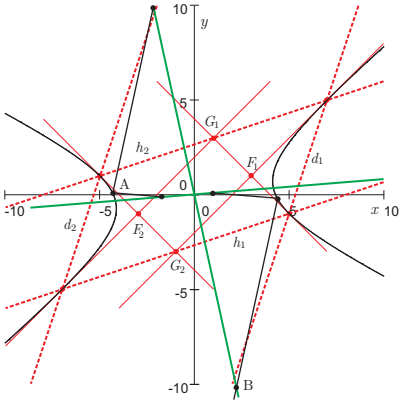

Figure 12: *A hyperbola as red quadrola and green grammola*

As a conic section the corresponding directrices have equations $3x - y - 16 = 0$ and $3x - y + 16 = 0$. This hyperbola also has another pair of red foci $G_1 = [1,3]$ and $G_2 = [-1,-3]$, with associated directrices $x - 3y + 8 = 0$ and $x - 3y - 8 = 0$.

As in the case of the ellipse we considered earlier, in each case the focus is the pole of the corresponding directrix,

meaning that it is the intersection of the tangents to the hyperbola at the directrix points. These tangents pass through two foci at a time, and are parallel to the red null directions. The parallelogram formed by the four foci is a blue and green rectangle.

So we could have found the red foci and directrices purely geometrically, by finding those points on the hyperbola where the tangents are parallel to the red null directions, and then forming intersections between these points. This is again quite different from finding the usual blue foci and directrices. Note that if we try to find green foci, vertical tangents are easy to find, but there are no horizontal tangents, thus the situation will necessarily be somewhat different.

Is the hyperbola also a grammola? It cannot be a blue grammola, since these are all ellipses, and it turns out not to be a red grammola either. But it *is* a green grammola with equation

$$\frac{\left(\left(119+8\sqrt{238}\right)x+51y\right)^2}{2\left(119+8\sqrt{238}\right)51}+\frac{\left(\left(119-8\sqrt{238}\right)x+51y\right)^2}{2\left(119-8\sqrt{238}\right)51}=\frac{128}{3}.$$

The green diagonals are shown in Figure 12.

The parabola

From the viewpoint of universal (affine) geometry, the most interesting conic is the *parabola*. Given a point F and a generic line l not passing through F, the locus of a point X such that $Q(X,F)=Q(X,l)$ is what we usually call a parabola, independent of which geometry we are considering. The generic parabola has a distinguished blue, red and green focus, and also a blue, red and green directrix.

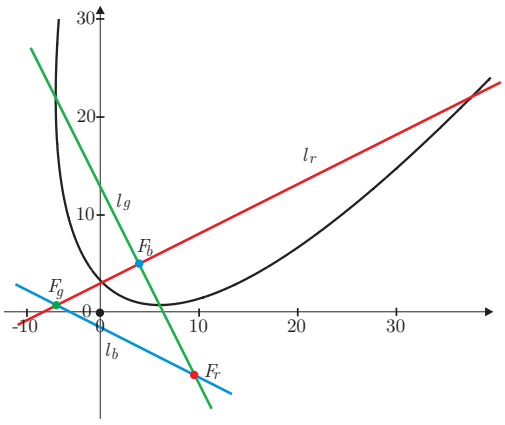

Figure 13: *Three foci and directrices of a parabola*

Figure 13 shows a parabola in the Cartesian plane and all three foci and directrices. A remarkable phenomenon appears: F_b is the intersection of l_r and l_g, F_r is the intersection of l_b and l_g, and F_g is the intersection of l_b and l_r. Furthermore l_r and l_g are blue perpendicular, l_b and l_g are red perpendicular, and l_b and l_r are green perpendicular—in other words we get a triple right triangle of foci. This means that once we know one of the focus/directrix pairs, the other two can be found simply by constructing the appropriate altitudes from the focus to the directrix together with their feet.

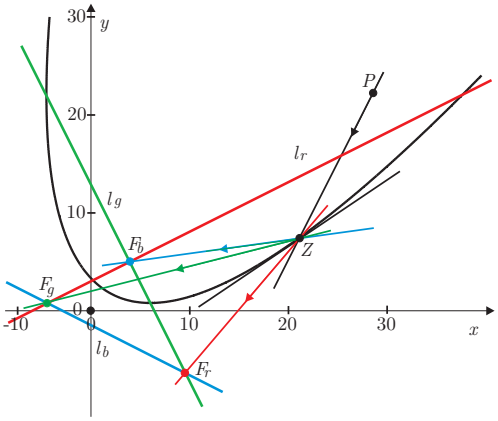

Figure 14: *Reflection properties of a parabola*

Although the various directrices are in different directions, the *axis* direction, defined as being perpendicular to the directrix, is common to all. Figure 14 shows the familiar reflection property of the parabola, where a particle P approaching the parabola along the axis direction and reflecting off the tangent (in either a blue, red or green fashion) always then passes through the corresponding focus.

The Figure 15 shows some interesting collinearities associated to a parabola, involving coloured vertices V (intersections of axes with the parabola), bases X (intersections of axes with directrices) and points Y formed by tangents to vertices.

Finally we show the three parabolas which have a given focus F and a given directrix l, both in black, each interpreted in one of the three geometries. Each of the three parabolas that share this focus and directrix have a focal triangle consisting of F and two of the feet of the altitudes from F to l, labelled F_b, F_r and F_g. The dotted line passes through the intersections of the red and green parabolas. Various vertices and axes are shown, and we leave the reader to notice interesting collinearities, and to try to prove them.

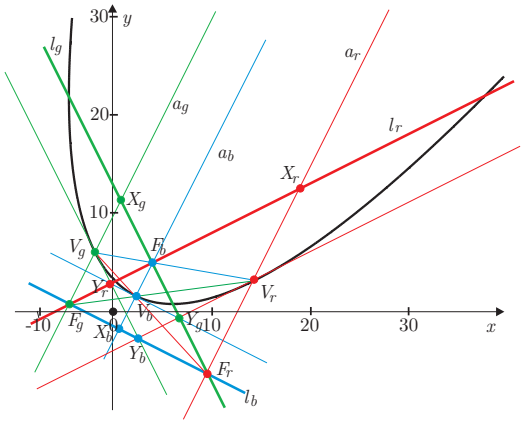

Figure 15: *Collinearities for a chromatic parabola*

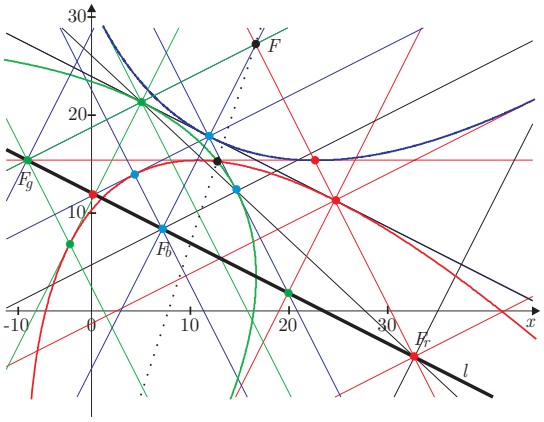

Figure 16: *Three parabolas with a common focus and directrix*

In conclusion, there may very well be other useful metrical definitions of conics; there are certainly still many rich discoveries to be made about these fascinating and most important geometric objects. Chromogeometry extends to many other aspects of planar geometry, for example to triangle geometry in [4].

References

[1] C. G. GIBSON, *Elementary Geometry of Algebraic Curves*, Cambridge University Press, Cambridge, 1998.

[2] N. J. WILDBERGER, *Divine Proportions: Rational Trigonometry to Universal Geometry*, Wild Egg Books, Sydney, 2005, http://wildegg.com.

[3] N. J. WILDBERGER, *Affine and projective universal geometry* (to appear, J. of Geometry), arXiv:math/0612499

[4] N. J. WILDBERGER, *Chromogeometry*, The Mathematical Intelligencer, DOI: 10.1007/s00283-009-9077-3, published online, 2009.

Norman John Wildberger
School of Mathematics and Statistics
UNSW Sydney 2052 Australia
e-mail: n.wildberger@unsw.edu.au

Stručni rad
Prihvaćeno 1. 12. 2009.

ŽELJKO GJURANIĆ

Konike i grafovi nekih polinoma pomoću NURBS krivulja

Conics and Graphs of Some Polynomials by Using NURBS Curves

ABSTRACT

This paper presents the definition of conics and the graphs of the 3rd and 4th degree polynomials by using NURBS curves, with a special description of the beam deflection line. The usage in AutoCAD is presented.

Key words: conics, NURBS curves, AutoCAD, beam deflection line

MSC 2010: 14Q05, 74B05, 65D17

Konike i grafovi nekih polinoma pomoću NURBS krivulja

SAŽETAK

U radu se prikazuje način zadavanja konika i grafova polinoma trećeg i četvrtog stupnja pomoću NURBS krivulja, s posebnim osvrtom na prikaz progibne linije elastičnog nosača. Prikazana je upotreba u AutoCAD-u.

Ključne riječi: konike, NURBS krivulje, AutoCAD, progibna linija

1 Uvod

Potreba za crtanjem konika (elipsa, parabola, hiperbola) javlja se u gotovo svim tehničkim strukama, a naročito u građevinskoj. Iako su konike matematički jednostavno definirane, većina CAD alata sadrži naredbe za crtanje samo kružnice i elipse. Ostale konike i druge krivulje mogu se, pomoću CAD alata, aproksimativno prikazati provlačenjem glatke krivulje kroz niz točaka.
Ovaj rad objašnjava drukčije određivanje konika, te nešto složenijih krivulja višeg reda, s posebnim osvrtom na AutoCAD kao najrašireniji CAD alat.

2 NURBS krivulje

Zadani interval $[t_0,t_m]$ podijelimo na m dijelova i djelišne točke, koje nazivamo *čvorovima*, označimo $(t_0,t_1,\ldots,t_m)$. Bazne *B-Spline* funkcije $N_{i,j}$ $(i+j\le m)$ definirane su na sljedeći način:

- Ako je $j=1$, tada vrijedi

$$N_{i,1}(t)=\begin{cases}1, & t\in[t_i,t_{i+1}\rangle\\ 0, & t\notin[t_i,t_{i+1}\rangle\end{cases},\qquad t\in[t_0,\,t_m\rangle. \tag{1}$$

Naravno, ova relacija vrijedi ako je $t_i\neq t_{i+1}$, u protivnom je $N_{i,1}=0$.

- Ako je $j>1$ tada se funkcije $N_{i,j}$ računaju rekurzivno pomoću formule

$$N_{i,j}(t)=N_{i,j-1}\cdot\frac{t-t_i}{t_{i+j-1}-t_i}+N_{i+1,j-1}\cdot\frac{t_{i+j}-t}{t_{i+j}-t_{i+1}}, \tag{2}$$

gdje je $t\in[t_0,\,t_m\rangle$.

Ako među čvorovima ima jednakih, neki od gornjih pribrojnika biti će oblika $0/0$. Takve ćemo pribrojnike smatrati jednakim nuli. [3], [2]

NURBS = *Non Uniform Rational B-Spline* je parametarski definirana krivulja, najčešće kvadratna ili kubna. NURBS krivulja je zadana kontrolnim točkama, od kojih svaka ima koordinate i "težinu". Laički rečeno, krivulja se ponaša kao elastična nit, gdje kontrolne točke predstavljaju magnete čiji intenzitet ovisi o težini kontrolne točke (slika 1).

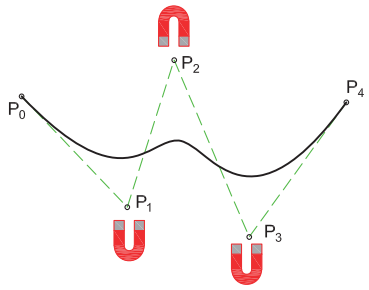

Slika 1: *NURBS krivulja*

Neka je $P_0, P_1, \ldots, P_n$ skup kontrolnih točaka, a $w = (w_0, w_1, \ldots, w_n)$ vektor težina tih točaka. Tada se NURBS krivulja definira izrazom:

$$C_k(t) = \frac{\sum_{i=0}^{n} w_i \cdot P_i \cdot N_{i,k}(t)}{\sum_{i=0}^{n} w_i \cdot N_{i,k}(t)}, \qquad (3)$$

gdje je $t \in [t_0,\ t_m\rangle$ i $m = n + k$.

Red krivulje k iznosi minimalno 2 (linearna krivulja). Krivulja drugog reda je neprekinuta, ali izlomljena, kontrolne točke su spojene ravnim linijama. Krivulja trećeg reda (kvadratna) je neprekinuta i glatka, te može točno predstaviti koniku. Najčešće je u upotrebi krivulja četvrtog reda (kubna), koja je neprekinuta, glatka, s kontinuiranom zakrivljenošću. Krivulje reda većeg reda od 6 općenito se izbjegavaju zbog numeričkih problema. [1], [2]

Većina CAD alata (uključujući AutoCAD) ne dozvoljava manipulaciju vektorom čvorova, koji je automatski generiran. Tako generiran vektor ima oblik {0,1,2,3,...} s tim da se prvi i zadnji član ponavljaju k puta. Broj elemenata vektora čvorova iznosi *red krivulje + broj kontrolnih točaka*.

Primjeri vektora čvorova:
3. red, 3 kontrolne točke $t_i = \{0,0,0,1,1,1\}$,
3. red, 4 kontrolne točke $t_i = \{0,0,0,1,2,2,2\}$,
4. red, 4 kontrolne točke $t_i = \{0,0,0,0,1,1,1,1\}$,
4. red, 5 kontrolnih točaka $t_i = \{0,0,0,0,1,2,2,2,2\}$.

Iz navedenog proizlaze određena svojstva NURBS krivulja:

- minimalni broj kontrolnih točaka jednak je redu krivulje,
- krivulja prolazi kroz prvu i zadnju kontrolnu točku,
- tangenta u prvoj točki prolazi drugom kontrolnom točkom,
- tangenta u zadnjoj točki prolazi predzadnjom kontrolnom točkom,
- više kontrolnih točaka s istim koordinatama smanjuje glatkoću krivulje, npr. ako kvadratna krivulja ima 2 kontrolne točke s istim koordinatama, krivulja će proći kroz te točke i na će tom mjestu postojati lom.

3 Konike

Sve konike su algebarske krivulje drugog stupnja, te se mogu odrediti pomoću NURBS krivulja zadanih baznim funkcijama drugog stupnja, odnosno NURBS krivuljama trećeg reda. Pošto u CAD alatima općenito nije moguće nacrtati beskonačnu krivulju, ovdje prikazujemo kako odrediti dio konike. Za određivanje dijela konike dovoljne su 3 kontrolne točke, osim za neke slučajeve kružnice i elipse.

3.1 Parabola

Od svih konika, pomoću NURBS krivulje, najjednostavije se određuje parabola (nazivnik u izrazu (3) jednak je 1). Prva i zadnja točka su rubne točke dijela parabole koji želimo prikazati, srednja točka je sjecište tangenata u prvoj i zadnjoj točki, a težine svih kontrolnih točaka moraju biti jednake 1.

U AutoCAD-u nije moguće direktno zadati kontrolne točke krivulje, stoga moramo koristiti slijedeći postupak:

1. Nacrtamo polyline kroz kontrolne točke (slika 2).
2. Odredimo red krivulje pomoću sistemske varijable `SPLINETYPE` –- moguće vrijednosti su 5 (bazne funkcije 2. stupnja) ili 6 (bazne funkcije 3. stupnja) (slika 3).
3. Pretvorimo polyline u segmentiranu krivulju pomoću naredbe `PEDIT`↩`L`↩`S`↩↩ (PEDIT, enter, slovo L, enter, slovo S, enter, enter) (slika 4).
4. Pretvorimo segmentiranu krivulju u spline pomoću naredbe `SPLINE`↩`O`↩`L`↩ (slika 5).

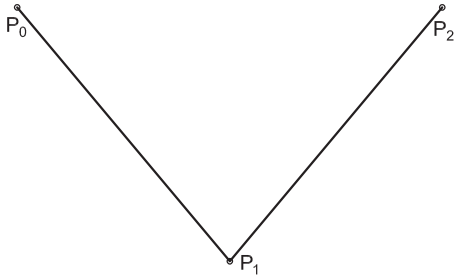

Slika 2: *Polyline kroz kontrolne točke*

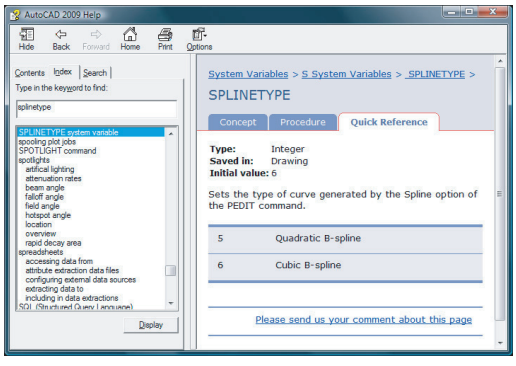

Slika 3: *Varijabla* `SPLINETYPE`

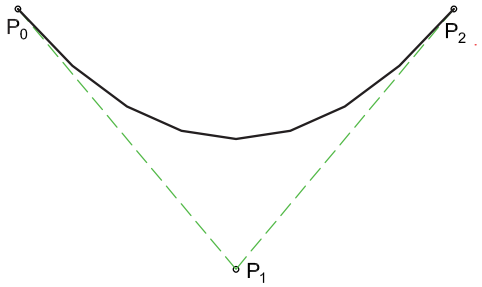

Slika 4: *Segmentirana krivulja*

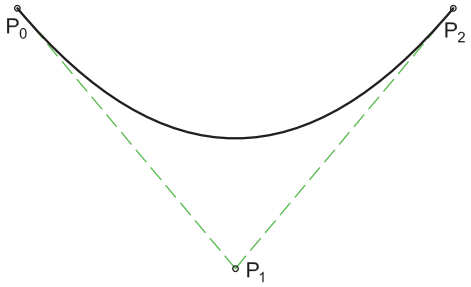

Slika 5: *Parabola*

3.2 Kružnica i elipsa

Kružni i eliptički lukovi u gotovo svim CAD alatima mogu se nacrtati bez pomoći NURBS krivulja, međutim, u nekim slučajevima potrebno ih je definirati kao NURBS krivulje, npr. crtanje nekih vrsta spirala.

Postupak crtanja kružnog luka sličan je postupku za crtanje parabole, međutim, težina srednje točke P_1 mora biti $w_1 = \cos(\alpha/2)$, a udaljenosti točke P_1 od točaka P_0 i P_2 moraju biti jednake (slika 6).

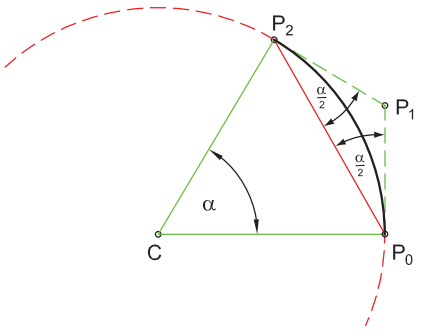

Slika 6: *Kružni luk*

Zbog jednostavnosti se obično koristi kut α od 90°, pri čemu w_1 iznosi $\sqrt{2}/2$. Ukoliko je potreban manji kut, nacrtana se krivulja može skratiti pomoću naredbe `TRIM`.

Postupak promjene težine srednje točke:
`SPLINEDIT↩L↩R↩W↩↩(nova težina)↩X↩X↩X↩↩`

Mali trik: u AutoCAD-u se umjesto brojke može upisati `LISP` izraz, tako da se vrijednost $\sqrt{2}/2$ može unijeti kao: `(/ (sqrt 2.0) 2.0)`

3.3 Hiperbola

Može se vidjeti da je težina srednje kontrolne točke između 0 i 1 za elipsu, točno 1 za parabolu, i veća od 1 za hiperbolu.

Ako je hiperbola zadana izrazom

$$\frac{x^2}{A^2} - \frac{y^2}{B^2} = 1 \tag{4}$$

i želimo ju prikazati na segmentu $x \in [A, X_1]$, najprije moramo pronaći sjecište njezinih tangenata u točkama P_0, P_2 kojima je 1. koordinata jednaka X_1 (slika 7). Pošto je hiperbola, dana jednadžbom (4), simetrična s obzirom na os x, sjecište tangenata nalazi se na x osi. Tangenta hiperbole u točki (X_1, Y_1) ima koeficijent smjera $S = \dfrac{B^2 \cdot X_1}{A^2 \cdot Y_1}$, iz čega proizlazi x koordinata sjecišta tangenata:
$X_0 = X_1 - \dfrac{Y_1}{S} = X_1 - \dfrac{A^2 \cdot Y_1^2}{B^2 \cdot X_1}$.
Težina srednje kontrolne točke određuje se prema izrazu $w_1 = \dfrac{X_1}{A}$.

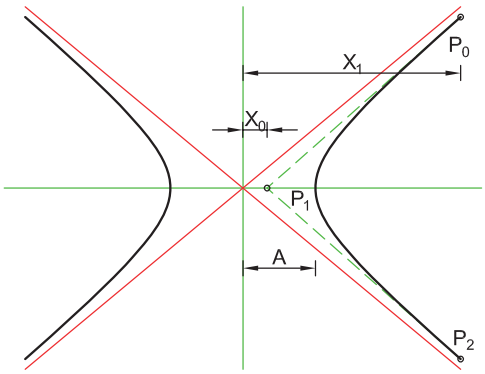

Slika 7: *Hiperbola*

4 Krivulje 4. i 5. reda

Pri statičkim proračunima često je potrebno prikazati dijagrame momenata savijanja, kuteve zaokreta i progibne linije nosača. Ukoliko na nosač djeluje jednoliko kontinuirano opterećenje, momentni dijagram je kvadratna parabola, odnosno NURBS krivulja 3. reda, dijagram kuteva zaokreta je krivulja 4. reda, a progibna linija krivulja 5. reda (slika 8).

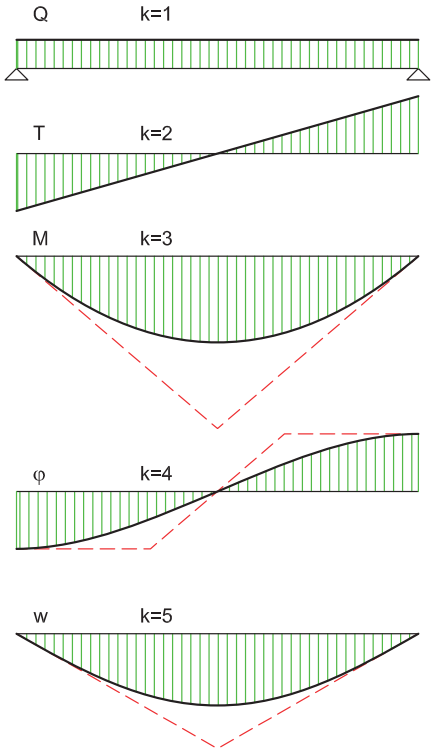

Slika 8: *Opterećenje, poprečne sile, momenti savijanja, kutevi zaokreta i progibna linija proste grede.*

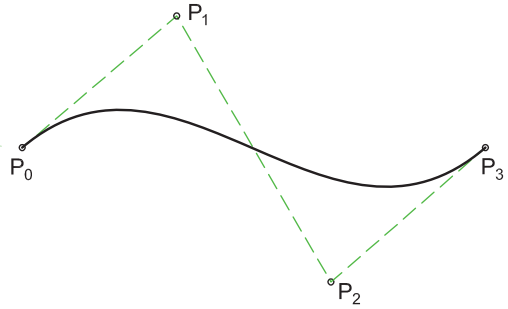

Slika 9: *Krivulja 4. reda*

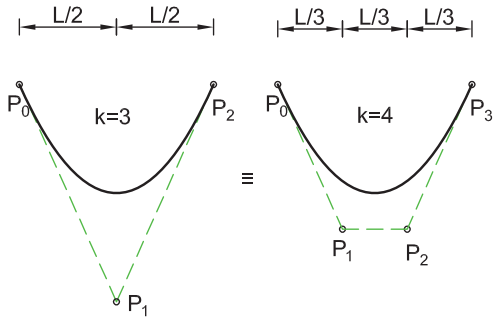

Slika 10: *Kvadratna parabola prikazana kao NURBS krivulja 3. i 4. reda*

Budući da su sve navedene krivulje grafovi polinoma $y = f(x)$, NURBS krivulje koje predstavljaju te funkcije imaju sljedeća svojstva:

- broj kontrolnih točaka je jednak redu krivulje,
- red krivulje je jednak redu polinoma + 1,
- sve kontrolne točke imaju težinu 1,
- x koordinate kontrolnih točaka su na jednakim razmacima.

Dakle, postupak crtanja krivulja 4. reda je vrlo jednostavan. Prva i zadnja kontrolna točka su krajevi krivulje, a preostale dvije kontrolne točke leže na tangentama u prvoj odnosno zadnoj točki (slika 9).

Naravno, pomoću krivulje 4. reda moguće je prikazati i kvadratnu parabolu (slika 10).

Ukoliko želimo nacrtati progibnu liniju nosača potrebna nam je NURBS krivulja 5. reda, koju je u AutoCAD-u nemoguće direktno nacrtati pa koristimo slijedeći postupak:

1. Nacrtamo polyline sa minimalnim brojem kontrolnih točaka (4) za krivulju 4. reda.
2. Odredimo 4. red krivulje pomoću sistemske varijable `SPLINETYPE` (6).
3. Pretvorimo polyline u segmentiranu krivulju pomoću naredbe `PEDIT↩L↩S↩↩`
4. Pretvorimo polyline u spline pomoću naredbe `SPLINE↩O↩L↩`
5. Pretvorimo krivulju 4. reda u krivulju 5. reda `SPLINEDIT↩L↩R↩E↩5↩X↩X↩`
6. Pomoću hvataljki pomaknemo kontrolne točke na potrebne pozicije (slika 11).

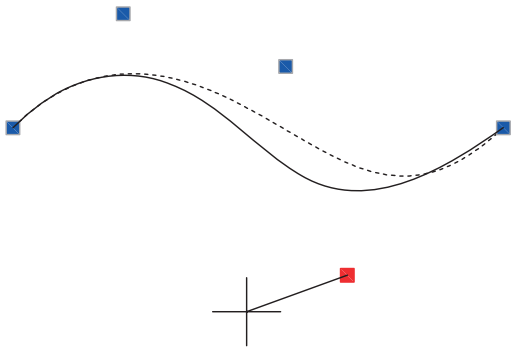

Slika 11: *Upotreba hvataljki u AutoCAD–u*

Ako krivulju zadanu izrazom

$$y = a \cdot x^4 + b \cdot x^3 + c \cdot x^2 + d \cdot x + e \tag{5}$$

želimo prikazati na intervalu $x \in [0,1]$, tada su koordinate kontrolnih točaka određene na sljedeći način:

$$P_0 = (0,e), \quad P_1 = (\frac{1}{4}, e + \frac{d}{4}), \; P_2 = (\frac{1}{2}, \frac{c}{6} + \frac{d}{2} + e),$$
$$P_3 = (\frac{3}{4}, \frac{b}{4} + \frac{c}{2} + \frac{3d}{4} + e), \; P_4 = (1, a+b+c+d+e).$$

Ukoliko promatramo elastični nosač, tada prema [4] za koeficijente iz jednadžbe (5) vrijedi sljedeće:

$e =$ pomak u prvom čvoru,

$d =$ kut zaokreta u prvom čvoru,

$c =$ moment savijanja u prvom čvoru $/(2 \cdot E \cdot I)$,

$b =$ poprečna sila u prvom čvoru $/(6 \cdot E \cdot I)$,

$a =$ opterećenje $/(24 \cdot E \cdot I)$,

gdje je E modul elastičnosti, a I tromost poprečenog presjeka.

Odnosno, u lokalnom koordinatnom sustavu nosača, koordinate kontrolnih točaka su:

$$P_0 = (0, w_0), \quad P_1 = (\frac{L}{4}, w_0 + \frac{\varphi_0 \cdot L}{4}),$$
$$P_2 = (\frac{L}{2}, \frac{M_0 \cdot L^2}{12 \cdot E \cdot I} + \frac{\varphi_0 \cdot L}{2} + w_0),$$
$$P_3 = (\frac{3}{4} \cdot L, w_1 - \frac{\varphi_1 \cdot L}{4}),$$
$$P_4 = (L, w_1).$$

PRIMJER 1: Slobodno oslonjena greda

Budući da je $M_0 = 0$, srednja kontrolna točka P_2 nalazi se u sjecištu tangenata u točkama P_0 i P_4, a y koordinata kontrolne točke P_2 iznosi $\frac{q \cdot L^4}{48 \cdot E \cdot I}$.

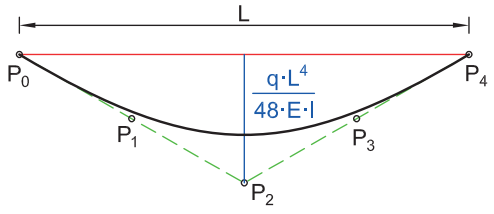

Slika 12: *Progibna linija slobodno oslonjene grede*

PRIMJER 2: Obostrano upeta greda

y koordinata srednje kontrolne točke P_2 iznosi $\frac{q \cdot L^4}{144 \cdot E \cdot I}$.

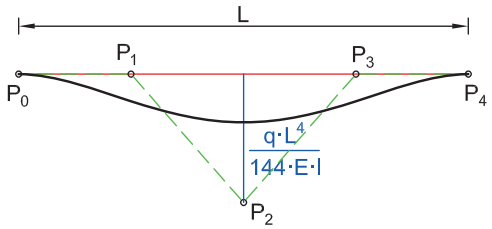

Slika 13: *Progibna linija obostrano upete grede*

PRIMJER 3: Jednostrano upeta greda (slika 14)

y koordinata srednje kontrolne točke P_2 iznosi $\frac{q \cdot L^4}{96 \cdot E \cdot I}$.

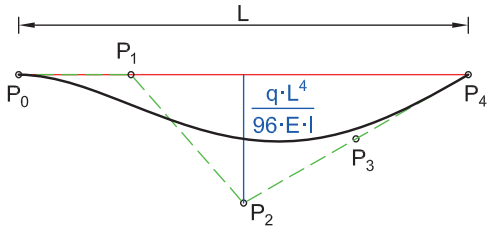

Slika 14: *Progibna linija jednostrano upete grede*

References

[1] http://web.cs.wpi.edu/~matt/courses/cs563/talks/nurbs.html

[2] http://www.cs.mtu.edu/ shene/COURSES/cs3621/NOTES/

[3] http://www.ibiblio.org/e–notes/Splines/Basis.htm

[4] V. SIMOVIĆ, Građevna statika I, Građevinski institut, Zagreb, 1988.

Željko Gjuranić
Emerson d.o.o., Selska cesta 93, 10000 Zagreb
e-mail: Zeljko.Gjuranic@Emerson.com

How to get KoG?

The easiest way to get your copy of KoG is by contacting the editor's office:

Nikoleta Sudeta
nsudeta@arhitekt.hr
Faculty of Architecture
Kačićeva 26, 10 000 Zagreb, Croatia
Tel: (+385 1) 4639 219
Fax: (+385 1) 4639 465

The price of the issue is €15 + mailing expenses €5 for European countries and €10 for other parts of the world.

The amount is payable to:

ACCOUNT NAME: Hrvatsko društvo za geometriju i grafiku
Kačićeva 26, 10000 Zagreb, Croatia

IBAN: HR862360000-1101517436

Kako nabaviti KoG?

KoG je najjednostavnije nabaviti u uredništvu časopisa:

Nikoleta Sudeta
nsudeta@arhitekt.hr
Arhitektonski fakultet
Kačićeva 26, 10 000 Zagreb
Tel: (01) 4639 219
Fax: (01) 4639 465

Za Hrvatsku je cijena primjerka 100 KN + 10 KN za poštarinu.

Nakon uplate za:

HDGG (za KoG), Kačićeva 26, 10000 Zagreb
žiro račun broj **2360000-1101517436**

poslat ćemo časopis na Vašu adresu.

Ako Vas zanima tematika časopisa i rad našega društva, preporučamo Vam da postanete članom HDGG (godišnja članarina iznosi 150 KN). Za članove društva časopis je besplatan.

INSTRUCTIONS FOR AUTHORS

SCOPE. "KoG" publishes scientific and professional papers from the fields of geometry, applied geometry and computer graphics.

SUBMISSION. Scientific papers submitted to this journal should be written in English or German, professional papers should be written in Croatian, English or German. The papers have not been published or submitted for publication elsewhere.
The manuscript with wide margins and double spaced should be sent in PDF format via e-mail to the one of the editors:

Sonja Gorjanc
sgorjanc@grad.hr

Jelena Beban - Brkić
jbeban@geof.hr

The first page should contain the article title, authors and coauthors names, affiliation, a short abstract in English, a list of keywords and the Mathematical subject classification.

UPON ACCEPTANCE. After the manuscript has been accepted for publication authors are requested to send its LaTeX file via e-mail to the address:

sgorjanc@grad.hr

Figures should be included in EPS or PS formats.

OFFPRINTS. The corresponding author and coauthors will receive hard copies of the issue free of charge and a PDF file of the article via e-mail.

UPUTE ZA AUTORE

PODRUČJE. "KoG" objavljuje znanstvene i stručne radove iz područja geometrije, primijenjene geometrije i računalne grafike.

UPUTSTVA ZA PREDAJU RADA. Znanstveni radovi trebaju biti napisani na engleskom ili njemačkom jeziku, a stručni na hrvatskom, engleskom ili njemačkom. Rad ne smije biti objavljen niti predan na recenziju drugim časopisima.
Rukopis sa širokim marginama i dvostrukim proredom šalje se u PDF formatu elektronskom poštom na adresu jedne od urednica:

Sonja Gorjanc
sgorjanc@grad.hr

Jelena Beban - Brkić
jbeban@geof.hr

Prva stranica treba sadržavati naslov rada, imena autora i koautora, podatke o autoru i koautorima, sažetak na hrvatskom i engleskom, ključne riječi i MSC broj.

PO PRIHVAĆANJU RADA. Tekst prihvaćenog rada autor dostavlja elektronskom poštom kao LaTeX datoteku, a slike u EPS ili PS formatu, na adresu:

sgorjanc@grad.hr

POSEBNI OTISCI. Svaki autor i koautor dobiva po jedan tiskani primjerak časipisa i PDF datoteku svog članka.

ISSN 1331-1611